DEVELOPMENT OF DYE SENSITIZED SOLAR CELLS FROM RUTHENIUM(II) COMPLEXES

PREEYAPAT PROMPAN

A THESIS SUBMITTED IN PARTIAL FULFILLMENT OF THE REQUIREMENTS
FOR THE DEGREE OF MASTER OF SCIENCE
MAJOR IN CHEMISTRY
FACULTY OF SCIENCE
UBON RATCHATHANI UNIVERSITY
ACADEMIC YEAR 2016

UBON RATCHATHANI UNIVERSITY
THESIS APPROVAL
MASTER OF SCIENCE
MAJOR IN CHEMISTRY FACULTY OF SCIENCE

TITLE DEVELOPMENT OF DYE SENSITIZED SOLAR CELLS FROM RUTHENIUM(II) COMPLEXES

AUTHOR MISS PREEYAPAT PROMPAN

EXAMINATION COMMITTEE

DR. NOPPORN RUANGSUPAPICHAT	CHAIRPERSON
ASST. PROF. DR. RUKKIAT JITCHATI	MEMBER
ASST. PROF. DR. KITTIYA WONGKHAN	MEMBER
ASST. PROF. DR. TINNAGON KAEWIN	MEMBER

ADVISORS

……………………………………………….……. ADVISOR
(ASST. PROF. DR. RUKKIAT JITCHATI)

…………………………………………………….. CO-ADVISOR
(ASST. PROF. DR. KITTIYA WONGKHAN)

…………………………….…………..….....
(ASSOC. PROF. DR. UTITH INPRASIT)
DEAN, FACULTY OF SCIENCE

..…………….……………….…………..….….....
(ASSOC. PROF. DR. ARIYAPORN PONGRAT)
VICE PRESIDENT
FOR ACADEMIC AFFAIRS

ACADEMIC YEAR 2016

ACKNOWLEDGEMENTS

I would like to acknowledge my advisor, Asst. Prof. Dr. Rukkiat Jitchati, for allowing me to undertake this project, all the brilliant ideas, his enthusiasm, advice and guiding me throughout the years. Thank for his support, patience, and encouragement throughout my graduate studies. It is not often that one finds an advisor and colleague that always finds the time for listening to the little problems and roadblocks that unavoidably crop up in the course of performing research. His technical and editorial advice was essential to the completion of this dissertation and has taught me innumerable lessons and insights on the workings of academic research in general. His advice was most valuable to understand the obtained results and to determine the next steps for the research presented in this thesis.

I would like to thanks many people who contributed their time and their advice. Thank to Asst. Prof. Dr. Kittiya Wongkhan for advice and support me in every problem especially in English and for writing my publication. Asst. Prof. Dr. Taweesak Sudyoadsuk, who set the instruments for the device measurement and for his guidance on the DSSCs fabrication and Mr. Chonchanok Talodthaisong are responsible for the device on the fabrication of all DSSCs presented in my work.

I would like to thank to the Organometallic and Catalytic Center (OCC), Department of Chemistry, Faculty of Science, Ubon Ratchathani University for the synthesis facilities.

Thanks everyone in the OCC group for contributed and helped me to make this research work possible at Ubon Ratchathani University. And finally, I must thank my family for their love and personal support during my study.

Preeyapat Prompan
Researcher

บทคัดย่อ

เรื่อง : การพัฒนาเซลล์พลังงานแสงอาทิตย์ชนิดสีย้อมไวแสงจากสารประกอบเชิงซ้อนของโลหะรูทีเนียม(II)
ผู้วิจัย : ปรียาภัทร พรมพันธุ์
ชื่อปริญญา : วิทยาศาสตรมหาบัณฑิต
สาขาวิชา : เคมี
อาจารย์ที่ปรึกษา : ผู้ช่วยศาสตราจารย์ ดร.รักเกียรติ จิตคติ
คำสำคัญ : เซลล์แสงอาทิตย์ชนิดสีย้อมไวแสง, สารประกอบเชิงซ้อนของโลหะรูทีเนียม(II), สีย้อมร่วม, สารประกอบเชิงซ้อนของโลหะรูทีเนียมชนิดไม่มีลิแกนด์ไทโอไซยาเนต

งานวิจัยนี้ได้รายงานการสังเคราะห์สารประกอบเชิงซ้อนของโลหะรูทีเนียม(II) 2 ชุด สารเป้าหมายทั้งหมดได้พิสูจน์เอกลักษณ์ทางโครงสร้าง ศึกษาสมบัติทางแสง สมบัติทางเคมีไฟฟ้า และการเป็นสีย้อมในเซลล์พลังงานแสงอาทิตย์ชนิดสีย้อมไวแสง ระบบอิเล็กโทรไลต์ ไอโอไดด์/ไตรไอโอไดด์ ภายใต้ความเข้มแสงมาตรฐานที่ AM 1.5 ความเข้มแสงเท่ากับ 100 mW/cm^2

ชุดที่ 1 สีย้อมร่วม ได้แก่ **P2+N719** และ **YN07+N719** ซึ่ง **P2** คือ 2-phenyl-5-(trifluoromethyl) pyrido) bis (2,2'-bipyridine-4,4'-dicarboxylic acid)ruthenium(II) hexafluorophosphate และ **YN07** คือ cis [bis(thiocyanato) bis (2,2'-biquinoline-4,4'-dicarboxylic acid (4-carboxy-2,2'-bipyridine-4'-caboxylate)ruthenium(II)] tetrabutylammonium พบว่าสีย้อมร่วมให้ประสิทธิภาพเป็น 2.37% และ 1.59% เมื่อเทียบกับ **P2** (1.42%), **YN07** (0.46%) และ **N719** (5.17%)

ชุดที่ 2 สีย้อมชนิดไม่มีลิแกนด์ไทโอไซยาเนต เป็น [Ru(dcbpy)$_2$(**ppy**)]PF$_6$: (**PP1**), [Ru(dcbpy)$_2$(**PL1**)]PF$_6$: (**PP2**), [Ru(dcbpy)$_2$(**PL2**)]PF$_6$: (**PP3**) และ [Ru(dcbpy)$_2$(**PL3**)]PF$_6$: (**PP5**) โดยที่ dcbpy คือ 2,2'-bipyridine-4,4'-dicarboxylic acid, **ppy** คือ 2-phenylpyridine, **PL1** คือ 2-phenylpyridine-3-(pyridin-2-yl)benzoate, **PL2** คือ methyl-2-phenylisonicotinate และ **PL3** คือ methyl-2-(3-(methoxycarbonyl)phenyl)isonicotinate จากการศึกษาพบว่าให้ประสิทธิภาพเท่ากับ 3.10%, 0.69%, 1.54% และ 1.53% ตามลำดับ เทียบกับ **N719** (7.44%)

ABSTRACT

TITLE : DEVELOPMENT OF DYE-SENSITIZED SOLAR CELLS FROM RUTHENIUM(II) COMPLEXES
AUTHOR : PREEYAPAT PROMPAN
DEGREE : MASTER OF SCIENCE
MAJOR : CHEMISTRY
ADVISOR : ASST. PROF. RUKKIAT JITCHATI, Ph.D
KEYWORDS : DYE-SENSITIZED SOLAR CELL (DSSC),
RUTHENIUM(II) COMPLEX, CO-SENSITIZATION,
THIOCYANATE FREE RUTHENIUM(II) COMPLEX

This thesis reported the synthesis of TWO series of ruthenium(II) complexes of which the physical, photophysical, and electrochemical properties of the target complexes were studied. The materials were studied by dye-sensitized solar cell (DSSCs) with iodide/tri-iodide electrolyte under standard AM 1.5 (100 mW/cm^2). In the first part, the co-sentisized dyes, specifically **P2+N719** and **YN07+N719** (**P2** was 2-phenyl-5-(trifluoromethyl)pyrido) bis (2,2'-bipyridine-4,4'-dicarboxylic acid)ruthenium(II) hexafluorophosphate and **YN07** was cis [bis(thiocyanato) bis (2,2'-biquinoline-4,4'-dicarboxylic acid(4-carboxy-2,2'-bipyridine-4'-caboxylate)ruthenium(II)] tetrabutyl-ammonium). It was found that the co-dyes showed photovoltaic efficiencies of 2.37% and 1.59% compared with pure dyes **P2** (1.42%), **YN07** (0.46%), and **N719** (5.17%). In the second part, the thiocyanate free ruthenium(II) complexes were coded as [Ru(dcbpy)$_2$(**ppy**)]PF$_6$: (**PP1**), [Ru(dcbpy)$_2$(**PL1**)]PF$_6$: (**PP2**), [Ru(dcbpy)$_2$(**PL2**)]PF$_6$: (**PP3**), and [Ru(dcbpy)$_2$(**PL3**)]PF$_6$: (**PP5**) (dcbpy was 2,2'-bipyridine-4,4'-dicarboxylic acid, **ppy** was 2-phenylpyridine, **PL1** was 2-phenylpyridine-3-(pyridin-2-yl)benzoate, **PL2** was methyl-2-phenylisonicotinate, and **PL3** was methyl-2-(3-(methoxycarbonyl)-phenyl)isonicotinate. It was found that DSSCs showed photovoltaic efficiencies at 3.10%, 0.69%, 1.54%, and 1.53% respectively, compared with **N719** (7.44%).

CONTENTS

CONTENTS (CONTINUED)

PAGE

LIST OF TABLES

LIST OF FIGURES

LIST OF FIGURES (CONTINUED)

LIST OF FIGURES (CONTINUED)

LIST OF FIGURES (CONTINUED)

LIST OF FIGURES (CONTINUED)

FIGURES **PAGE**

LIST OF FIGURES (CONTINUED)

LIST OF ABBREVIATIONS

ABBREVIATION	**DEFINITION**
A	Ampare
Ag/AgCl	Silver/ Silver chloride (reference electrode)
AR.	Analysis reagent
Aq.	Aqueous
AM	Air mass
anh.	Anhydrous
ATR	Attenuated total reflectance
conc.	Concentrated
cm^{-1}	Reciprocal centimeter (unit of wavenumber)
^{13}C NMR	Carbon nuclear magnetic resonance
^{o}C	Degree Celsius
CB	Conduction band
cm	Centimeter
cm^{3}	Centimeter cubic unit
CV	Cyclic voltammetry
d	Doublet (for NMR spectral data)
dcbpy	2,2'-Bipyridine-4,4'-dicarboxylic acid
$dFppyCF_3$	2-(2,4-Difluorophenyl)-5-trifluoromethyilpyridine
dd	Double of doublet (for NMR spectral data)
DCM	Dichloromethane
dcbiq	4,4'-Dicarboxy-2,2' -biquinoline
DFT	Density functional theory
DI	Deionized Water
DMF	Dimethylformamide
DMSO	Dimethyl sulfoxide
DSSCs	Dye-Sensitized Solar Cells
E	Energy

LIST OF ABBREVIATIONS (CONTINUED)

ABBREVIATION	**DEFINITION**
E_g	Energy gap
E_{ap}	Anodic peak potentials
E_{cp}	Cathodic peak potentials
eV	Electron volt
E_{ox}	Oxidation potential
$E_{ox, onset}$	Onset oxidation potential
E_{red}	Reduction potential
$E_{red, onset}$	Onset reduction potential
ESI-MS	Electrospray ionization mass spectrometry
EtOAc	Ethyl acetate
Fc/Fc^+	Ferrocene/Ferrocenium
FF	Fill factor
FTIR	Fourier transform infrared spectroscopy
FTO	Fluoride doped tin oxide
HOMO	Highest occupied molecular orbital
Hz	Hertz
I_0	The energy of incident sunlight (100 mW/cm^2)
IPCE	Incident Photon to Current Conversion Efficiency
IR	Infrared
J	Coupling constant (for NMR spectral data)
J_{max}	Maximum current
J_{SC}	Short circuit current density
J_{ph}	The short circuit photocurrent density generated by mono chromatic light
L	Liter
LUMO	Lowest unoccupied molecular orbital
M	Molarity

LIST OF ABBREVIATIONS (CONTINUED)

ABBREVIATION	**DEFINITION**
m	Multriplet (for NMR spectral data)
m^2	Square meter
MHz	Mega hertz
ml	Milliliter
MLCT	Metal to ligand charge transfer
mM	Millimolar
mmol	Millimol
mV	Millivolt
MW	Molecular weight
Red	Reduction
S	The ground state
S^*	The excited state
S^+	The oxidized dye
s	Singlet (for NMR spectral data)
s	Second
TBAOH	Tetra butyl ammonium hydroxide
TCO	Transparent conducting oxides
TDDET	Time-dependent density functional theory
TLC	Thin layer chromatography
TMS	Tetra methylsilane
t	Triplet (for NMR spectral data)
UV-Vis	Ultra violet-visible
V	Voltage
v/v	Volume/volume
V_{max}	Maximum voltage
V_{OC}	Open circuit voltage
W	Watt

LIST OF ABBREVIATIONS (CONTINUED)

ABBREVIATION	**DEFINITION**
δ	Chemical shift (for NMR spectral data)
η	The power conversion efficiency
µA	Microampare
µm	Micrometer
µW	Microwatt
α	Alpha
Ω	Ohm (Unit of electrical resistance)
p	Para-substitution
ε	Molar extinction coefficient
λ	Wavelength
π	Pi-orbital
Δ	Delta
%	Percent

CHAPTER 1

INTRODUCTION

1.1 Importance in research and development

Energy is one of the most important factors to human life. The energy can produce from many sources: biomass energy, fossil, fuels-coal, petroleum and natural gas which are the nonrenewable energy. Hence, the scientists need to find alternative energy sources.

The sun light is one of the best renewable energy because it is clean, sustainable and environmental friendly. Sun light can be converted directly to electricity which called photovoltaic cell or solar cell. In 1954, photovoltaic P-N type semiconductor single crystal silicon has developed to give high performance. Until now, P-N solar cells give power conversion efficiencies around 18-45% [1], [2]. However, the synthesis process to produce P-N solar cell need high technology and purity of semiconductor materials. So, there are the several researchers have developed other solar.

In 1991, dye-sensitized solar cells (DSSCs) were invented by O'Regan Grätzel [3]. There was due to its low cost of production, high performance compared with the traditional photovoltaic cells [4].

1.2 Dye sensitized solar cells (DSSCs)

DSSCs have attracted much attention because of their high solar light to electricity conversion efficiency.

1.2.1 Structure and materials of DSSCs

The DSSC is a multilayer structure, comprised of three distinct functional components. It includes a dye sensitizer, semiconductor working electrode (anode), a redox electrolyte and a platinized counter electrode (Pt cathode). The most important component is a dye which should absorb all region of the sun light. The DSSCs structures are shown in Figure 1.1.

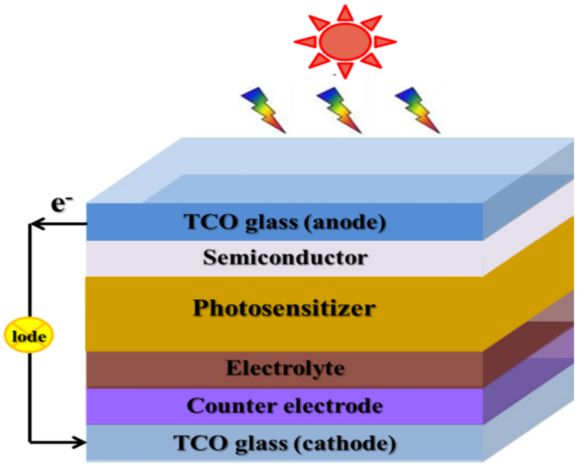

Figure 1.1 Sandwiched structure and components of the DSSCs

1.2.1.1 Transparent conducting oxide (TCO) substrate

Transparent conducting oxide is used as the substrate for semiconductor (TiO_2) normally using fluoride doped tin oxide (SnO_2: F, FTO). For high solar cell performance, the substrates have low sheet resistance, high transparency and should resistance independent to temperature.

1.2.1.2 Semiconductor

Several semiconductor can be used in DSSCs, for example, Si, ZnO, SnO_2, Nb_2O_5 GaAs, InP and CdS. In contrast, TiO_2 show good chemical stability under visible-light irradiation. In addition, it is nontoxic and inexpensive. The TiO_2 holds the dye molecules, collected the photogenerated electrons from the LUMO level of the dye molecules. Therefore, TiO_2 materials have to satisfy several requirements including high surface area to load a large amount of dye molecules, conduction band energy level less than the LUMO level of the dye and more than the redox level of the electrolyte. Today, TiO_2 becomes the best choice for semiconductor.

1.2.1.3 Photosensitizer (dye)

Normally, the well knows dyes are the ruthenium complex which was developed by Grätzel’s group shown in Figure 1.2. The dye can absorb visible light and inject electrons from the excited state into the conduction band of semiconductor. The injected electrons move through the semiconductor to the current collector and the dye will be regenerated by obtaining an electron from electrolyte. At the same time, electrolyte was obtained electron from the counter electrode.

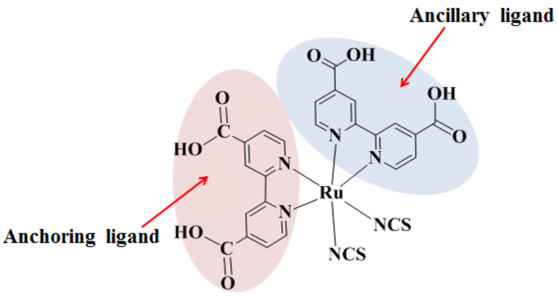

Figure 1.2 Structure of ruthenium complex (N3)

Anchoring ligand with carboxylic acid groups will hold the TiO_2 surface which results to effect electron injection from ruthenium complex into the TiO_2. The ruthenium complex adsorbed on the TiO_2 surface by carboxylate bidentate coordination or ester bonding (–C(=O)O–). In contrast, the role of ancillary ligand is absorbing light in a wide range of the visible to near-IR region from 400 to 900 nm which is attributing to the metal to ligand charge transfer (MLCT) transition.

1.2.1.4 Electrolyte

The electrolyte normally used in the DSSCs is I^-/I^-_3 couple, which is mediate electrons between the TiO_2 and the counter electrode. Iodide electrolyte concentrations of 0.1 to 0.5 M and 0.05 to 0.1 M I_2 in nonprotonic solvents (e.g. acetonitrile, propionitrile, methoxyacetonitrile and propylene carbonate) are employed. Viscosity of solvents directly affects ion conductivity in the electrolyte and consequently the cell performance.

1.2.1.5 Counter electrode

The role of counter electrode is to compensate an electron to the tri-iodide ions (I^-_3), formed by the reduction of dye$^+$, in the Figure 1.3. Basically, the Pt coated on FTO substrate is used as the counter electrode.

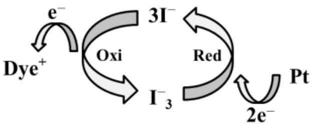

Figure 1.3 The mechanism of a iodide/tri-iodide redox couple on the platinized FTO glass electrode

1.2.2 The principle of dye sensitized solar cell

The principles of operation and a generic energy level DSSCs are shown in the Figure 1.4.

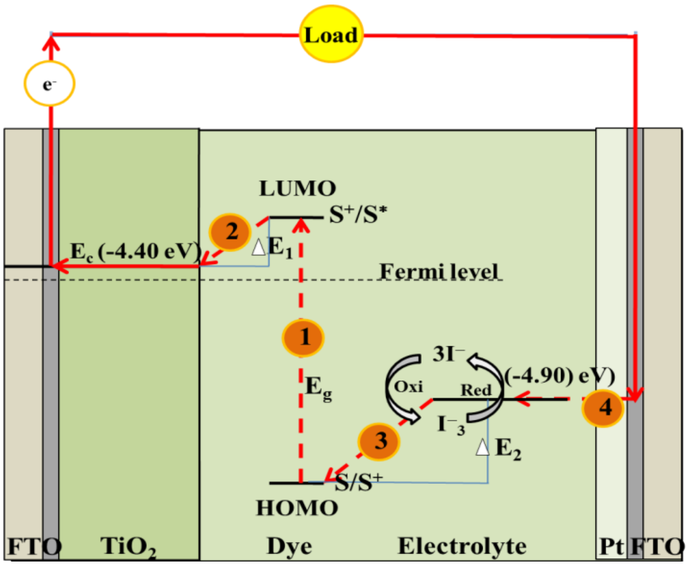

Figure 1.4 Schematic energy diagram and operating principle of DSSCs

1.2.2.1 The photosensitizers on the TiO_2 are excited from the ground state (S) to the excited state (S^*) (equation 1) which is called photo excitation.

$$S + h\nu \longrightarrow S^* \text{ (photo excitation)} \qquad (1)$$

1.2.2.2 The excited electrons are injected into the conduction band of the TiO_2 electrode, resulting in the oxidation of the photosensitizer (equation 2) which is called electron injection. The electron injection occurred from photosensitizers into the conduction band of TiO_2 with in 10^{10} - 10^{12} s^{-1}.

$$S^* \rightarrow S^+ + e^- \text{ (CB of } TiO_2\text{) (electron injection)} \qquad (2)$$

1.2.2.3 The oxidized sensitizers (S^+) obtain electrons from the I^-/I^-_3 electrolyte. The I^-/I^-_3 couple is regenerate the ground state (S), and I^- is oxidized to the oxidized state, I^-_3 (equation 3) which is called regeneration of dye.

$$2S^+ + 3I^- \rightarrow 2S + I^-_3 \text{ (regeneration of dye)} \quad (3)$$

1.2.2.4 The oxidized redox (I^-_3) diffuses toward the counter electrode and re-reduced to I^- ions which is regeneration of electrolyte (equation 4).

$$I^-_3 + 2e^- \text{ (Pt)} \rightarrow 3I^- \text{ (regeneration of electrolyte)} \quad (4)$$

Overall, electric power is generated without permanent chemical transformation. The performance of DSSCs is importantly based on three energy levels of the component as follows;

(1) The excited state (LUMO) of the photosensitizer

(2) The ground state (HOMO) of the photosensitizer

(3) The redox potential of I^-/I^-_3 in the electrolyte

The LUMO level and the conduction band of TiO_2 (ΔE_1) is important which the energy gap between excited state (LUMO) of dyes are higher than conduction band of TiO_2 at approximately -4.40 eV, giving suitable driving force for electron injection. The ground state (HOMO) of sensitizers is more negative than the redox potential of I^-/I^-_3 redox at -4.90 eV, giving a thermodynamic driving force for efficient dye regeneration. The energy gap between HOMO and I^-/I^-_3 are ΔE_2. The energy gaps, ΔE_1 and ΔE_2, must be larger than approximately 0.2 eV as driving force for each of the electron transfer to take place with optimal efficiency [5], [6], [7].

1.2.3 The development of ruthenium sensitizers

The ruthenium(II) complex for DSSC can be divided into 2 types.

1.2.3.1 Ruthenium(II) complex with thiocyanate ligands

The common thiocyanate ruthenium(II) sensitizer consist of bipyridine (N^N ligand) and thiocyanate ($^-$NCS) ligand. The well know ruthenium(II) complex with thiocyanate ligands is cis-di(thiocyanato) bis (bpy-4,4'-dicarboxylic acid) ruthenium(II) (**N3**). It has shown the power conversion efficiency at 10% under one sun illumination (AM 1.5) due to light driven MLCT transition that promotes rapid charge injection into the semiconductor [8]. This is attributed to their strong MLCT in the visible region and easy redox. The **N3** dye shows λ_{max} at 520 nm, the higher short circuit current and long term stability. Both HOMO and LUMO provide favorable electron density distribution for the electron injection and the sensitizer regeneration processes shown in Figure 1.5.

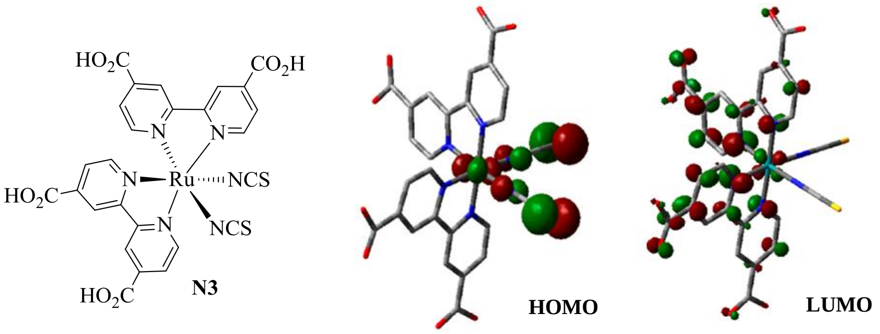

Figure 1.5 Structure and the HOMO and LUMO of N3 dye [8]

Later, enhancing the absorption of the lower energy region of the spectrum was reported the tri(cyanato)-2',2",2"terpyridyl-4',4",4"-tricarboxylate ruthenium(II): **Black dye** (in Figure 1.6) which their visible absorption extending into the near-IR region up to 920 nm. Its overall energy conversion efficiency is around 11.4% under AM 1.5 solar light which shows higher efficiency than **N3** [9].

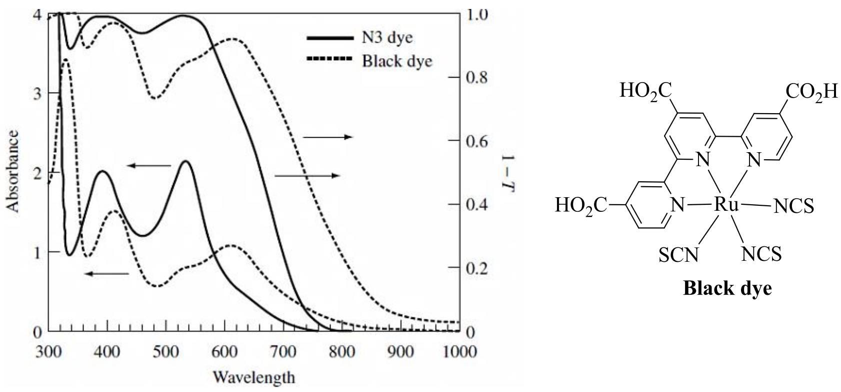

Figure 1.6 Absorption spectra and light-harvesting efficiency of N3 and Black dye

The dye (cis-bis(isothiocyanato) bis (2,2'-bipyridyl-4,4'-dicarboxylato) ruthenium(II) bis(tetrabutylammonium)) (**N719**) was developed from **N3** dye. It has shown efficiencies over 11.18% [10]. However, the main defect of the **N3** and **N719** sensitizer is the absence of strong absorption in the red region of the visible spectrum [11].

After that, the (4,4'-dicarboxylic acid-2,2'-bipyridine)(4,4'-dinonyl-2,2'-bipyridine)$(NCS)_2$ ruthenium(II) (**Z907**), containing aliphatic side chains moiety, was synthesized. The chemical structure is shown in the Figure 1.7.

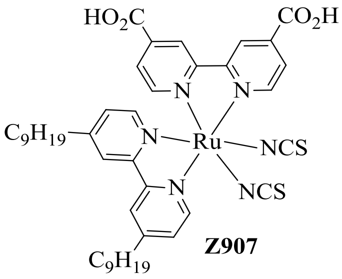

Figure 1.7 Chemical structure of Z907 dye

Z907 shows efficiencies at 9.5% under AM 1.5 which is significantly lower than that **N3** dye [12]. However, the aliphatic side chains played a major role for the lower power efficiency with a better stability of DSSC compared with those of **N3** dye [13].

The ruthenium(II) complex with thiocyanate shows high efficiency. However, it was found that thiocyanate is a monodentate ligand, which can coordinate either sulfur or nitrogen atom. Hence, it can be easily replaced by other competing ligands yielding less efficient.

1.2.3.2 Ruthenium(II) complex without thiocyanate ligands

The thiocyanate free ruthenium(II) complex consist of bipyridine and phenylpyridine (C^N) ligands.

Bessho et al. developed thiocyanate free ruthenium(II) complex, bis (4,4'-dicarboxy-2,2'-bipyridine)-2-(2,4-difluorophenylpyridine) ruthenium(II); **Complex 1**. They found that, **Complex 1** shows three absorption bands at 406, 490 and 560 nm which are attributed to MLCT band. **Complex 1** shows high efficiency at 10.1% compared with **N719** at 10% [14]. By extending the π-conjugation, the DSSCs efficiency can be improved. It shows high molar absorptivity and high stability. Moreover, application of TDDFT calculation has provided valuable information on the nature of the electronic transitions that are involved in the light absorption and electron transfer process are shown in Figure 1.8.

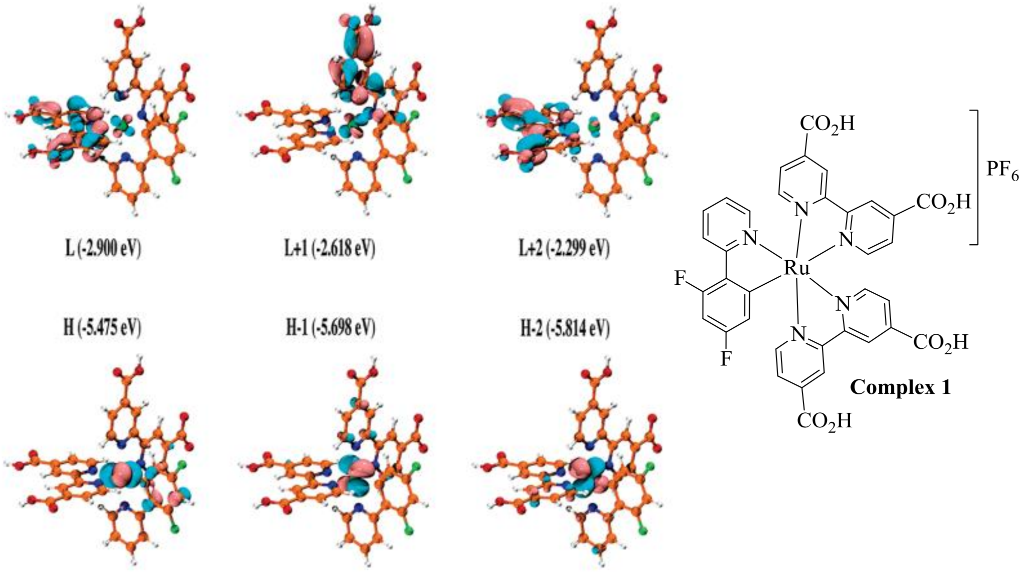

Figure 1.8 Computed isosurface plots of selected Kohn-Sham molecular orbitals (from HOMO-2 to LUMO+2) of complex 1

1.2.4 The trend for dye sensitizer development

In the development of new ruthenium(II) sensitizers for DSSCs application, four features will be considered:

1.2.4.1 The sensitizer should have strong absorption over a broad spectral range extending into the near-IR region in order to harvest most wavelengths in the solar irradiance spectrum and absorb light as much as possible such as using co-sensitization, by replacing the thiocyanate ligands with C^N or N^N ligands and extending electron-rich π-conjugated in dye molecule.

1.2.4.2 The sensitizer have to tightly attach to the semiconductor surface through anchoring moiety such as carboxylic acids, phosphonic acids and nitro group. Strong electronic coupling between the conduction band of the semiconductor and the sensitizer will smooth the electron injection process resulting in high charge separation efficiency.

1.2.4.3 The LUMO level of dye must be higher than that of the conduction band of the TiO_2 and the HOMO of dye must be more negative than the electrolyte (iodide/tri-iodide).

1.2.4.4 The sensitizer should have long term and thermal stability.

1.2.5 Photovoltaic performance of DSSCs

Figure 1.9 illustrates the photovoltaic parameters of the DSSCs. The performance is evaluated based on four parameters. These include the open circuit voltage (V_{OC}), the short circuit current (J_{SC}), the incident photon to current conversion efficiency (IPCE) and the power conversion efficiency (η).

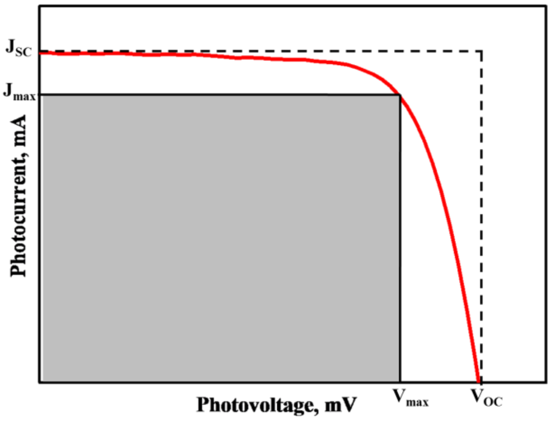

Figure 1.9 The current-voltage characteristic of DSSCs

The two parameters, V_{OC} and J_{SC}, are obtained from the current-voltage characteristic (I-V curve) of the DSSCs. The intersections between the I-axis and V-axis are J_{SC} and V_{OC}, respectively. The ratio of the obtained maximal output of power ($J_{max} \times V_{max}$) to the theoretical power ($J_{SC} \times V_{OC}$) is defined as the fill factor (FF) which gives an indication of the ability for solar cell (equation 5).

$$FF = \frac{J_{max} \times V_{max}}{J_{SC} \times V_{OC}} \quad (5)$$

The IPCE is another important characteristic of DSSCs, which is defined as the ratio of the observed photocurrent to the incident photon flux measured as a function of excitation wavelength. This measurement serves as an indicator for the conversion ability of the solar cell to produce electrical current from the incident photons [15], [16]. The greater IPCE values at each wavelength, the more efficient were obtained. The IPCE is plotted as a function of the monochromatic excitation wavelength, which can be calculated using equation 6.

$$\text{IPCE (\%)} = \frac{1240 \times J_{ph}}{\lambda \times I_0} \tag{6}$$

Where, J_{ph} is the short circuit photocurrent density generated by mono chromatic light and I_0 is the energy of incident sunlight (100 mW/cm^2).

Solar energy to electricity conversion efficiency (η) is defined as the ratio of the maximum output electrical power of the DSSC to the energy of incident sunlight (I_0) under white light irradiation (AM 1.5). The electricity conversion efficiency can be obtained by the following equation 7.

$$\eta = \frac{J_{SC} \times V_{OC} \times FF}{I_0} \tag{7}$$

In the photovoltaic field, the global air mass 1.5 spectrum is typically referred to as the standard solar spectrum. The performance of the solar cells measured at different times and locations are usually compared to the AM 1.5.

The sunlight passes through the atmosphere, it absorbed and scattered by water, carbon dioxide, ozone and other substances. The continuous spectrum results in bands with many sharp peaks at various wavelengths, especially in the infrared region are shown in Figure 1.10. The average energy reaching the earth is approximately at 100 mW/cm^2 [17].

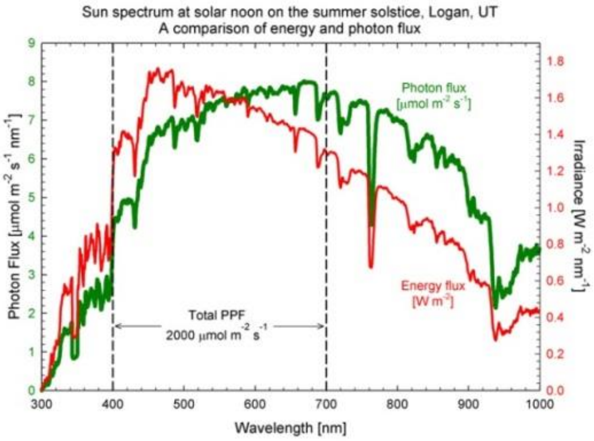

Figure 1.10 The spectrum of the area solar simulator from PV measurements compared to the reference AM 1.5 Global [17]

1.3 Objectives

1.3.1 To synthesize and characterize of ruthenium(II) complexes (**P2**, **YN07** and **N719**)

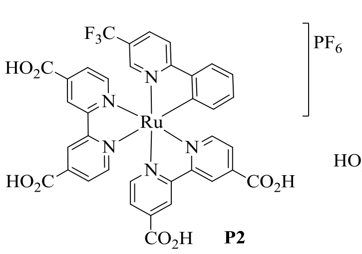

P2

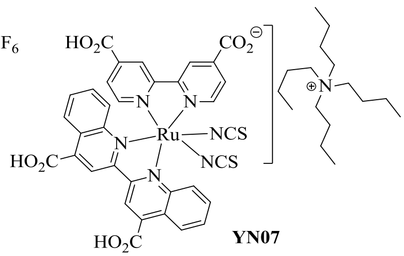

YN07

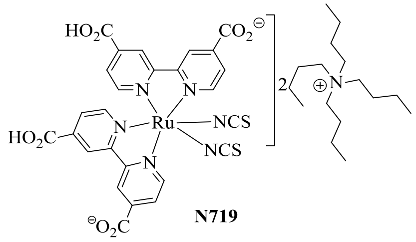

N719

1.3.2 To study the co-sensitizers which are a combination of **P2+N719** and **YN07+N719** in DSSCs

1.3.3 To synthesize and characterize of thiocyanate free ruthenium(II) complexes by varying the position of ester groups on the phenyl pyridine ligand

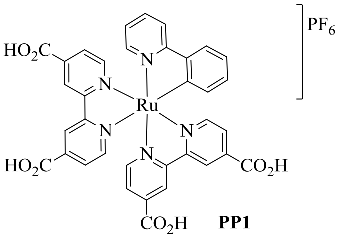

PP1

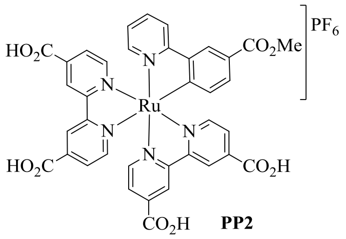

PP2

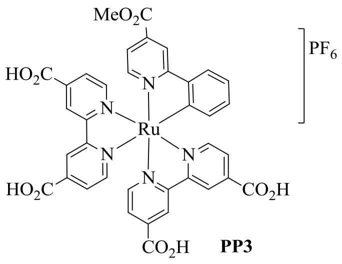

PP3

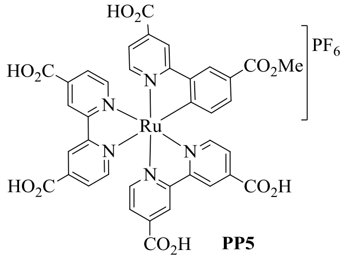

PP5

1.3.4 To study the photophysical and electrochemical properties of ruthenium(II) complexes

1.3.5 To fabricate and investigate the DSSCs devices using ruthenium(II) complexes

CHAPTER 2

LITERATURE REVIEWS

A dye-sensitized solar cell based on ruthenium sensitizers has studied intensively due to its high cell performance. At present, DSSCs have achieved remarkable conversion efficiencies over 11% under AM 1.5 which photon to current conversion efficiency (IPCE) was obtained 80% at 450 - 600 nm. Several groups have successfully developed efficient of ruthenium sensitizers by introducing extended conjugation units, using co-sensitization and thiocyanate free ruthenium complexes to improve the light-harvesting efficiency *via* an enhanced absorption coefficient, the stability of the solar cell and long term efficiency.

2.1 Co-sensitization

Basically, there is a single sensitizer shows a specific absorption covering a wide ranges from visible to IR region. Therefore, co-sensitizer with a dye combination of two or more can solve this problem.

Kuang et al. reported the photovoltaic performance of organic dyes with two dyes (**SQ1** and **JK2**). The current-voltage characteristics and structure of **SQ1** and **JK2** are shown in the Figure 2.1. They found that the co-dyes show efficiency value about 6.28% compared with **SQ1** (3.78%) and **JK2** (6.02%) [18].

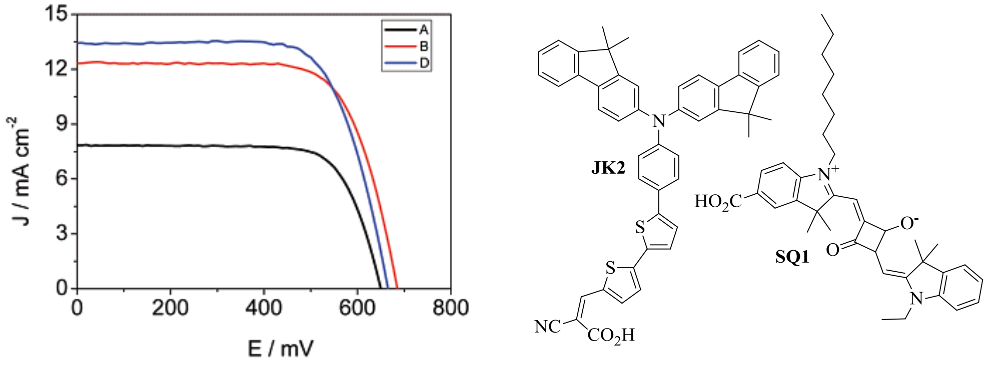

Figure 2.1 The current density-voltage characteristics of DSSCs device, A (SQ1), B (JK2) and D (co-sensitization of SQ1+JK2)

Lin et al. also reported the co-dyes (**JD1+SQ2**). The **JD1** dye has a molar absorption coefficient of 38,500 $M^{-1}cm^{-1}$ and show a maximum IPCE higher than 75% between the wavelengths of 400 and 600 nm. **SQ2** dye has high molar absorption coefficient of 319,000 $M^{-1}cm^{-1}$ and an absorption maximum at 662 nm. The UV-visible absorption spectra characteristics of **JD1**, **SQ2** and co-dyes are shown in Figure 2.2. They found that the 6:4 molar ratio of **JD1+SQ2** show efficiency value about 6.36% compared with **JD1** (5.44%) and **SQ2** (4.11%) [19].

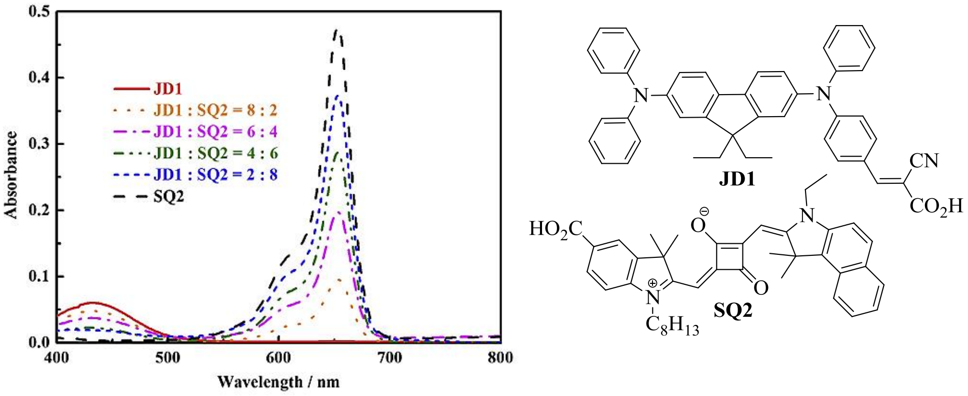

Figure 2.2 **The absorption spectra of dyes solution (JD1, SQ2 and co-sensitizers at different molar ratios)**

Yu et al. synthesized zinc phthalocyanine (**Zn-tri-PcNc-1**) which combined D-π-A triarylamine-bithiophene-cyanoacrylate (**DH-44**) for co-sensitized solar cell. The IPCE curves and structure of **Zn-tri-PcNc-1** and **DH-44** are shown in Figure 2.3.

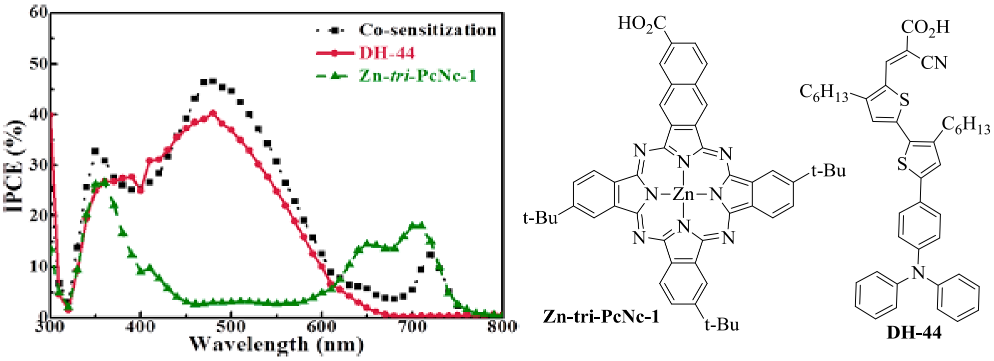

Figure 2.3 **The incident light harvesting efficiency of dyes; Zn-tri-PcNc-1, DH-44 and co-sensitization**

The resulting co-sensitization of **Zn-tri-PcNc-1+DH-44** showed complementary absorption spectra in the range of 320 - 750 nm. The co-dye shows power conversion efficiency of 6.61% with compared **Zn-tri-PcNc-1** (2.38%) and **DH-44** (5.16%) [20].

Singh et al. studied the amphiphilic heteroleptic ruthenium complex sensitizer (**Ru dye**) co-adsorbed with organic dye (**Y3**) for DSSCs. They found that the device of **Ru dye+Y3** show high power conversion efficiency about 6.29% more than **Ru dye** (5.21%) and **Y3** (3.30%) [21]. The absorption spectra and structures of **Ru dye** and **Y3** are shown in Figure 2.4.

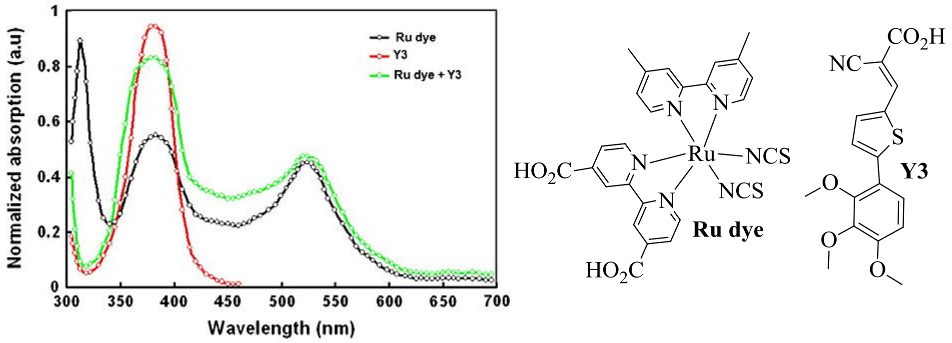

Figure 2.4 Normalized absorption spectra of Ru dye, Y3 and Ru dye+Y3

Ogura et al. reported the efficiency of co-dyes (**black dye+D131**). They found that the device of multiple dye system showed high IPCE, in Figure 2.5. The multiple dye showed high power conversion efficiency about 11.00% more than **black dye** (10.04%) and **D131** (5.06%) [22].

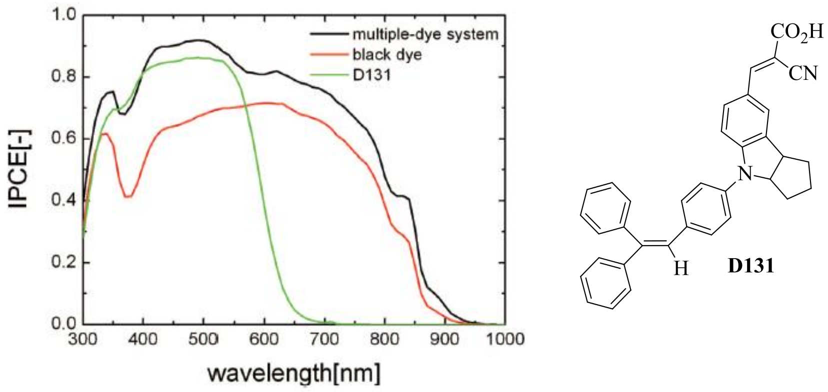

Figure 2.5 The IPCE of multiple-dyes system, black dye and D131

Shi et al. studied ruthenium(II) complex (**XS49**) for DSSC. The **XS49** dye shows high molar absorption coefficient and power conversion efficiency at 7.12%. Moreover, the co-dyes (**XS49+MXD1**) were fabricated using 2 processes; simultaneous (a) and the sequential adsorption (b), in Figure 2.6. The result showed that the sequential adsorptions gave a better result than the simultaneous process with power conversion efficiency about 8.16% [23].

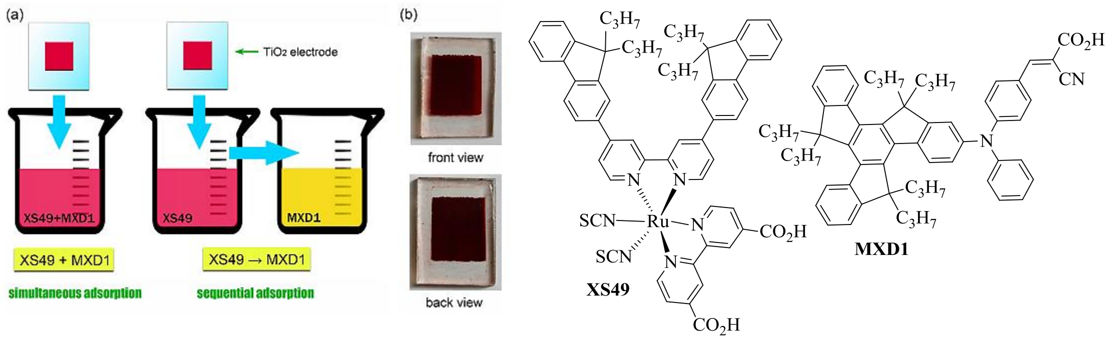

Figure 2.6 Typical process of the simultaneous adsorption and the sequential adsorption; (b) the front and back view of TiO_2 film stained in XS49 for 12 h

Ranasinghe et al. also reported the photovoltaic performance of co-dyes (**N719+black dye**). They found that the co-dyes show efficiency 4.60% with compered **N719** (3.80%) and **black dye** (3.00%), in Figure 2.7 [24].

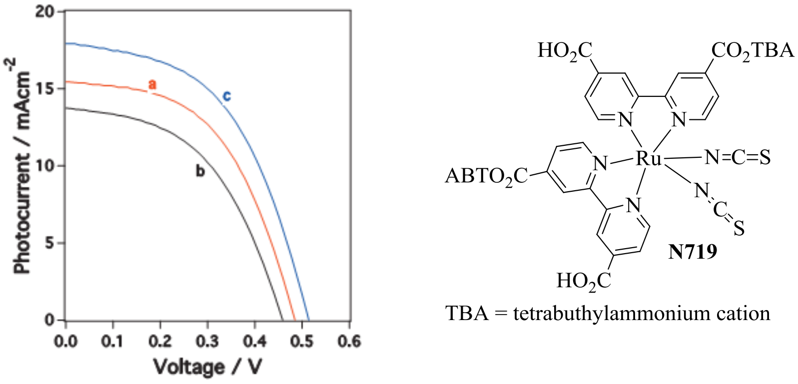

TBA = tetrabuthylammonium cation

Figure 2.7 The current density-voltage characteristics of DSSCs device of (a) N719, (b) black dye and (c) N719+black dye in 1:1 mixture of *t*-butanol and acetonitrile solution

2.2 Thiocyanate free ruthenium(II) complex

In spite of the efficiency, DSSCs needs to be improved the power conversion efficiency with the increasing of UV-Vis absorption, enhancing of the light harvesting ability and a red shifted of the MLCT. Thiocyanate free ruthenium(II) complex can improved the efficiency of DSSCs with extending the π-conjugation. The thiocyanate ligand was replaced with C^N ligand. Therefore, thiocyanate free ruthenium(II) complexes can enhance the optical properties and increase the power conversion efficiencies. Furthermore, the C^N ligand is a bidentate ligand which can coordinate to the ruthenium stronger than a thiocyanate monodentate ligand.

Siu et al. synthesized ruthenium complexes (**D1-D4**) which combines thiazole, benzothiazole, carbazole and triphenylamine (Figure 2.8). The C^N ligands are strong electron donating which extend the π-electron delocalization to improve the absorption spectral coverage and molar extinction coefficient. The result showed that the **D3** dye showed highest power conversion efficiency of 2.98% under AM 1.5, with a J_{SC} = 6.25 mA/cm^2, V_{OC} = 0.659 V and fill factor = 0.724. It was found that the performance efficiency correlate with the molar extinction coefficient of the dyes [25].

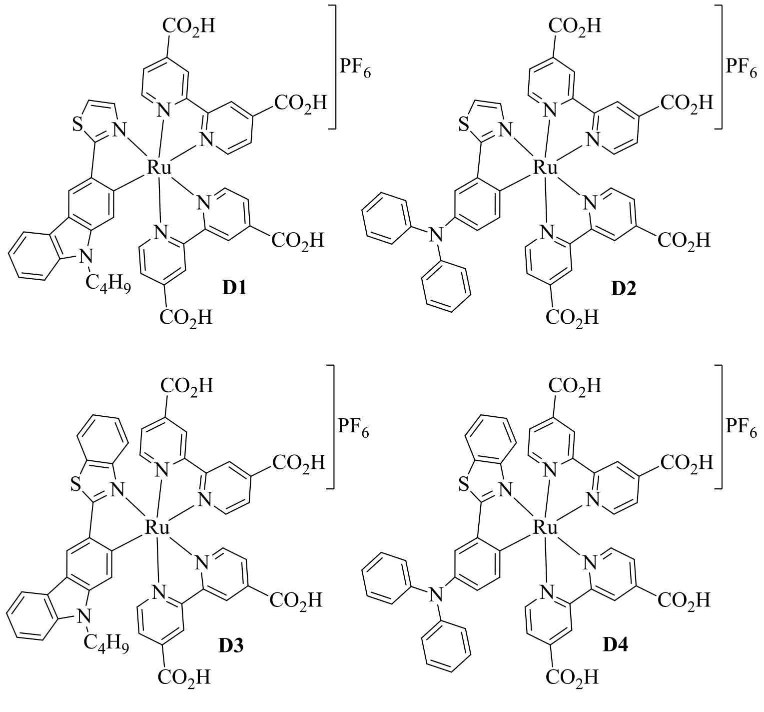

Figure 2.8 Chemical structures of ruthenium(II) complexes; D1-D4

Dragonetti et al. studied thiocyanate free ruthenium complexes which is a pyrid-2-yltetrazolate (**Tetrazpy**) ligand, in Figure 2.9. The UV-visible absorption spectrum showed three absorption bands in the visible region. The sensitizer shows power conversion efficiency of 3% (J_{SC} = 7.6 mA/cm^2, V_{OC} = 0.60 V and FF = 0.65) [26].

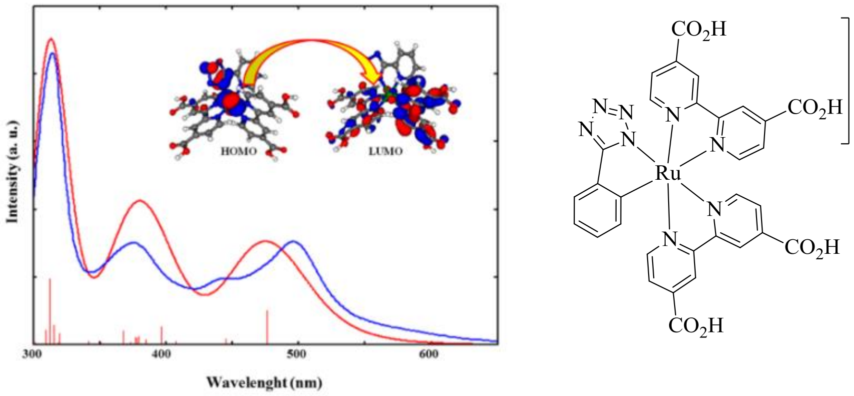

Figure 2.9 Computed (red lines) and experimental (blue lines), UV-Vis spectra of ruthenium dye with a tetrazpy ligand in DMSO

Singh et al. reported thiocyanate free ruthenium complex (**H1S1**) for solar cells, in Figure 2.10. The **H1S1** dye shows broad absorption spectrum. It was found that the power conversion efficiency of 4.76% (J_{SC} = 11.21 mA/cm^2, V_{OC} = 0.62 V and FF = 0.68) obtained under standard AM 1.5 [27].

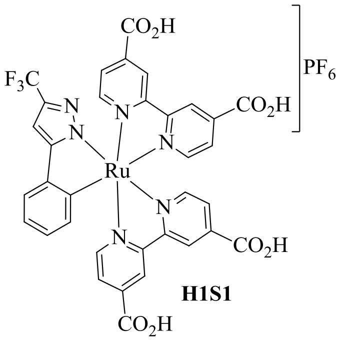

Figure 2.10 Chemical structure of bis(4,4'-dicarboxy-2,2'-bipyridine) 5-phenyl-3-(trifluoromethyl)-1H-pyrazole ruthenium(II)

Funaki et al. reported the thiocyanate free cyclometalated ruthenium(II) complexes (**FT22** and **FT61**). They found that the maxima absorption of complexes show red shifted more than **N719** (Figure 2.11). The **FT22** and **FT61** dyes gave the power conversion efficiency of 3.8% and 5.5%, respectively with compared **N719** (7.4%) [28].

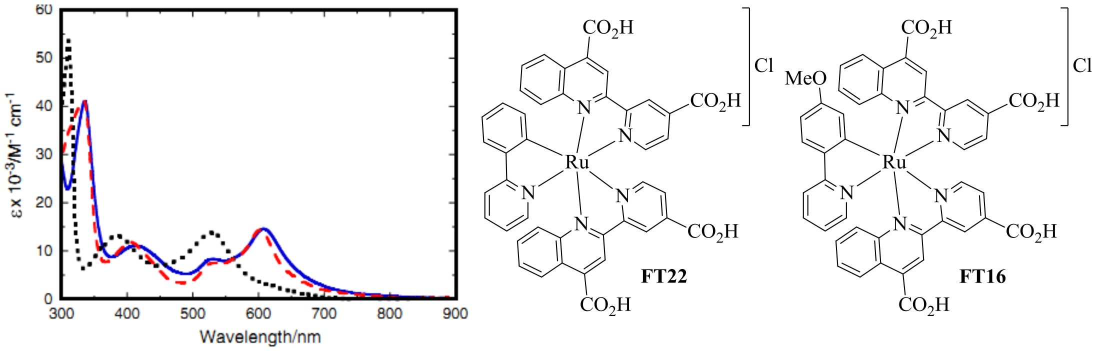

FT22 **FT16**

Figure 2.11 The absorption spectra and chemical structures of FT22 and FT16

Dragonetti et al. studies thiocyanate free cyclometallated ruthenium complex, [Ru(dFppyCF$_3$)(dcbpy)$_2$]PF$_6$; where **dcbpy** is 2,2'-bipyridine-4,4'-dicarboxylic acid and dFppyCF$_3$ is 2-(2,4-difluorophenyl)-5-trifluoromethylpyridine (Figure 2.12). The complex was synthesized and used as photosensitizer in DSSC. They found that the complex showed the power conversion efficiency of 3.7% [29].

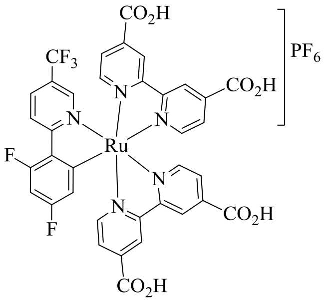

Figure 2.12 Chemical structure of [Ru(dFppyCF$_3$)(dcbpy)$_2$]

Schott et al. reported the theoretical calculations. They studied the influence of electron-donor and electron acceptor in ruthenium complexes by using ZORA-SO, in Figure 2.13. It was found the -CO$_2$H group was a suitable for covalent interactions with TiO$_2$ nanoparticles [30].

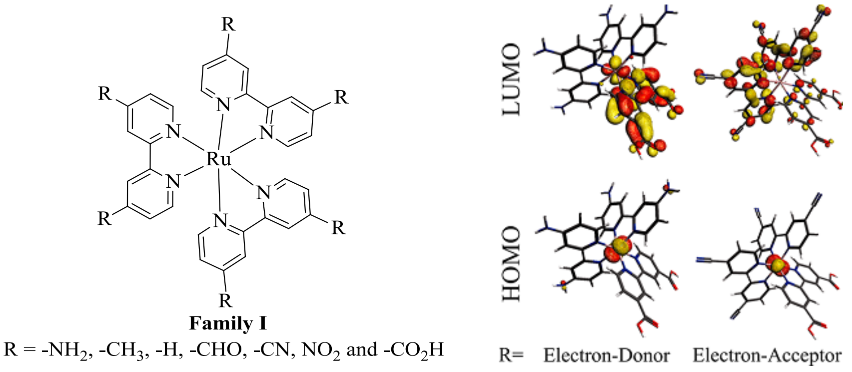

Figure 2.13 Chemical structures of the ruthenium complexes; Family I

Bomben et al. developed of ruthenium complexes containing of the -CO_2H substituents in C^N ligands (**5a** and **5b**) shown in Figure 2.14 (right). The complexes can absorb the sun light from 350 - 700 nm. They studied the molecular orbital calculations with the local density approximation, in Figure 2.14 (left) [31]. They found that the electron distribution of HOMO and LUMO are the ruthenium metal unit and ligand with carboxylic acid group, respectively.

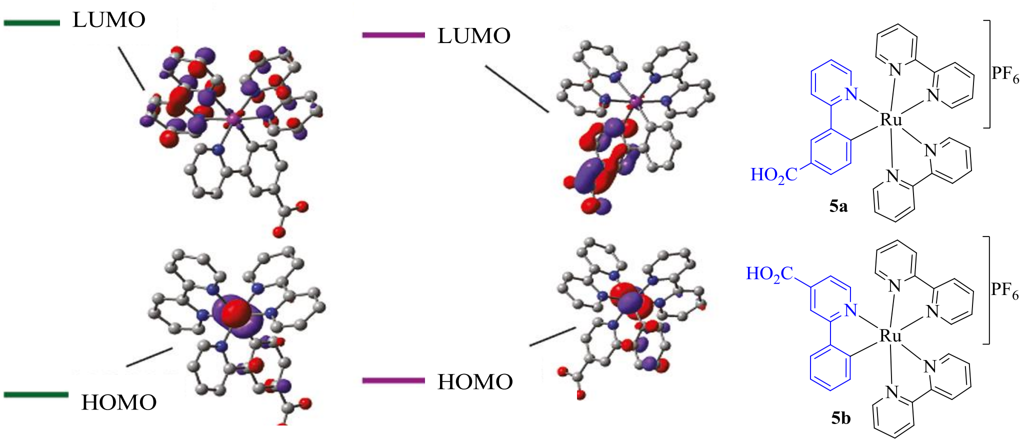

Figure 2.14 The molecular orbitals and chemical structures of 5a and 5b [31]

Bomben et al. reported the ruthenium complexes (**1-5**) by varying the position of the -NO_2 groups (Figure 2.15). They found that the complex **3** shows highest molar extinction coefficients (ε) because the meta -NO_2 group lead to enhanced π-electron conjugation while the complex **2** and **4** shows less ε more than **3** due to the steric interactions [32].

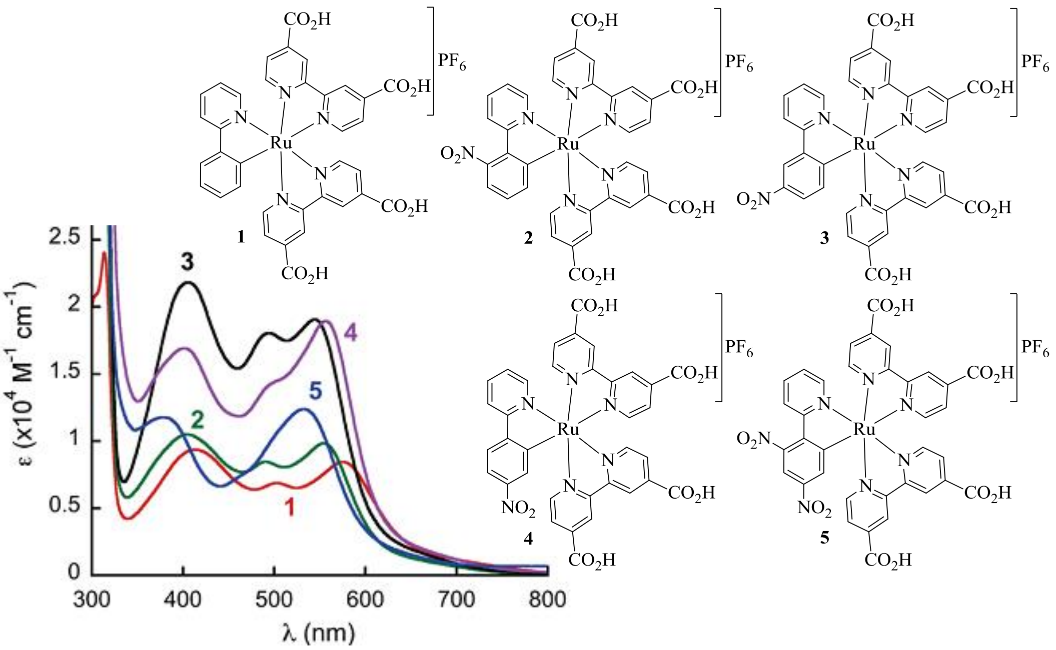

Figure 2.15 The absorption spectra for the -NO_2 series 1-5 which contain aromatic substituents

Ocakoglu et al. reported the tris(4,4'-dicarboxy-2,2'-bipyridyl)ruthenium complex (**K303**). The UV-visible spectrum shows broad absorption bands between 430 - 600 nm due to MLCT band. The photo to electrical conversion efficiency of **K303** was obtained at 6.33% (J_{SC} = 19.58 mA/cm^2, V_{OC} = 570 mV and FF = 0.58) [33]. Moreover, they studied the calculation of HOMO and LUMO energy levels of **K303** (Figure. 2.16).

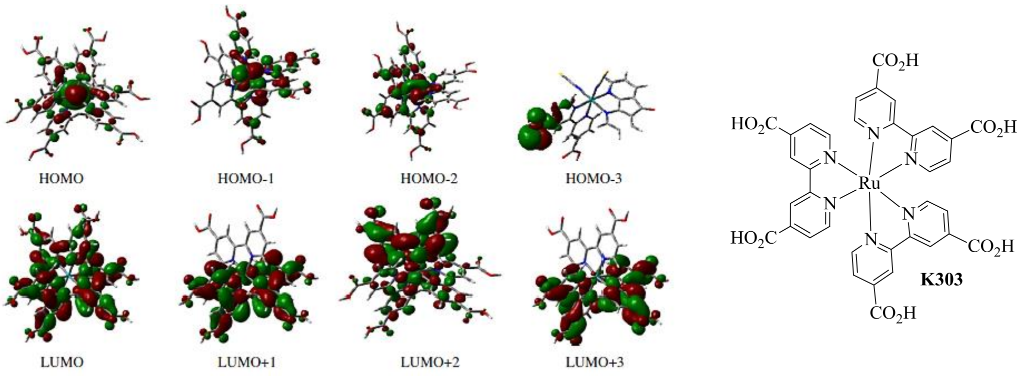

Figure 2.16 Schematic representation of the molecular orbitals obtained from DFT (B3LYP/LANL2DZ) method [33] and chemical structure of K303

Huang et al. designed and synthesized thiocyanate free ruthenium(II) complexes (**D-bisCF$_3$**, **D-CF$_3$**, **D-OMe** and **D-DPA**). The device based on **D-CF$_3$** showed the best performance at 8.74% compared with **N719** (8.70%) [34]. Furthermore, they studied the long-term stability of DSSCs. It was found that the overall efficiency of **D-bisCF$_3$** slightly decreases from 5.45% to 5.14% and remains at 94% of the initial value while the **D-CF$_3$** decrease of from 7.52% to 6.85% under 100 mW/cm^2 light soaking at 60 °C for 400 hours (Figure 2.17).

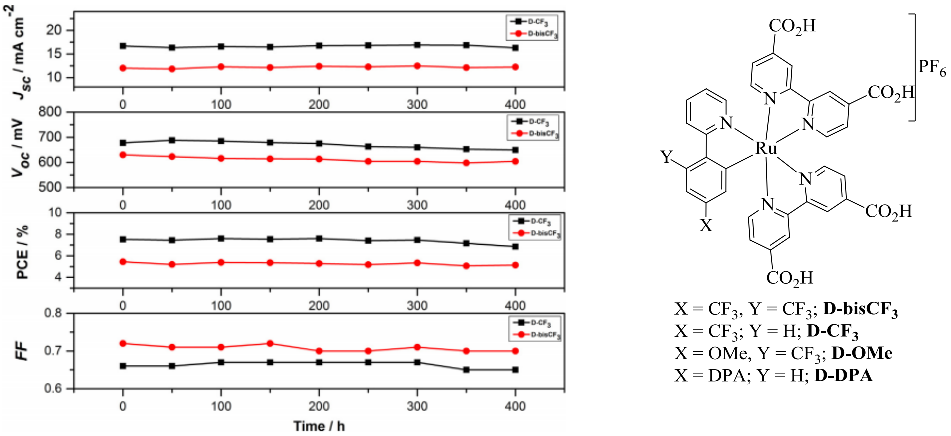

X = CF$_3$, Y = CF$_3$; **D-bisCF$_3$**
X = CF$_3$; Y = H; **D-CF$_3$**
X = OMe, Y = CF$_3$; **D-OMe**
X = DPA; Y = H; **D-DPA**

Figure 2.17 Variations of photovoltaic parameters (η, J_{SC}, V_{OC}, and FF) with aging time for DSSC devices based on D-bisCF$_3$ and D-CF$_3$ under AM 1.5 light soaking at 60 °C

CHAPTER 3

EXPERIMENTAL

3.1 Chemicals

All the chemicals used in this synthesis part are shown in Table 3.1.

Table 3.1 Chemicals for the synthesis

Chemicals	Formula	Grade	Manufacturer
Acetonitrile	CH_3CN	ACS-for analysis	CARLO ERBA
Acetone	CH_3COCH_3	Commercial	CARLO ERBA
Alpha-phellandrene	$C_{10}H_{16}$	AR	SAFE
Ammonium thiocyanate	NH_4SCN	99%	ACROS
2-Bromopyridine	C_5H_4BrN	99%	ACROS
1 M Tetrabutylammonium hydroxide in methanol	$(C_4H_9)_4NOH$	AR	ACROS
4,4'-Dimethyl-2,2'-bipyridine	$C_{12}H_{12}N_2$	99%	ACROS
4,4'-Dicarboxy-2,2'-biquinoline	$C_{20}H_{12}N_2O_4$	99% (TLC)	SIGMA-ALDRICH
Chloroform-d	$CDCl_3$	D, 99.8%, 1% v/v TMS	SIGMA-ALDRICH
Dichloromethane	CH_2Cl_2	Commercial	CARLO ERBA
2-Chloropyridine	C_5H_4ClN	99%	ACROS
2-Chloroisonicotinic acid	$C_6H_4ClNO_2$	97%	MAYBRIDGE
Ethanol	CH_3CH_2OH	ACS-for analysis	CARLO ERBA
Diethyl ether stabilized	$(CH_3CH_2)_2O$	AR	PANREAC
Ethyl acetate	$C_4H_8O_2$	Commercial	CARLO ERBA
Ferrocene	$C_{10}H_{10}Fe$	98%	ACROS
Hexane	C_6H_{14}	Commercial	CARLO ERBA

Table 3.1 Chemicals for the synthesis (continued)

Chemicals	Formula	Grade	Manufacturer
Hydrochloric acid	HCl	37%, for analysis	CARLO ERBA
Methanol	CH_3OH	Commercial and AR	CARLO ERBA
Methanol-d_4	CD_3OD	D, 99.8%	Cambridge isotope laboratories
N,N'-Dimethylformamide	$HCON(CH_3)_2$	ACS-for analysis	CARLO ERBA
Dimethyl sulfoxide-d_6	$(CD_3)_2SO$	D, 99.9%	SIGMA-ALDRICH
3-Methoxycarbonyl-phenylboronic acid	$C_8H_9BO_4$	97%	ACROS
Nitric acid	HNO_3	65% Pro analysis	MERCK
1,4-Dioxane	$C_4H_8O_2$	AR	CARLO ERBA
Phenylboronic acid	$C_6H_5B(OH)_2$	98%	ACROS
Potassium hexafluorophosphate	KPF_6	99%, extra pure	ACROS
Potassium permanganate	$KMnO_4$	AR	CARLO ERBA
Ruthenium(III) chloride hydrate	$RuCl_3.xH_2O$	Hygroscopic	Pressure chem.Co.
Sodium dichromate	Na_2CrO_7	99.5%	Aldrich
Sodium hydroxide	$NaOH$	ACS- for analysis	CARLO ERBA
Sodium sulfate	Na_2SO_4	ACS- for analysis	CARLO ERBA
Sulfuric acid	H_2SO_4	96%	CARLO ERBA

3.2 Chemicals for DSSCs devices fabrication

The chemical used for DSSCs fabrication are listed in Table 3.2.

Table 3.2 Chemicals for the devices fabrication

Chemicals	Formula	Grade	Manufacturer
Isopropanol	C_3H_8O	ACS-for analysis	CARLO ERBA
(Cis-bis (isothiocyanato) bis (2,2'-bipyridyl-4,4'-dicarboxylato) ruthenium(II) bis(tetrabutylammonium) (**N719**)	$C_{58}H_{86}N_8O_8$-RuS_2	95% NMR	Dyesol
Chloroplatinic acid	H_2PtCl_6	40% Pt	ACROS
Lithium iodide	LiI	99%, pure analysis	ACROS
3-Methoxy ethanol	$C_3H_8O_2$	99.8% anhydrous	CARLO ERBA
Tetra propyl ammonium iodine	$C_{12}H_{28}NI$	98%	ACROS
Titanium(IV) oxide	TiO_2	Ti-nanoxide 20T/SP, D/SP	Solaronix
Titanium(IV) oxide	TiO_2	Ti-Nanoxid R/SP	Solaronix
Titanium tetrachloride	$TiCl_4$	0.09 M in 20% HCl	Sigma-Aldrich
4-Tertbutyl pyridine (TBP)	$C_9H_{13}N$	96%	ACROS
Valernitrile	$CH_3(CH_2)_3CN$	98%	ACROS

3.3 Instruments and general chemical characterization techniques

The FTIR spectra were recorded by attenuated total reflectance (ATR) technique using neat sample with a Perkin-Elmer Spectrum RX.I one Fourier transform infrared spectrophotometer over the 550 - 4000 cm^{-1}. The data of FTIR spectra are reported as follows: frequency (cm^{-1}).

UV-Visible spectra were recorded in a 1 cm path length quartz cell using a UV-2600 spectrophotometer high resolution. The samples were dissolved in ethanol and diluted to a concentration of 4 - 5×10^{-5} M.

^{1}H and ^{13}C NMR spectra were performed in $CDCl_3$, DMSO-d_6 or CD_3OD recorded on Bruker AVANCE 300 MHz spectrometer, using TMS as the internal reference. Data for NMR spectra are reported as followed: chemical shift (δ ppm), multiplicity, coupling constant (J) (Hz) and integration.

Cyclic voltammetry was conducted on a Autolab Metrohm PG11. The 1×10^{-3} M solutions of the corresponding complexes were prepared in DMF containing 0.1 M tetrabutylammonium hexafluorophosphate (Bu_4NPF_6) as supporting electrolyte and purged with argon gas for 30 min prior to use at a scan rate of 100 mV/s at room temperature. The working electrode was a glassy carbon electrode. The auxiliary electrode was a Pt electrode and Ag^+/AgCl (3 M KCl) electrode was used as reference electrode.

Molecular weight of ligands and ruthenium(II) complexes were measured by the high resolution mass spectra were recorded employing the time of flight (TOF) mode on a Bruker MicroTOF model by electrospray ionization techniques (ESI).

3.4 Experimental section

This experimental section describe the synthesis of the ruthenium(II) complexes. The organization of this thesis can be divided into two main parts, which are; 1) investigate the performance of co-sensitization from a combination of ruthenium complexes and 2) study the performance of a new thiocyanate free ruthenium complexes. The ligands and the complexes were synthesized and characterized by ^{1}H, ^{13}C NMR, FTIR and mass technique. Then, the photophysical and electrochemical of complexes were studied. For the photovoltaic performance of DSSCs, the co-dyes and thiocyanate free ruthenium complexes were tested under a standard AM 1.5.

The overall experimental flow chart is shown in Figure 3.1.

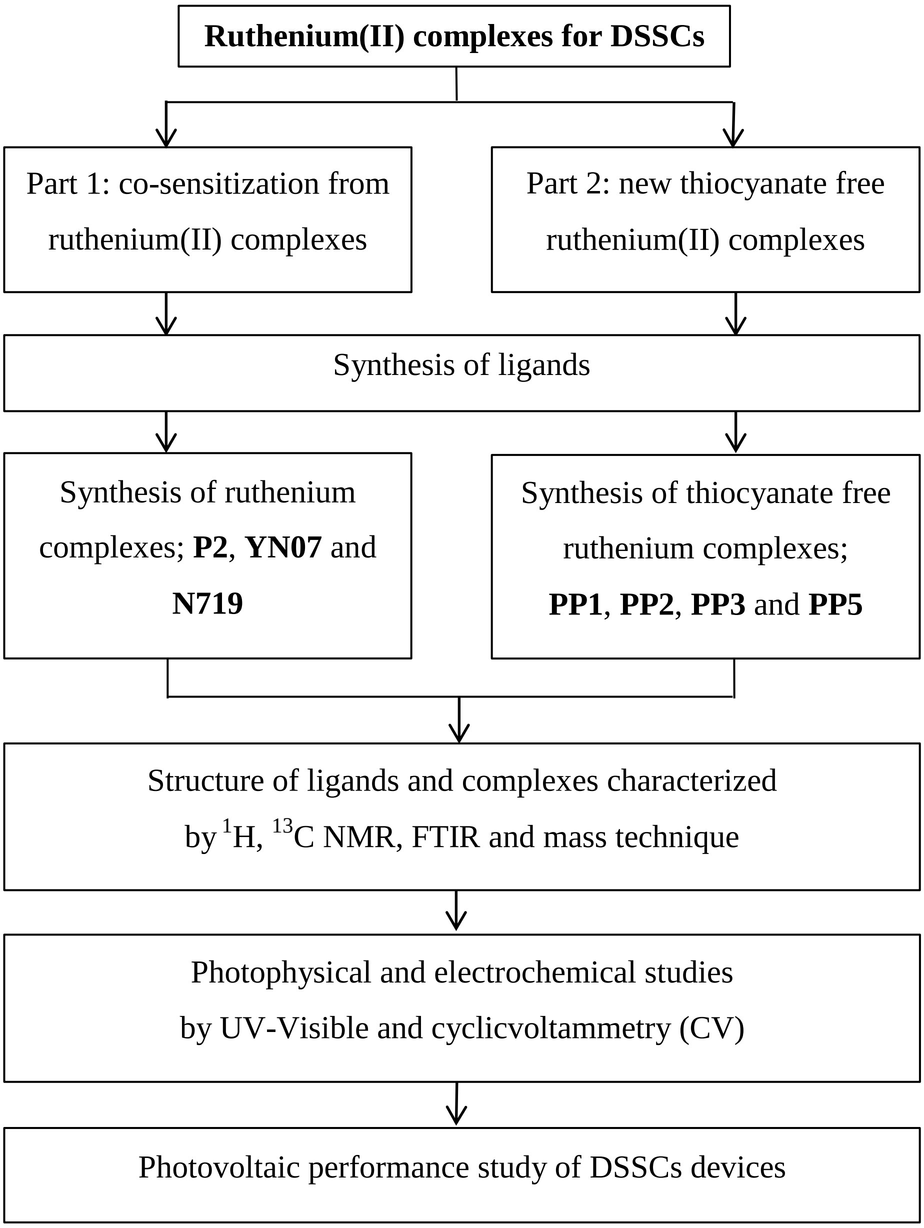

Figure 3.1 Experimental chart model of this work

Generally, the common ruthenium(II) complexes sensitizers can be synthesized by two method.

In the thesis, thiocyanate ruthenium(II) complexes **YN07** and **N719** were synthesized form one-pot reaction *via* the reaction of ruthenium dimer with N^N ligands and NH_4SCN, respectively.

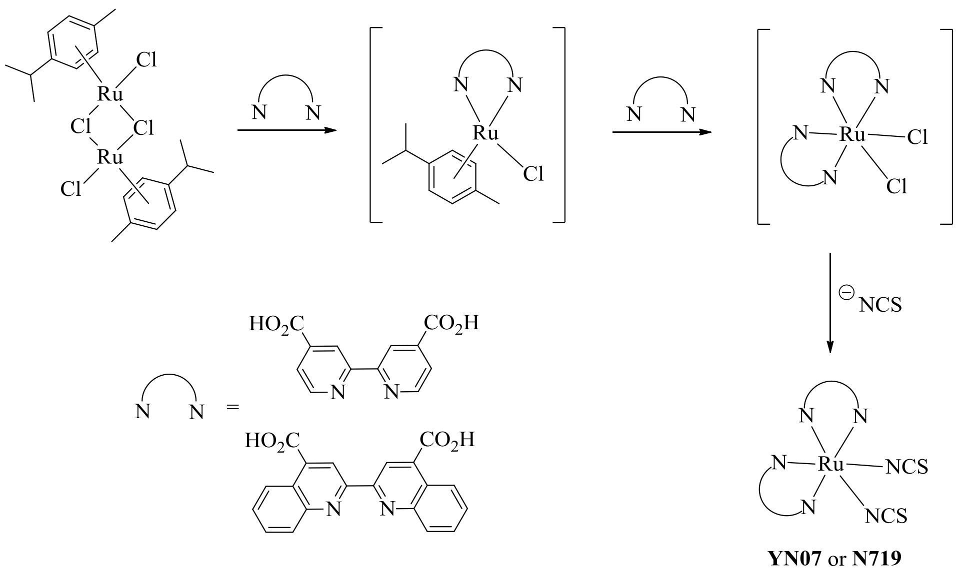

The thiocyanate free ruthenium(II) complex can be synthesized by two steps *via* the reaction of the ruthenium dimer with the corresponding ligands (step 1) to yield the ruthenium intermediates, followed by the addition of N^N ligand to afford the target complex (step 2).

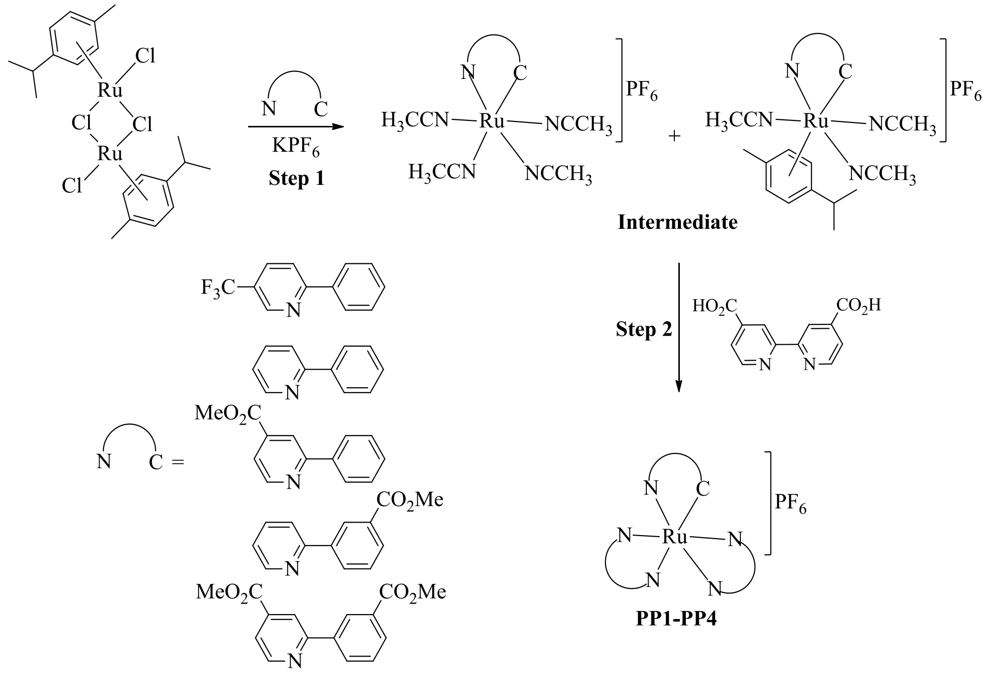

3.4.1 Co-sensitization of ruthenium(II) complexes

3.4.1.1 Synthesis and characterization of 2,2'-bipyridine-4,4'-dicarboxylic acid (**dcbpy**)

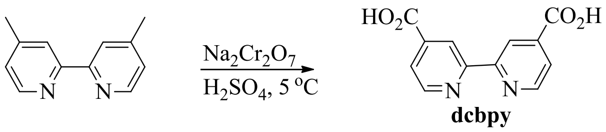

By using a similar procedure as used for the synthesis of **dcbpy** [35] using 25 ml of conc. H_2SO_4 and $Na_2Cr_2O_7$ (1.35 g, 8.69 mmol) were added in 100 ml round bottom flask. During the vigorous stirring, the 4,4'-dimethyl-2,2'-bipyridine (0.40 g, 2.17 mmol) was slowly added for 30 min (color changed from red to green) and then poured the mixture solution into 200 ml ice water and kept at 5 °C for 1 h. The yellow precipitate was filtered and then washed with ice water (10 ml × 3). The obtained yellow solid was dissolved with 25% NaOH and acidified with conc. HCl until a precipitate was formed. The solid portion was isolated and washed with ice water to afford a white solid product (0.32 g, 60%); ^{1}H NMR (300 MHz, DMSO-d_6) δ 8.90 (d, J = 4.7 Hz, 2H), 8.83 (s, 2H), 7.90 (d, J = 4.4 Hz, 2H); ^{13}C NMR (75 MHz, DMSO-D_6) δ 166.4, 155.9, 151.1, 139.0, 120.0, 119.8; ATR-FTIR (neat) 3113, 2491, 1708, 1562, 1458, 1364, 1284, 1238, 1011, 763, 680 cm^{-1}; MS (ESI$^+$) m/z calcd for $C_{12}H_6N_2O_4$ [M^+-$2H^+$] 242. 0328, found 242.2855.

3.4.1.2 Synthesis and characterization of ruthenium complexes

1) Synthesized of di-μ-chlorobis[(η^6-benzene)dichlororuthenium (**Ru-cymene**)

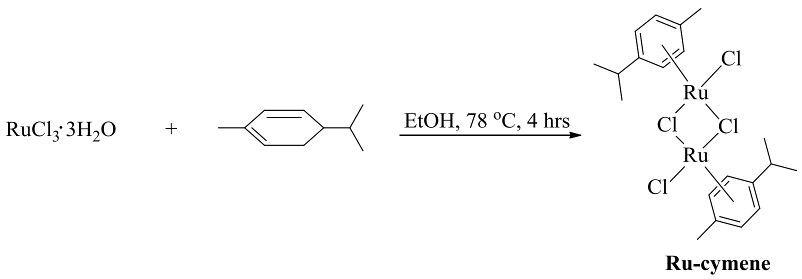

By using a similar procedure as used for the synthesis of **Ru-cymene** [36] using ruthenium(III) trichloride trihydrated (1.0129 g, 3.88 mmol), α-phellandrene (5 ml, 30 mmol) and 12 ml of ethanol were added in round bottom flask. The reaction mixture was refluxed at 78 °C for 4 hours. After the solvent was removed by rotary evaporator, filtered and washed the precipitate product with hexane. The product was obtained as the orange solid (1.0350 g, 45%); ^{1}H NMR (300 MHz, $CDCl_3$) δ 5.48 (d, J = 5.5 Hz, 4H), 5.34 (d, J = 5.4 Hz, 4H), 3.01 - 2.81 (m, 2H), 2.16 (s, 6H), 1.28 (d, J = 6.8 Hz, 12H); ^{13}C NMR (75 MHz, $CDCl_3$) δ 101.2, 96.7, 81.3, 80.5, 30.6, 22.1, 18.9; ATR-FTIR (neat) 3051, 2959, 2922, 2866, 1446, 386, 1055, 876 cm^{-1}.

2) Synthesized of (2-phenyl-5-(trifluoromethyl)pyrido) bis(2,2'-bipyridine-4,4'-dicarboxylic acid)ruthenium(II) hexafluorophosphate (**P2**)

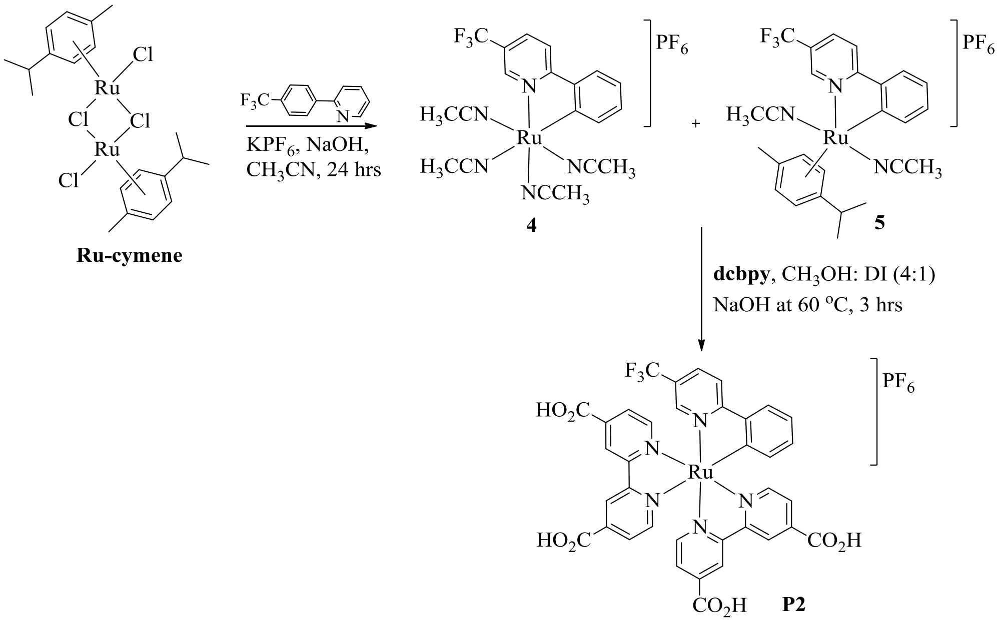

By using a similar procedure as used for the synthesis of **P2** [37] using **Ru-cymene** (0.20 g, 0.33 mmol), 2-phenyl-5-trifluoromethylpyridine (0.15 g, 0.67 mmol), NaOH (0.03 g, 0.75 mmol), KPF_6 (0.24 g, 1.30 mmol) and 5 ml of dried CH_3CN were placed in a 50 ml two necked round bottom flask. The reaction was stirred at 45 °C for 24 hours under N_2. After the reaction completed, the reaction was cooled to room temperature and the solvent was removed by using rotary evaporator under vacuum. The crude solid was filtered by using dichloromethane: acetonitrile (9:1 v/v) solvent through the celite pad to obtain the yellow-green solid mixture intermediate products (**4** and **5**). The product from this step was used without further purification.

Then, the **dcbpy** (0.05 g, 0.20 mmol), NaOH (0.02 g, 0.40 mmol) and 5 ml of CH_3OH: DI (4:1 v/v) were placed in a 50 ml two necked round bottom flask. The reaction was degassed with N_2 balloon for 3 times and was heated at 60 °C for 40 minutes. The intermediate **4** and **5** (0.07 g, 0.11 mmol) were added and continued reflux for 3 hours. The reaction mixture color was changed from yellow-green to dark-purple. After the reaction was completed, the solvent was removed by rotary evaporator. The solid was reconstituted in 40 ml of water, followed by the addition of 0.02 M HNO_3 until the formation of a precipitate was observed. The precipitate was collected on a sintered glass crucible by suction filtration and was washed with water and mix solvent (acetone: diethyl ether) to obtained a target complex. The precipitate was dissolved with methanol, filtrated by sintered glass to collect the solution fraction. The solvent was removed and dried at 80 °C for 24 hours. The **P2** complex was achieved as dark purple solid (0.0424 g, 40%); ^1H NMR (300 MHz,) δ 9.12 (s, 1H), 9.03 (s, 1H), 8.96 (s, 1H), 8.94 (s, 1H), 8.28 (d, J = 8.9 Hz, 1H), 8.19 (d, J = 6.0 Hz, 1H), 8.08 (d, J = 5.6 Hz, 1H), 8.04 - 7.94 (m, J = 7.1, 3.3 Hz, 4H), 7.90 (d, J = 6.2 Hz, 1H), 7.81 - 7.71 (m, 3H), 7.69 (d, J = 1.9 Hz, 1H), 6.97 (dd, J = 11.4, 4.0 Hz, 1H), 6.90 (dd, J = 13.2, 7.1 Hz, 1H), 6.41 (d, J = 6.6 Hz, 1H); ATR-FTIR (neat) 3500 - 2400 (broad), 3437, 3073, 2926, 2855, 1715, 1612, 1325, 1225, 1134, 1008, 769 cm^{-1}; MS (ESI^+) m/z calcd for $C_{36}H_{23}F_3N_5O_8Ru$ [M^+-PF^-_6] 812.0547, found 812.0549.

3) Synthesized of cis[bis(thiocyanato)bis(2,2'-bipyridine-4,4'-dicarboxylic acid)ruthenium(II)] tetrabutylammonium (**N719**)

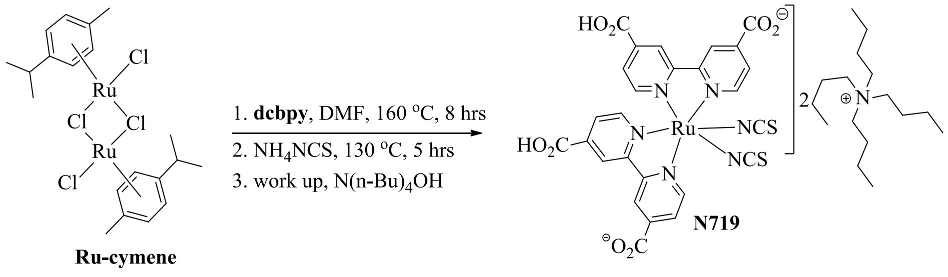

By using a similar procedure as used for the synthesis of **N719** [38] using **Ru-cymene** (0.1602 g, 0.33 mmol), **dcbpy** (0.15 g, 0.63 mmol) and 25 ml of dry DMF were placed in a 100 ml two necked round bottom flask. The solution was refluxed at 160 °C for 8 hours under N_2 balloon in the dark. Next, an excess of NH_4NCS (0.12 g, 1.53 mmol) was added to the resulting dark solution and continued stirring for another 4 hours at 130 °C. The reaction mixture temperature was cooled down to room temperature and the solvent was removed by using rotary evaporator. After that, 40 ml of water was added to induce the precipitate and filtered on a sintered glass crucible, respectively. The solid was washed with water, followed by 1:4 v/v acetone/ diethylether. Next step, the resulting solid was dissolved in 0.1 M tetrabutylammonium hydroxide in methanol to confer solubility by deprotonation of the carboxylic group and purified on a sephadex LH-20 column with methanol as the eluent. In this step, the crude product was collected by using a similar procedure as used for the synthesis of **P2**. The **N719** complex was obtained as dark purple solid (0.0584 g, 60%); ^{1}H NMR (300 MHz, CD_3OD) δ 9.59 (d, J = 5.6 Hz, 1H), 9.07 (s, 1H), 8.91 (s, 1H), 8.31 (d, J = 5.6 Hz, 1H), 7.78 (d, J = 5.6 Hz, 1H), 7.65 (d, J = 5.8 Hz, 1H), 3.28 - 3.19 (m, 8H), 1.76 - 1.43 (m, 8H), 1.41 (m, J = 14.5, 7.3 Hz, 8H), 1.01 (t, J = 7.2 Hz, 12H); ^{13}C NMR (75 MHz, CD_3OD) δ 165.9, 165.4, 159.0, 157.5, 153.4, 153.0, 140.6, 140.0, 134.8, 126.6, 125.7, 123.3, 122.9, 58.0, 23.5, 19.7, 13.6; ATR-FTIR (neat) 3500 - 2400 (broad), 3450, 3084, 2964, 2873, 2098, 1715, 1606, 1408, 1225, 1016.65, 770 cm^{-1}; MS (FAB$^+$) m/z calcd for $C_{33}H_{19}N_5O_8RuS$ [$M^+-(C_4H_9)_4N^+-SCN^-+4H^+$)] 749.7312, found 749.7320.

4) Synthesized of cis[bis(thiocyanato)bis(2,2'- biquinoline-4,4'-dicarboxylic acid(4-carboxy-2,2'-bipyridine-4'-caboxylate)ruthenium(II)] tetrabutylammonium (**YN07**)

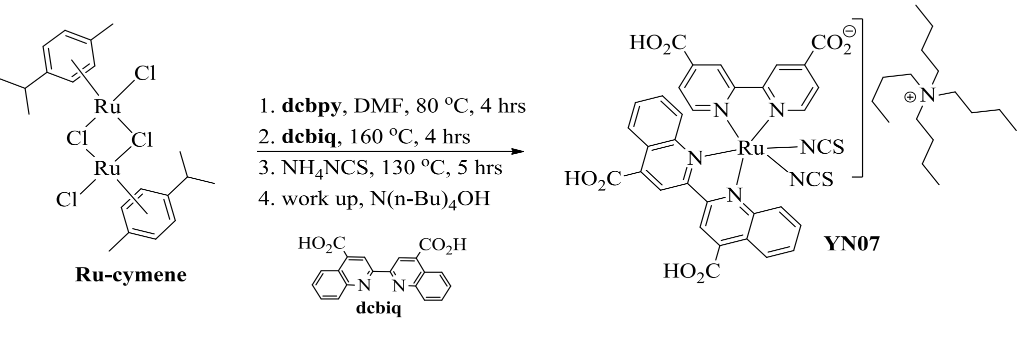

By using a similar procedure as used for the synthesis of **YN07** [39] using **Ru-cymene** (0.1028 g, 0.16 mmol), **dcbpy** (0.0818 g, 0.32 mmol) and 25 ml of dry DMF were placed in a 100 ml two necked round bottom flask. The reaction mixture was stirred at 80 °C for 4 hours under N_2 in the dark. Subsequently, 2,2'-biquinoline-4,4'-dicarboxylic acid (**dcbiq**) (0.1156 g, 0.16 mmol) was added and the reaction mixture was stirred at 160 °C for 4 hours. At last, an excess of NH_4SCN 0.15 g was added to the resulting dark solution and continued stirring for another 4 hours at 130 °C. After that, the crude product was collected by using a similar procedure as used for the synthesis of **N719**. The **YN07** complex was achieved as a green solid (0.0760 g, 70%); ^{1}H NMR (300 MHz, CD_3OD) δ 9.58 (d, J = 5.9 Hz, 1H), 9.23 (d, J = 8.6 Hz, 1H), 9.07 (d, J = 9.1 Hz, 1H), 9.03 - 8.90 (m, 2H), 8.87 (s, 1H), 8.83 (s, 1H), 8.67 (q, J = 6.2 Hz, 1H), 8.32 (d, J = 11.1, 5.3 Hz, 1H), 8.02 - 7.84 (m, J = 10.5, 5.6 Hz, 2H), 7.85 - 7.71 (m, 1H), 7.65 (dd, J = 5.9, 1.9 Hz, 1H), 7.58 - 7.49 (m, 1H), 7.33 - 7.11 (m, 2H), 3.27 - 3.16 (m, 8H), 1.71 - 1.56 (m, J = 11.8, 10.1, 6.1 Hz, 8H), 1.47 - 1.32 (m, 8H), 1.00 (t, J = 7.3 Hz, 12H); ^{13}C NMR (75 MHz, DMSO-d_6): δ 168.1, 167.5, 167.3, 165.6, 165.3, 162.1, 160.3, 159.8, 158.0, 155.3, 154.7, 154.3, 152.1, 151.4, 148.5, 139.7, 139.2, 138.9, 138.8, 137.7, 135.8, 131.6, 131.4, 131.0, 130.6, 130.3, 129.8, 129.4, 127.1, 126.1, 125.3, 124.7, 123.9, 119.7, 57.9, 23.5, 19.3, 13.9; ATR-FTIR (neat) 3500 - 2400 (broad), 3485, 3079, 2964, 2875, 2103, 1715, 1550, 1404, 1224, 1135, 1024, 771 cm^{-1}; MS (ESI$^+$) m/z calcd for $C_{34}H_{20}N_6O_8RuS_2Na$ [M^+-$C_{16}H_{36}N^+$+Na^++H^+] 828.9728, found 828.9761.

3.4.2 The thiocyanate free ruthenium complexes

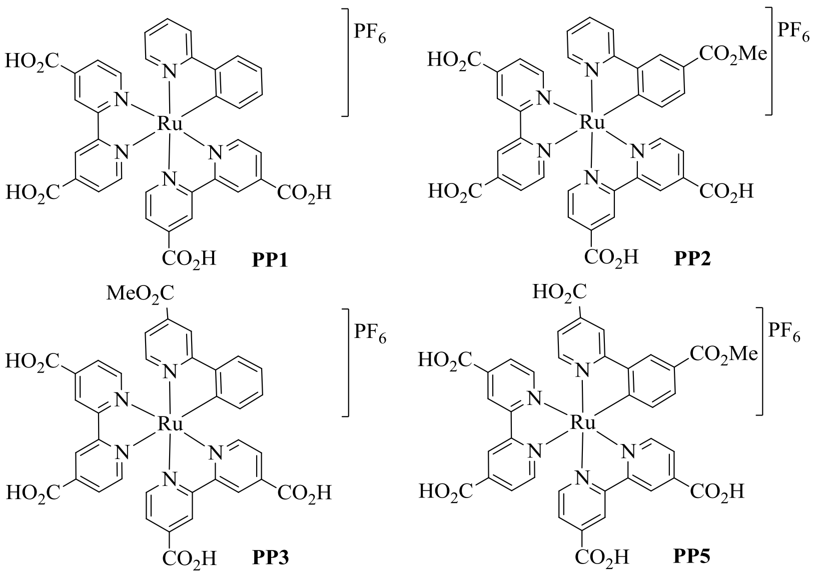

Figure 3.2 Structures of target molecule

3.4.2.1 Synthesis and characterization of C^N ligands

1) Synthesized of methyl 2-chloroisonicotinate

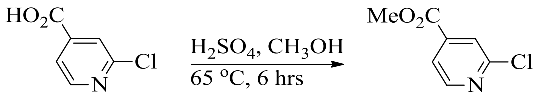

By using a similar procedure as used for the synthesis of 2-chloroisonicotinate [40] using 2-chloroisonicotinic acid (1.0030 g, 6.00 mmol), 10 ml of methanol and 2 ml of conc. H_2SO_4 in 50 ml round bottom flask was heated to reflux at 65 °C for 6 hours. The reaction was cooled to room temperature and extracted into dichloromethane (10 ml × 3 times). The organic fractions were combined and dried over Na_2SO_4 anhydrous and filtered. The crude reaction was evaporated to dryness and then passed through silica column chromatography using 3% (v/v) ethyl acetate: hexane to give the target product as a yellow liquid (0.7515 g, 73%); ^{1}H NMR (300 MHz, $CDCl_3$) δ 8.51 (d, J = 5.0 Hz, 1H), 7.84 (s, 1H), 7.74 (d, J = 5.0 Hz, 1H), 3.94 (s, 3H); ^{13}C NMR (75 MHz, $CDCl_3$) δ 164.2, 152.4, 150.5, 140.2, 124.0, 121.5, 52.9; ATR-FTIR (neat) 3069, 2954, 2849, 1732, 1552, 1435, 1367, 1292, 1268, 1144, 970, 754 cm^{-1}.

2) Synthesized of 2-phenylpyridine (**ppy**)

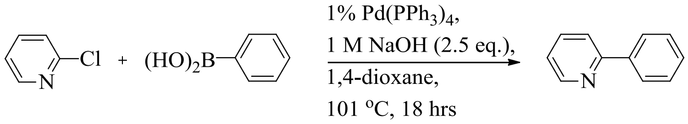

By using a similar procedure as used for the synthesis of **ppy** [41] using 2-chloropyridine (1.1955 g, 3.51 mmol), phenylboronic acid (1.284 g, 3.51 mmol), 1 M NaOH (18 ml, 18.84 mmol) and 25 ml of 1,4-dioxane in 100 ml two neck round bottom flask were degassed with N_2 balloon for 3 times. Then, 1% $Pd(PPh_3)_4$ (0.1218 g, 0.0351 mmol) was added in to a solution. The mixture solution was degassed before refluxed at 101 °C for 18 hours. After being cooled to room temperature, water was added and the mixture was extracted with dichloromethane. The organic fractions were combined and dried over Na_2SO_4 anhydrous and filtered. The solvent was removed by using rotary evaporator. The crude product was purified through silica column chromatography using hexane as eluent to afford **ppy** as a yellow liquid (1.466 g, 90%); ^{1}H NMR (300 MHz, $CDCl_3$) δ 8.69 (d, J = 4.8 Hz, 1H), 7.99 (d, J = 7.4 Hz, 2H), 7.79 - 7.67 (m, 2H), 7.51 - 7.36 (m, 3H), 7.28 - 7.16 (m, J = 7.9, 7.2, 5.0 Hz, 1H); ^{13}C NMR (75 MHz, $CDCl_3$) δ 157.5, 149.6, 139.4, 136.7, 128.9, 128.7, 126.9, 122.0, 120.5; ATR-FTIR (neat) 3060, 3005, 1582, 1467, 1423, 1151, 739, 691 cm^{-1}.

3) Synthesized of 2-phenylpyridine 3-(pyridin-2-yl)benzoate (**PL1**)

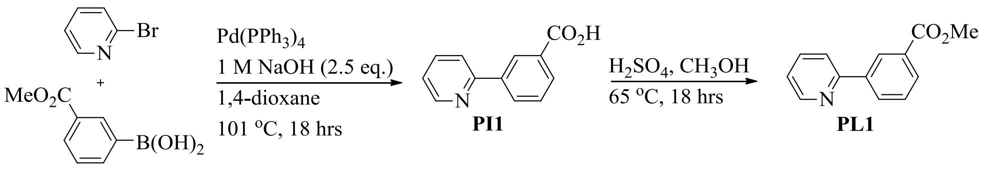

Compound 3-(pyridin-2-yl)benzoic acid (**PI1)** was synthesized a similar procedure as for **ppy** using 2-bromopyridine (0.7770 g, 4.92 mmol), 3-methoxycarbonyl phenylboronic acid (0.9735 g, 5.40 mmol), 1 M NaOH

(12 ml, 12.75 mmol), 25 ml of 1,4-dioxane and 2% $Pd(PPh_3)_4$ (0.1419 g, 0.12 mmol) were refluxed at 101 °C for 18 hours. After the reaction completed, the reaction mixture was extracted into dichloromethane (10 ml × 3 times). The water fractions were combined and acidified with 10 M HCl until a precipitate was formed. The solid was filtered and washed with ice water to achieve **PI1** as a yellow solid (0.7809 g, 80%); ^{1}H NMR (300 MHz, DMSO-d_6) δ 8.69 (d, J = 5.2 Hz, 1H), 8.66 (s, 1H), 8.30 (d, J = 7.9 Hz, 1H), 8.00 (t, J = 8.5 Hz, 2H), 7.90 (t, J = 7.8 Hz, 1H), 7.61 (t, J = 7.7 Hz, 1H), 7.39 (dd, J = 7.2, 5.1 Hz, 1H); ^{13}C NMR (75 MHz, DMSO-d_6) δ 167.6, 150.1, 139.4, 137.9, 131.9, 131.1, 130.2, 129.6, 127.7, 123.5, 120.8; ATR-FTIR (neat) 3000 - 2400 (broad), 3044, 1678, 1592, 1466, 1301, 1269, 1005, 742 cm^{-1}; MS (ESI$^+$) m/z calcd for $C_{12}H_{10}NO_2$ [M$^+$+H$^+$] 200.0712, found 200.0723.

Compound **PL1** was synthesized a similar procedure as for methyl 2-chloroisonicotinate using **PI1** (0.3960 g, 1.20 mmol), 15 ml of methanol and 1 ml of conc. H_2SO_4 were refluxed at 65 °C for 18 hours. The reaction was purified by silica column chromatography using 5% (v/v) ethyl acetate: hexane as eluent to afford **PL1** as a yellow liquid (0.3082 g, 73%); ^{1}H NMR (300 MHz, $CDCl_3$) δ 8.72 (d, J = 5.0 Hz, 1H), 8.64 (s, 1H), 8.24 (d, J = 8.4 Hz, 1H), 8.09 (d, J = 7.8 Hz, 1H), 7.79 (d, J = 4.4 Hz, 2H), 7.56 (t, J = 7.7 Hz, 1H), 7.29 (d, J = 4.8 Hz, 1H), 3.95 (s, 3H); ^{13}C NMR (75 MHz, $CDCl_3$) δ 166.9, 156.3, 149.8, 139.7, 136.8, 131.3, 130.7, 129.9, 128.9, 127.9, 122.5, 120.6, 52.1; ATR-FTIR (neat) 3029, 2951, 2850, 1710, 1558, 1432, 1298, 1248, 1108, 1081, 744 cm^{-1}; MS (ESI$^+$) m/z calcd for $C_{13}H_{12}NO_2$ [M$^+$+H$^+$] 214.0868, found 214.0872.

4) Synthesized of methyl 2-phenylisonicotinate (**PL2**)

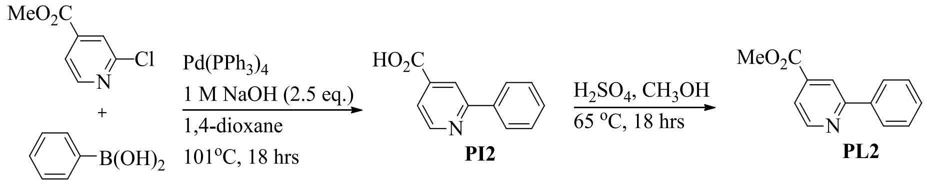

Compound **PL2** was synthesized a similar procedure as for **PL1** using methyl 2-chloroisonicotinate (0.6027 g, 3.51 mmol), phenyl boronic acid (0.4695 g, 3.85 mmol), 1 M NaOH (9 ml, 8.64 mmol), 25 ml of 1,4-dioxane and

1% $Pd(PPh_3)_4$ (0.0380 g, 0.032 mmol) were obtained the intermediate product 2-phenylisonicotinic acid (**PI2)** as yellow solid (0.4920 g, 70%); ^{1}H NMR (300 MHz, DMSO-d_6) δ 8.84 (d, J = 4.8 Hz, 1H), 8.27 (s, 1H), 8.11 (d, J = 7.2 Hz, 2H), 7.76 (d, J = 4.7 Hz, 1H), 7.60 - 7.40 (m, 3H); ^{13}C NMR (75 MHz, DMSO-d_6) δ 166.6, 157.6, 151.1, 139.9, 138.4, 130.0, 129.4, 127.1, 121.9, 119.4; ATR-FTIR (neat) 3090, 2379 (broad), 1712, 1611, 1563, 1403, 1384, 1316, 1228, 1011, 768, 662 cm^{-1}; MS (ESI$^+$) m/z calcd for $C_{12}H_{10}NO_2$ [M$^+$+H$^+$] 200.0712, found 200.0721.

Then, **PI2** (0.4719 g, 2.37 mmol), 10 ml of methanol and 1 ml of conc. H_2SO_4 were refluxed for 18 hours. The **PL2** was afforded as yellow liquid (0.5136 g, 61%); ^{1}H NMR (300 MHz, $CDCl_3$) δ 8.83 (d, J = 5.6 Hz, 1H), 8.29 (s, 1H), 8.05 (dd, J = 8.6, 1.4 Hz, 2H), 7.76 (d, J = 5.4, 1.4 Hz, 1H), 7.56 - 7.37 (m, 3H), 3.98 (s, 3H); ^{13}C NMR (75 MHz, $CDCl_3$) δ 165.7, 158.4, 150.4, 138.5, 138.1, 129.4, 128.8, 126.9, 121.1, 119.6, 52.6; ATR-FTIR (neat) 3004, 2951, 2850, 1728, 1556, 1435, 1394, 1299, 1244, 1118, 756, 728, 689 cm^{-1}.

5) Synthesized of methyl 2-(3-(methoxycarbonyl)phenyl) isonicotinate (**PL3**)

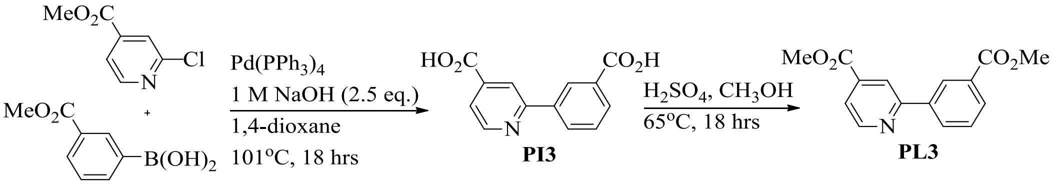

Compound **PL3** was synthesized a similar procedure as for **PL1** using methyl 2-chloroisonicotinate (0.6037 g, 3.52 mmol), 3-methoxycarbonyl phenylboronic acid (0.6937 g, 3.85 mmol), 1 M NaOH (9 ml, 9.42 mmol), 25 ml of 1,4-dioxane and 3% $Pd(PPh_3)_4$ (0.1400 g, 0.12 mmol) were used instead. The 2-(3-carboxyphenyl) isonicotinic acid (**PI3**) was achieved as a yellow solid (0.4490 g, 53%); ^{1}H NMR (300 MHz, DMSO-d_6) δ 8.88 (d, J = 4.9 Hz, 1H), 8.67 (s, 1H), 8.36 (d, J = 8.0 Hz, 1H), 8.33 (s, 1H), 8.03 (d, J = 7.8 Hz, 1H), 7.81 (d, J = 4.9 Hz, 1H), 7.65 (t, J = 7.7 Hz, 1H); ^{13}C NMR (75 MHz, DMSO-d_6) δ 167.5, 166.5, 156.5, 151.3, 140.0, 138.6, 131.9, 131.3, 130.6, 129.8, 127.8, 122.4, 119.5; ATR-FTIR (neat) 3100 - 2300 (broad), 3098, 1679, 1608, 1442, 1306, 1221, 1014, 737, 672 cm^{-1}; (ESI$^+$) m/z calcd for $C_{13}H_{10}NO_4$ [M$^+$+H$^+$] 244.0610, found 244.9618.

Next step, **PI3** (0.2220 g, 0.92 mmol), 10 ml of methanol and 2 ml of conc. H_2SO_4 were heated at 65 °C for 18 hours. The product **PL3** was achieved as white solid (0.1850 g, 75%); ^{1}H NMR (300 MHz, $CDCl_3$) δ 8.86 (d, J = 4.9 Hz, 1H), 8.70 (s, 1H), 8.36 (s, 1H), 8.30 (d, J = 7.8 Hz, 1H), 8.13 (d, J = 7.7 Hz, 1H), 7.82 (d, J = 4.9 Hz, 1H), 7.59 (t, J = 7.8 Hz, 1H), 4.01 (s, 3H), 3.97 (s, 3H); ^{13}C NMR (75 MHz, $CDCl_3$) δ 166.8, 165.6, 157.3, 150.5, 138.8, 138.4, 131.4, 130.9, 130.4, 129.0, 128.0, 121.6, 119.7, 52.7, 52.2; ATR-FTIR (neat) 3029, 2923, 2853, 1726, 1594, 1557, 1432, 1288, 1258, 1118, 950, 749 cm^{-1}; MS (ESI$^+$) m/z calcd for $C_{15}H_{14}NO_4$ [M$^+$+H$^+$] 272.0923, found 272.0924.

3.4.2.2 Synthesis and characterization of thiocyanate free ruthenium(II) complexes

1) Synthesized of [triacetonitrile(η^6-*p*-cymene)(2-phenylpyridine)-ruthenium(II)] hexafluorophosphate (**PI4**)

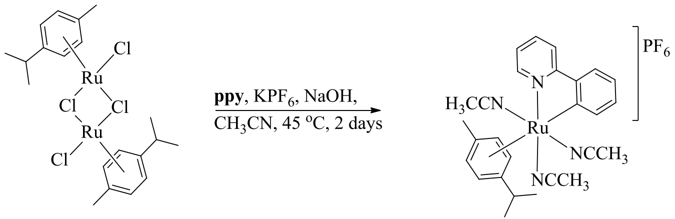

Ru-cymene **PI4**

Compound **PI4** was synthesized a similar procedure as for mixture **4** and **5** [37], [42] using **Ru-cymene** (0.1010 g, 0.16 mmol), **ppy** (0.0690 g, 0.33 mmol), NaOH (0.0190 g, 0.37 mmol), KPF_6 (0.1268 g, 0.66 mmol) and 5 ml of CH_3CN was degassed with N_2 balloon for 3 times, which was then heated at 45 °C for 2 days. The solvent was removed using a rotary evaporator. The crude reaction was purified by silica column chromatography using (2:8 v/v) acetonitrile: dichloromethane as eluent. The first yellow band was isolated and then reconstituted in dichloromethane to afford intermediate **PI4** as a green solid (0.0900 g, 90%); ^{1}H NMR (300 MHz, $CDCl_3$) δ 9.32 (d, J = 5.0 Hz, 1H), 8.05 (d, J = 7.0 Hz, 1H), 7.89 - 7.70 (m, 2H), 7.66 (d, J = 7.3 Hz, 1H), 7.37 - 7.24 (m, 1H), 7.24 - 7.08 (m, 2H), 5.88 (d, *J* = 5.6 Hz, 1H), 5.82 (d, *J* = 5.5 Hz, 1H), 5.69 (d, *J* = 5.5 Hz, 1H), 5.51 (d, *J* = 5.5 Hz, 1H), 2.41 - 2.25 (m, *J* = 13.1, 6.5 Hz, 1H), 2.14 (s, 3H), 2.00 (s, 3H), 1.26 (s, 6H), 0.97 (d, *J* = 6.6 Hz, 3H), 0.84 (d, *J* = 6.3 Hz, 3H); ATR-FTIR (neat) 2922, 2853, 2205, 1645, 1644, 1461, 1375, 831 cm^{-1}; MS (ESI$^+$) m/z calcd for $C_{21}H_{22}NRu$ [M^+-PF^-_6-3(CH_3CN)] 390.0796, found 390.0742.

2) Synthesized of [triacetonitrile(η^6-*p*-cymene)(2-phenylpyridine 3-(pyridin-2-yl)benzoate)ruthenium(II)] hexafluorophosphate (**PI5**)

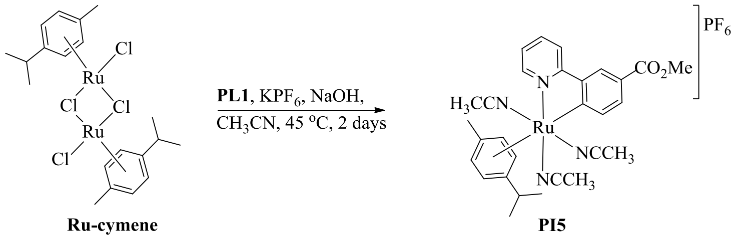

Ru-cymene **PI5**

Compound **PI5** was synthesized a similar procedure as for **PI4** using **Ru-cymene** (0.1025 g, 0.16 mmol), **PL1** (0.0665 g, 0.32 mmol), NaOH (0.0240 g, 0.60 mmol), KPF_6 (0.1255 g, 0.68 mmol) and 5 ml of CH_3CN were used instead. The **PI5** was obtained as green solid (0.0540 g, 47%); ^{1}H NMR (300 MHz, $CDCl_3$) δ 9.34 (d, *J* = 5.9 Hz, 1H), 8.30 (s, 1H), 8.18 (d, *J* = 8.0 Hz, 1H), 7.95 - 7.77 (m, 3H), 7.42 - 7.30 (m, *J* = 8.8, 4.2 Hz, 1H), 5.98 (d, *J* = 6.3 Hz, 1H), 5.84 (d, *J* = 6.2 Hz, 1H), 5.71 (d, *J* = 6.0 Hz, 1H), 5.52 (d, *J* = 5.9 Hz, 1H), 3.94 (s, 3H), 2.36 - 2.27 (m, 1H), 2.15 (s, 3H), 2.05 (s, 3H), 1.25 (s, 6H), 0.91 (dd, *J* = 10.5, 6.9 Hz, 3H), 0.84 (d, *J* = 7.4 Hz, 3H); ATR-FTIR (neat) 2922, 2853, 2278, 1710, 1585, 1459, 1252, 1190, 830 cm^{-1}; MS (ESI$^+$) m/z calcd for $C_{23}H_{24}NO_2Ru$ [M^+-PF^-_6-3(CH_3CN)+H^+] 448.0851, found 448.0829.

3) Synthesized of [triacetonitrile(η^6-*p*-cymene)(methyl-2-phenyl-isonicotinate)ruthenium (II)] hexafluorophosphate (**PI6**)

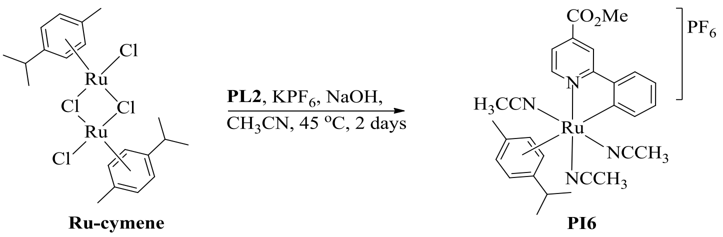

Ru-cymene **PI6**

Compound **PI6** was synthesized a similar procedure as for **PI4** using **Ru-cymene** (0.1011 g, 0.16 mmol), **PL2** (0.0700 g, 0.33 mmol), NaOH (0.0260 g, 0.37 mmol), KPF_6 (0.1300 g, 0.66 mmol) and 5 ml of CH_3CN were used instead. The **PI6** was achieved as a green solid (0.0580 g, 50%); ^1H NMR (300 MHz, $CDCl_3$) δ 9.50 (d, *J* = 6.1 Hz, 1H), 8.29 (s, 1H), 8.05 (d, *J* = 7.3 Hz, 1H), 7.89 - 7.69 (m, 2H), 7.37 - 7.05 (m, 2H), 5.93 (d, *J* = 6.1 Hz, 1H), 5.85 (d, *J* = 6.3 Hz, 1H), 5.73 (d, *J* = 6.3 Hz, 1H), 5.56 (d, *J* = 6.2 Hz, 1H), 4.00 (s, 3H), 2.47 - 2.19 (m, *J* = 17.7, 16.8, 5.5 Hz, 1H), 2.14 (s, 3H), 2.01 (s, 3H), 1.26 (s, 6H), 0.96 (d, *J* = 6.8 Hz, 3H), 0.86 (dd, *J* = 15.8, 7.3 Hz, 3H); ATR-FTIR (neat) 2922, 2853, 2282, 1727, 1612, 1455, 1251, 1114, 829 cm^{-1}; MS (ESI^+) m/z calcd for $C_{2}3H_{2}4NO_{2}Ru$ $[M^+\text{-}PF^-_6\text{-}3(CH_3CN)+H^+]$ 448.0851, found 448.0799.

4) Synthesized of [triacetonitrile(η^6-*p*-cymene)(methyl-2-(3(methoxycarbonyl)phenyl)isonicotinate)ruthenium(II)] hexafluorophosphate (**PI7**)

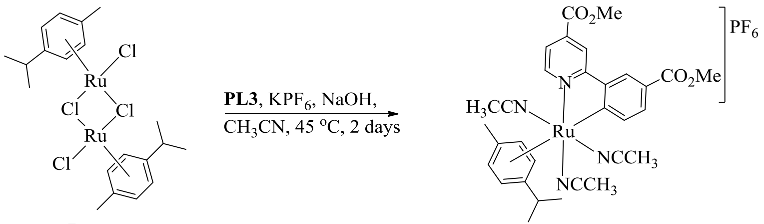

Ru-cymene **PI7**

Compound **PI7** was synthesized a similar procedure as for **PI4** using **Ru-cymene** (0.1028 g, 0.16 mmol), **PL3** (0.0900 g, 0.33 mmol), NaOH (0.0189 g, 0.47 mmol), KPF_6 (0.0980 g, 0.66 mmol) and 5 ml of CH_3CN were used instead. The **PI7** was achieved as green solid (0.0805 g, 65%); ^1H NMR (300 MHz, $CDCl_3$) δ 9.54 (d, *J* = 5.5 Hz, 1H), 8.42 (s, 2H), 8.17 (d, *J* = 7.9 Hz, 1H), 7.87 (d, *J* = 6.3 Hz, 2H), 6.01 (d, *J* = 5.6 Hz, 1H), 5.85 (d, *J* = 5.4 Hz, 1H), 5.80 (d, *J* = 5.8 Hz, 1H), 5.60 (d, *J* = 5.5 Hz, 1H), 4.03 (s, 3H), 3.97 (s, 3H), 2.39 - 2.22 (m, 1H), 2.15 (s, 3H), 2.04 (s, 3H), 1.26 (s, 6H), 0.95 (d, *J* = 6.5 Hz, 3H), 0.86 (d, *J* = 6.5 Hz, 3H); ATR-FTIR (neat) 2921, 2852, 2279, 1711, 1644, 1585, 1245, 1111, 829 cm^{-1}; MS (ESI^+) m/z calcd for $C_{25}H_{26}NO_4Ru$ $[M^+\text{-}PF^-_6\text{-}3(CH_3CN)+H^+]$ 506.0907, found 506.0878.

5) Synthesized of 2-phenylpyridine-bis(2,2'-bipyridine-4,4'-dicarboxylic acid)ruthenium(II) hexafluorophosphate (**PP1**)

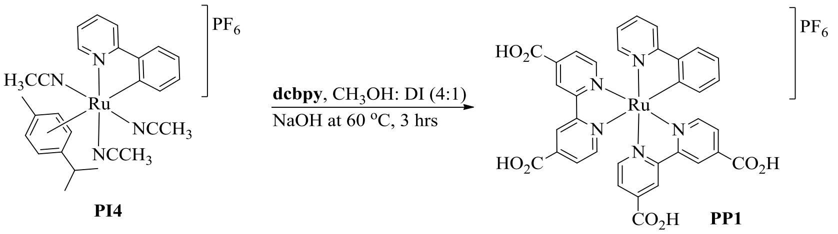

Compound **PP1** was synthesized a similar procedure as for **P2** (in page 31) using **dcbpy** (0.070 g, 0.32 mmol), NaOH (0.0210 g, 0.65 mmol), 5 ml of CH_3OH: DI water (4:1 v/v) and **PI4** (0.1000 g, 0.16 mmol). After purification, the dark purple solid complex was obtained (0.0275 g, 20%); ^{1}H NMR (300 MHz, CD_3OD) δ 9.05 (s, 1H), 8.97 (s, 1H), 8.91 (s, 2H), 8.19 (d, J = 5.6 Hz, 1H), 8.08 (d, J = 7.5 Hz, 1H), 8.00 - 7.82 (m, 4H), 7.76 - 7.58 (m, 4H), 7.58 - 7.39 (m, J = 15.6, 5.6 Hz, 1H), 7.20 - 7.01 (m, 1H), 7.02 - 6.88 (m, 1H), 6.90 - 6.68 (m, 2H), 6.39 - 6.28 (m, 1H); ATR-FTIR (neat) 3373, 2924, 2852, 1696, 1536, 1467, 1366, 1231, 1012 cm^{-1}; MS (ESI$^+$) m/z calcd for $C_{24}H_{14}N_4O_6Ru$ [M^+-PF^-_6-$C_{11}H_9N$+$3H^+$] 558.9717, found 558.3804.

6) Synthesized of 2-phenylpyridine 3-(pyridin-2-yl)benzoate-bis (2,2'-bipyridine-4,4'-dicarboxylic acid)ruthenium(II) hexafluorophosphate (**PP2**)

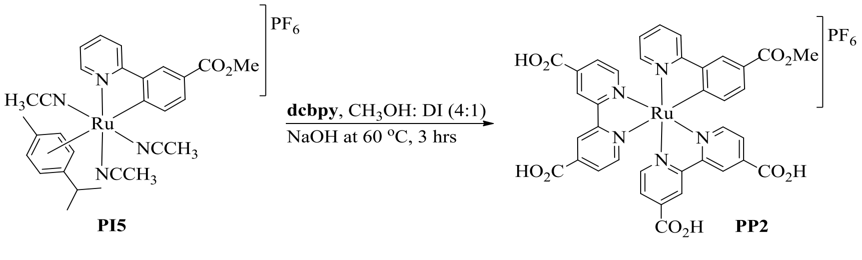

Compound **PP2** was synthesized a similar procedure as for **P2** using **dcbpy** (0.0446 g, 0.19 mmol), NaOH (0.0160 g, 0.40 mmol), 5 ml of CH_3OH: DI water (4:1 v/v) and **PI5** (0.0608 g, 0.09 mmol). After purification, the pure dark purple solid complex was obtained (0.0160 g, 20%); ^{1}H NMR (300 MHz, CD_3OD) δ 9.06 (s, 1H), 8.98 (s, 1H), 8.93 (s, 1H), 8.92 (s, 1H), 8.46 (s, 1H), 8.18 (d, *J* = 8.0 Hz, 1H), 8.08 (d, *J* = 5.8 Hz, 1H), 8.01 - 7.84 (m, 4H), 7.85 - 7.51 (m, 5H), 7.42 (d, *J* = 7.7 Hz, 1H), 7.05 (t, *J* = 6.3 Hz, 1H), 6.57 (d, *J* = 7.9 Hz, 1H), 3.85 (s, 3H); ATR-FTIR (neat) 3383, 2923, 2857, 1709, 1584, 1369, 1231, 1012, 761 cm^{-1}; MS (ESI$^+$) m/z calcd for $C_{37}H_{23}N_5O_{10}Ru$ $[M^+-PF^-_6-3H^++H_2O]$ 816.1824, found 816.0875.

7) Synthesized of methyl 2-phenylisonicotinate-bis(2,2'-bipyridine-4,4'-dicarboxylic acid)ruthenium(II) hexafluorophosphate (**PP3**)

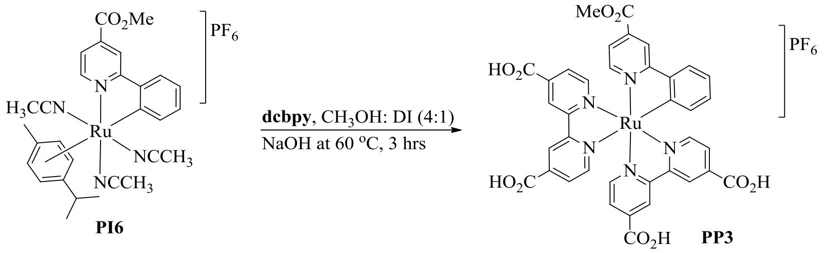

Compound **PP3** was synthesized a similar procedure as for **P2** using **dcbpy** (0.0446 g, 0.19 mmol), NaOH (0.0160 g, 0.40 mmol), 5 ml of CH_3OH: DI water (4:1 v/v) and **PI6** (0.0600 g, 0.09 mmol). After purification, the pure dark purple solid complex was obtained (0.0490 g, 60%); ^{1}H NMR (300 MHz, CD_3OD) δ 9.07 (s, 1H), 8.99 (s, 1H), 8.93 (s, 1H), 8.91 (s, 1H), 8.50 (s, 1H), 8.16 (dd, *J* = 9.1, 5.9 Hz, 1H), 8.04 - 7.86 (m, 4H), 7.75 (d, *J* = 6.0 Hz, 2H), 7.70 (d, *J* = 5.9 Hz, 2H), 7.44 (d, *J* = 5.8 Hz, 1H), 7.10 (d, *J* = 8.7 Hz, 1H), 6.95 (t, *J* = 7.3 Hz, 1H), 6.85 (dd, *J* = 14.3, 5.2 Hz, 1H), 6.37 (t, 1H), 3.95 (s, 3H); ATR-FTIR (neat) 3408, 3078, 2923, 2853, 1715, 1603, 1406, 1369, 1228, 1008, 765 cm^{-1}; MS (ESI$^+$) m/z calcd for $C_{37}H_{26}N_5O_{10}Ru$ $[M^+-PF^-_6]$ 802.0744, found 802.0744.

8) Synthesized of 2-(3-(methoxycarbonyl)phenyl)isonicotinic acid-bis(2,2'bipyridine-4,4'-dicarboxylic acid)ruthenium(II) hexafluorophosphate (**PP5**)

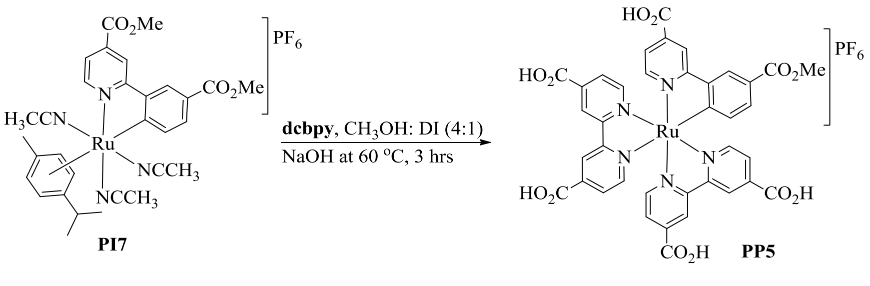

Compound **PP5** was synthesized a similar procedure as for **P2** using **dcbpy** (0.0355 g, 0.15 mmol), NaOH (0.0150 g, 0.37 mmol), 5 ml of CH_3OH: DI water (1:4 v/v) and **PI7** (0.0530 g, 0.07 mmol). After purification, the pure dark purple solid complex was obtained (0.0235 g, 35%); ^1H NMR (300 MHz, CD_3OD) δ 9.07 (s, 1H), 8.99 (s, 1H), 8.94 (s, 1H), 8.92 (s, 1H), 8.59 (s, 1H), 8.53 (s, 1H), 8.06 (d, J = 5.7 Hz, 1H), 7.94 (dd, J = 12.4, 5.7 Hz, 2H), 7.87 (d, J = 5.8 Hz, 2H), 7.78 - 7.64 (m, 4H), 7.47 (dd, J = 11.5, 7.2 Hz, 2H), 6.60 (d, J = 7.9 Hz, 1H), 3.86 (s, 3H); ATR-FTIR (neat) 3407, 3074, 2923, 2853, 1707, 1583, 1370, 1229, 1111, 1011, 768 cm^{-1}; MS (ESI$^+$) m/z calcd for $C_{38}H_{24}N_5O_{12}RuNa$ [M^+-PF_6^--$2H^+$+Na^+] 866.0290, found 866.7410.

3.5 Fabrication of DSSC devices using sensitizer

3.5.1 Fabrication of DSSC devices using co-sensitizer

3.5.1.1 Preparation of working electrode of pure and co-dyes shown in Figure 3.3.

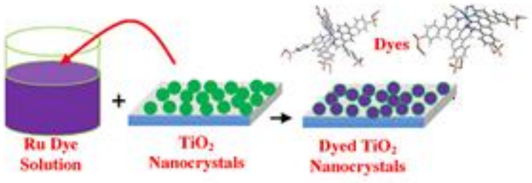

Figure 3.3 Schematic drawing of working electrode steps [43]

By using a similar procedure was reported by Talodthaisong [44], fluorine-doped tin oxide (FTO) conducting glasses (8 Ω/sq, Solaronix) were used for electrodes. The FTO conducting glasses were immersed in an aqueous solution of 4×10^{-2} M $TiCl_4$ at 70 °C in water saturation for 30 min and then washed with water and ethanol, respectively. The $TiCl_4$-treated-FTO were coated with 3 layers of a transparent (Ti-Nanoxide 20T/SP, Solaronix) and 1 layer of a scattering (Ti-Nanoxide R/SP, Solaronix) by screen printing method, respectively. Then, they were gradually sintered in stepwise at 325 °C for 5 min, at 375 °C for 5 min, at 450 °C for 5 min, at 500 °C for 30 min and cooled to 80 °C. Prior to dye sensitization, the TiO_2 electrodes were immersed in an aqueous solution of 4×10^{-2} M $TiCl_4$ at 70 °C in a water saturation atmosphere for 30 min. The TiO_2 electrodes were sintered again at 325 °C for 5 min, at 375 °C for 5 min, at 450 °C for 5 min, at 500 °C for 30 min and then cooled to ca. 80 °C. The prompted TiO_2 electrodes are shown in Figure 3.4.

Figure 3.4 The picture of TiO_2 electrode

The electrodes were dipped in dyes solution (3×10^{-4} M in ethanolic) in the dark at room temperature for 24 hours. The co-dyes solutions of **P2**+**N719** and **YN07+N719** were prepared in 1:1 ratios. The colors of pure and co-dyes solutions are shown in Figure 3.5.

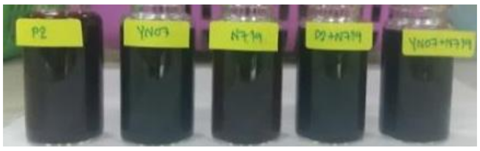

Figure 3.5 The color of pure and co-dyes solution

Then, the electrodes were washed with water and ethanol. They were dried on heater at 50 °C to completed the working electrodes as shown in Figure 3.6.

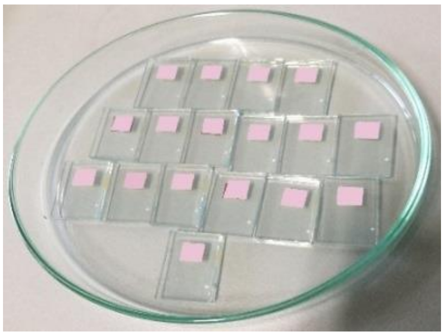

Figure 3.6 The picture of the completed working electrode

3.5.1.2 Preparation of counter electrodes

The FTO conducting glasses (8 Ω/sq, Solaronix) were used for electrodes. The 1×2 cm of FTO conducting glasses were prepared. Then, FTO glass was washed with detergent, acetone, ethanol, DI water and hexane, respectively. Next step, the electrodes were gradually sintered at 80 °C for 2 hours and cooled to room temperature.

The counter electrodes were prepared by placing a drop of H_2PtCl_6 solution (18 microliters × 2 times) on an FTO conducting glasses shown in Figure 3.7 (left). After that they were heated at 375 °C for 30 min. The counter electrodes are shown in Figure 3.7 (right).

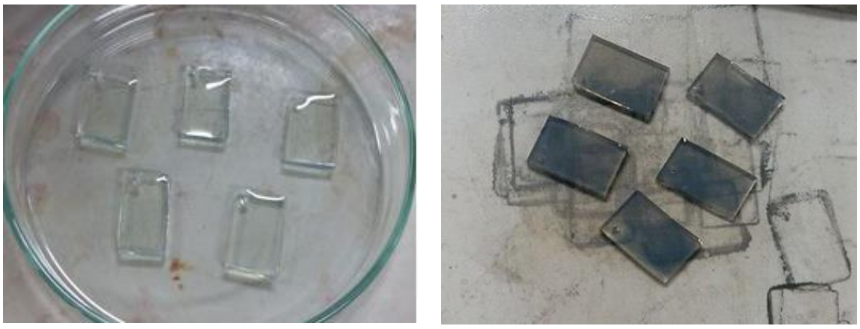

Figure 3.7 The H_2PtCl_6 solution dropped on FTO (left) and the completed counter electrodes (right)

3.5.1.3 Preparation of electrolyte

The electrolyte solution was prepared from 0.05 M I_2, 0.1 M LiI, 0.4 M t-butylpyridine (t-BPy) and 0.6 M tetrapropyl ammonium iodide (TPAI) in 85:15 v/v acetonitrile/valeronitrile solvent.

3.5.1.4 Assembling of DSSCs

The working electrodes and the counter electrodes were assembled into a sealed sandwich-type cell at 120 °C, 1.30 min (in Figure 3.8) by heating a surlyn film as a spacer between the electrodes.

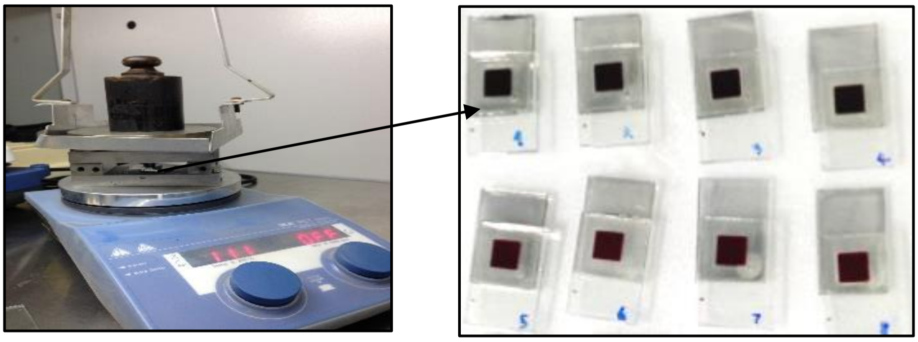

Figure 3.8 Pressing process (left) and the assembling device (right)

After the electrode was seated, then the liquid electrolyte was filled through the predrilled hole by a vacuum backfilling shown in Figure 3.9.

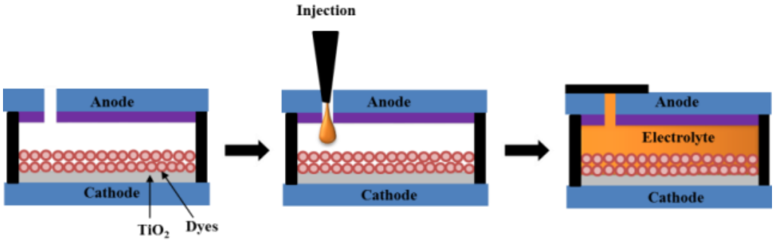

Figure 3.9 Injection step of electrolyte into the cell

Finally, the space left for contacts on both electrodes was stuck with copper film. Then, the cells were painted with silver paint to increase the conductivity. Both solar cell electrodes were contacted with copper wire by soldering method to get the competed the cells (Figure 3.10).

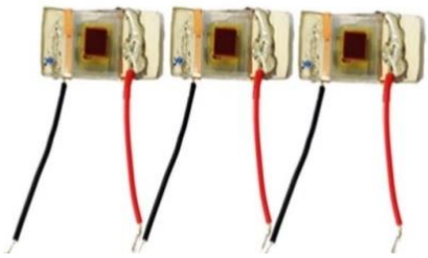

Figure 3.10 The completed dye-sensitized solar cells of P2+N719, YN07+N719 and N719

3.5.2 Fabrication of DSSC devices using thiocyanate free ruthenium sensitizer (PP1, PP2, PP3 and PP5)

3.5.2.1 Preparation of working electrode

The working electrodes of **PP1**, **PP2**, **PP3**, **PP5** and **N719** were prepared without $TiCl_4$-treatment. However, the FTO were coated with three layers of transparent (Ti-Nanoxide 20T/SP, Solaronix) and two layers of scattering (Ti-Nanoxide R/SP, Solaronix) TiO_2 which are slightly different from the preparation of pure and co-dyes (*i.e.*, three transparent layers and one scattering layer). Then, they were gradually sintered in stepwise at 125 °C for 10 min, at 125 °C for 10 min, at 450 °C for 30 min, at 500 °C for 30 min and cooled to 80 °C. After cooling to about 80 °C, the electrodes were immersed in **PP1**, **PP2**, **PP3**, **PP5** and **N719** solution (3×10^{-4} M in ethanol) in the dark at room temperature for 24 hours. The dyes solutions are shown in Figure 3.11.

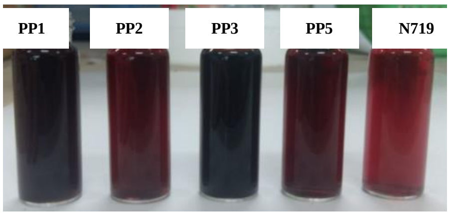

Figure 3.11 The color of PP1, PP2, PP3, PP5 and N719 dye solution

By using the same procedure as use for pure and co-dyes. The counter electrodes, electrolyte and assembling of **PP1**, **PP2**, **PP3**, **PP5** and **N719** were obtained as shown in Figure 3.12.

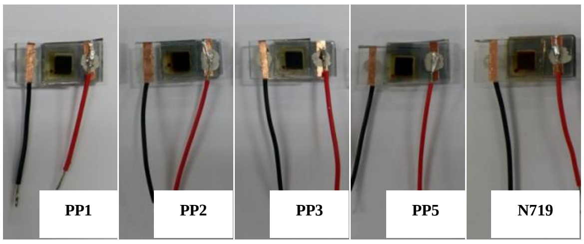

Figure 3.12 The completed dye-sensitized solar cells (PP1, PP2, PP3, PP5 and N719)

3.6 DSSCs characterization

The current-voltage (I-V) measurement were carried out with an active area of 0.16 cm^2 by a Keithley 2400 source meter unit under AM 1.5 sun simulated sunlight (100 mW.cm^{-2}) which was produced by a 150 W xenon arclamp (6255 Newport) with an IR-cutoff filter (KG5-Newport).

The incident photon to current conversion efficiency (IPCE) measurement is given by a 150 W xenon arc lamp (6255 Newport) fitted with a 1/8 Monochromator (74000 Newport).

CHAPTER 4

SYNTHESIS, CHARACTERIZATION, PHOTOPHYSICAL, ELECTROCHEMICAL PROPERTY AND PHOTOVOLTAIC PERFORMANCE OF CO-SENSITIZERS FOR DSSCs

The limitation of ruthenium(II) complex with thiocyanate ligand in DSSC is weak absorption in the red and IR regions. To overcome this problem, the co-sensitization is an effective approach. In this chapter, the combination of the ruthenium(II) complexes which are 2-phenyl-5-(trifluoromethyl)pyrido) bis (2,2'-bipyridine-4,4'-dicarboxylic acid) ruthenium(II) hexafluorophosphate (**P2**) and cis [bis(thiocyanato) bis (2,2'-biquinoline-4,4'-dicarboxylicacid(4-carboxy-2,2'-bipyridine-4'-caboxylate)ruthenium(II)] tetrabutyl-ammonium (**YN07**) and cis-bis(isothiocyanato) bis (2,2'-bipyridyl-4,4'-dicarboxylato) ruthenium(II) bis(tetrabutylammonium) (**N719**) was used as co-dyes in DSSCs. The synthetic routes of **YN07** and **N719** were reported by Nazeeruddin [38] and Thathong [39]. The retrosynthetic analysis of **P2** is shown in Figure 4.1.

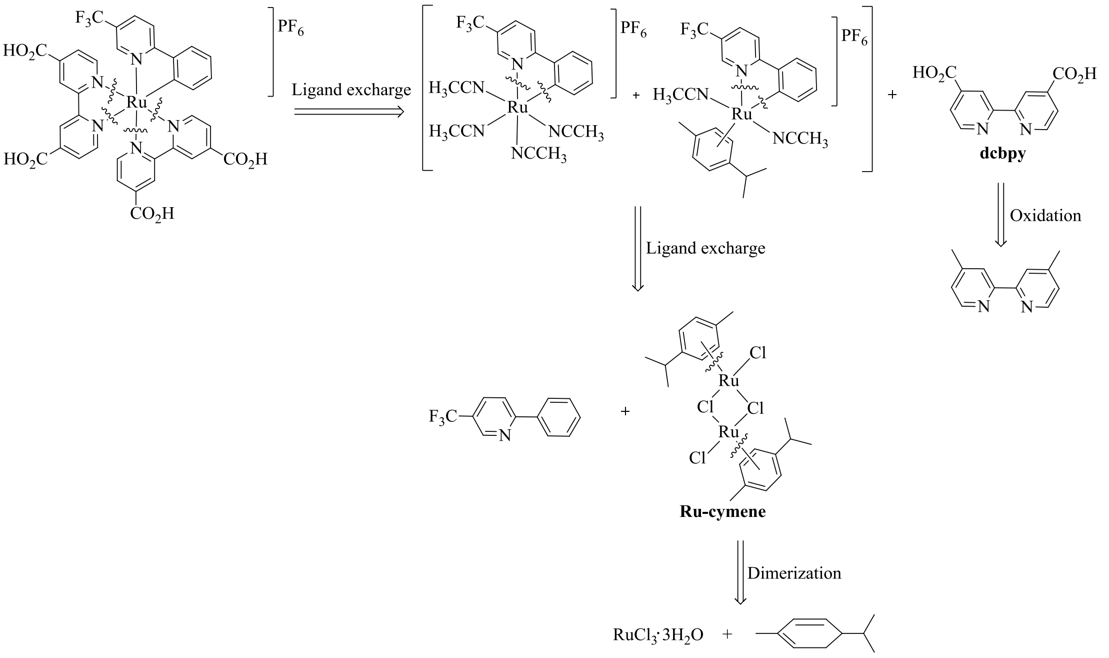

Figure 4.1 The retrosynthetic route of P2

4.1 Synthesis and characterization of 2,2'-bipyridine-4,4'-dicarboxylic acid (dcbpy)

Dcbpy ligand was synthesized by oxidation reaction of dimethyl on bipyridine. It was oxidized by sodium dichromate ($Na_2Cr_2O_7$) in acidic condition to give aldehyde. Then, the resulting intermediate was further oxidized to carboxylic acid to obtained as a white solid in 60% yield. The mechanism of the oxidation reaction can be explained in Figure 4.2.

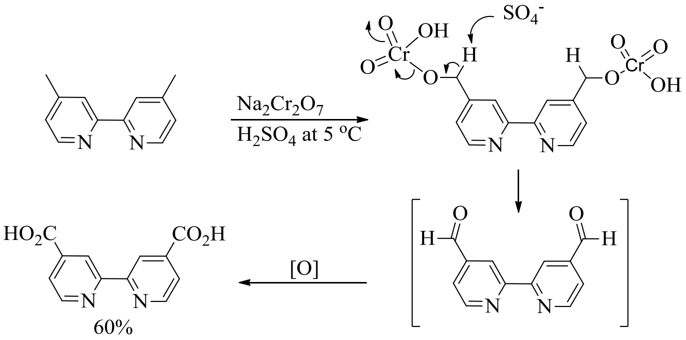

Figure 4.2 The oxidation mechanism of dcbpy

The product was characterized by ^{1}H NMR. The **dcbpy** is a symmetric molecule as only 3 protons signals of pyridine ring was observed. The spectrum was observed without the proton of the carboxylic groups in DMSO-d_6. The ^{1}H NMR spectrums appear the two doublets signal at 8.90 and 7.90 ppm assigned to H^1 and H^2, respectively, in Figure 4.3. The H^1 of pyridine shows the signal in the downfield region due to high electronegativity of nitrogen. Correspondingly, the coupling constant of H^1 and H^2 was observed about 4 Hz. The molecular structure of ligand was supported with ^{13}C NMR. The ^{13}C spectra show 5 carbon resonances for aromatic pyridine carbon and one signal for carbonyl group. Furthermore, **dcbpy** ligand showed the characteristic peaks for the functional group with a solid sample ATR-FTIR technique. The broad weak band above 2491 cm^{-1} assigned for O–H stretching of the carboxylic acid. The medium peak located around 1700 cm^{-1} is the C=O stretch vibration of carboxylic acid and the sharp peaks in the region of 1500 - 1300 cm^{-1} were assigned to the C=C bonds in the pyridine rings. The molecular weight was confirmed by mass spectroscopy. The mass spectra show the peaks at 242.2855 m/z assigned to M^+-$2H^+$ (in Figure A.1, appendices).

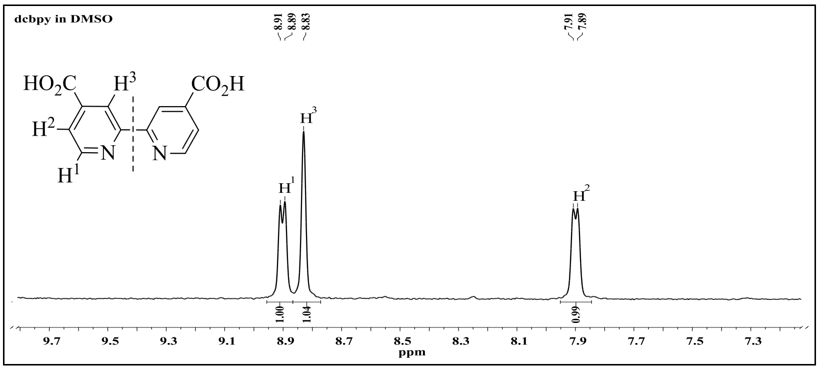

Figure 4.3 The ^{1}H NMR spectrum of dcbpy in DMSO-d_6

4.2 Synthesis and characterization of di-μ-chlorobis[(η^6-benzene) dichloro-ruthenium(II)] (Ru-cymene)

The **Ru-cymene** was synthesized from the addition reaction of the $RuCl_3.3H_2O$ and α-phellandrene in ethanol solution to give the complex as orange solid, 48% yield as shown in Figure 4.4.

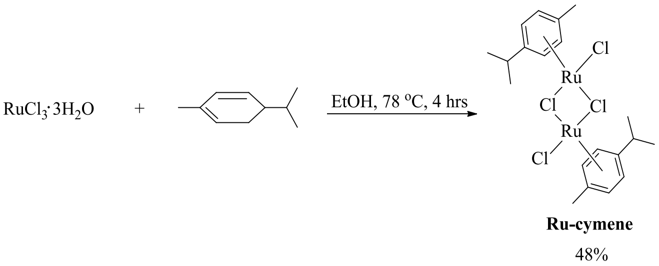

Figure 4.4 The synthesis of Ru-cymene

The complex is a symmetric molecule as only 14 protons was observed. The ^{1}H NMR spectra of **Ru-cymene** appear the two doublet signals at 5.48 (2×2H) and 5.34 (2×2H) ppm represented to the proton of phenyl ring. The proton of isopropyl shows at 2.92 (2×1H) and 1.28 (2×6H) ppm. The last singlet signal at 2.16 (2×3H) ppm was assigned to metyl group, in Figure 4.5. Furthermore, the molecular structure was confirmed with ^{13}C NMR. The ^{13}C spectra show 4 signals for 6 aromatic carbon resonances and 3 signals for alkyl group. The molecular structure was confirmed with ATR-FTIR and mass. From, IR spectra, the sharp peaks at 1446 and 1386 cm^{-1} were assigned for the C=C bonds in the phenyl rings (in Figure A.2, appendices).

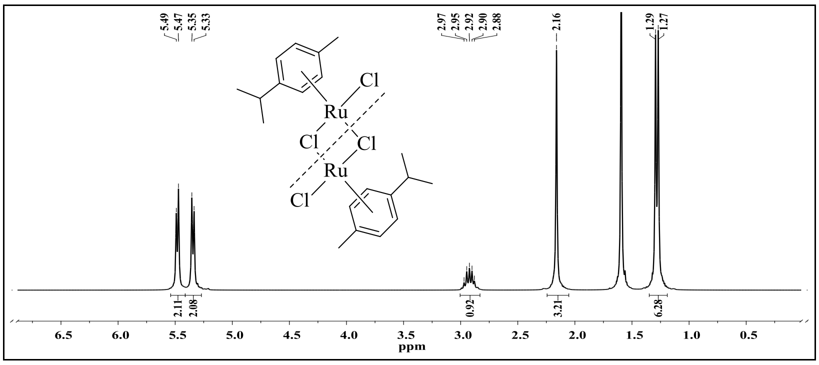

Figure 4.5 The ^{1}H NMR spectrum of Ru-cymene in $CDCl_3$

4.3 Synthesis and characterization of ruthenium complexes

4.3.1 2-Phenyl-5-(trifluoromethyl)pyrido-bis(2,2'-bipyridine-4,4'-dicarboxylic acid)ruthenium(II) hexafluorophosphate (P2)

The **P2** complex was synthesized a similar procedure as reported in the literature [30]. [31], involving two steps; in the first step, the **Ru-cymene** and 2-phenyl-5-trifluoromethylpyridine were reacted by ligand exchange reaction to obtain the acetonitrile and *p*-cymene ruthenium complexes (**4** and **5**). The ^{1}H NMR spectra of intermediate is show in Figure A.3, (appendices). Next step, the acetonitrile ligands were exchanged by **dcbpy** ligand to give the complex **P2** as dark purple solid, 40% yield, in Figure 4.6.

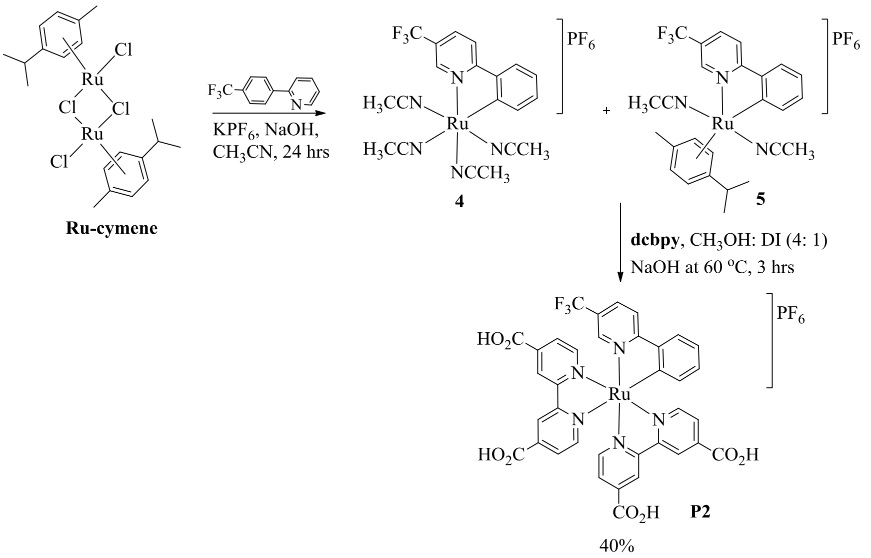

Figure 4.6 The synthesis of P2

The ruthenium(II) sensitizers was coordinated with phenylpyridine derivative and **dcbpy** ligands. The structure of complex was investigated with ^{1}H NMR. The spectrum obtained from methanol-d_4 with clearly resolved peaks. The **P2** complex gives 14 signals of a total 19 protons of phenylpyridine and bipyridine ligands without a proton from carboxylic acid. It was that the 4 singlet signals at 9.12, 9.03, 8.96 and 8.94 ppm with integration number 1:1:1:1, respectively are the H^1, H^2, H^3 and H^4 of pyridine ring (in Figure 4.7). The H^1 and H^2 show downfield region due to the anisotropic effect of C^N ligand. Moreover, this structure was characterized by FTIR. The broad peak of O–H stretching at 3437 cm^{-1} was observed and the medium peak located around 1715 cm^{-1} was assigned to the C=O stretching of carboxylic acid groups. Additionally, the sharp peaks in the region of 1325 cm^{-1} was assigned for the C–O stretching. The molecular weight of the complex was observed at 812.0549 m/z assigned to M^+-PF^-_6 (in Figure A.4, appendices).

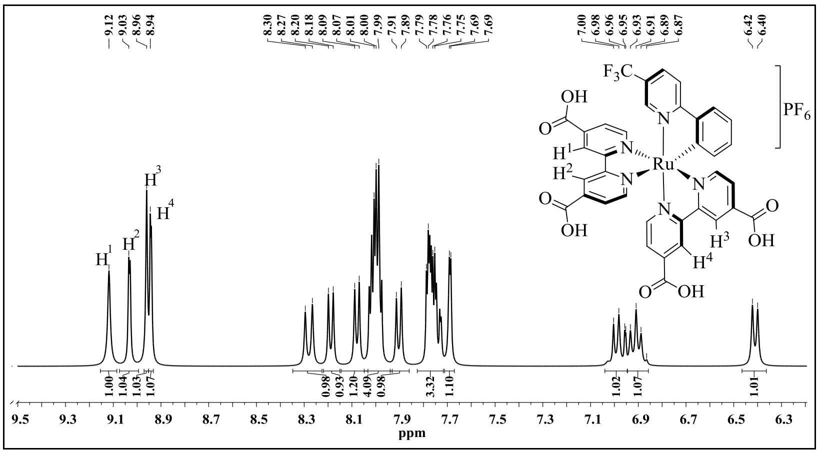

Figure 4.7 The ^{1}H NMR spectrum of P2 in CD_3OD

4.3.2 Cis[bis(thiocyanato)bis(2,2'-bipyridine-4,4'-dicarboxylic acid) ruthenium(II) tetrabutylammonium (N719)

We successfully synthesized the complex **N719** by using ligand exchange reaction between **Ru-cymene**, **dcbpy** and ammoniumthiocyanate to obtained the **N3** complex. Then, the **N3** was dissolved in 0.1 M tetrabutylammonium hydroxide in methanol to confer solubility by deprotonation of the carboxylic group, in Figure 4.8.

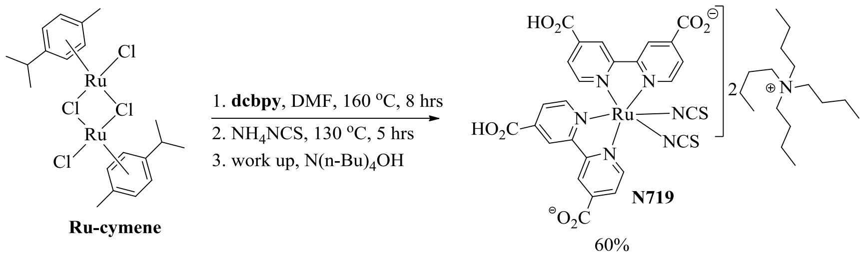

Figure 4.8 The synthesis of N719

The complex **N719** was achieved as dark purple solid, 60% yield. The molecular structure was characterized ^{1}H, ^{13}C NMR and ATR-FTIR was also reported in the literature [45].

The structure of complex was investigated with ^{1}H NMR. The **N719** complex is a symmetrical molecule as only 42 protons was observed. The spectrum shows singlet signal in the aromatic region corresponding to pyridine rings, in Figure 4.9. The signals of aliphatic region represent to tetrabutylammonium cations. The integrated ratio of the aliphatic to aromatic protons confirmed the presence of two tetrabutylammonium cations. The ^{13}C NMR, ATR-FTIR and mass spectrum are shown in Figure A.5, appendices.

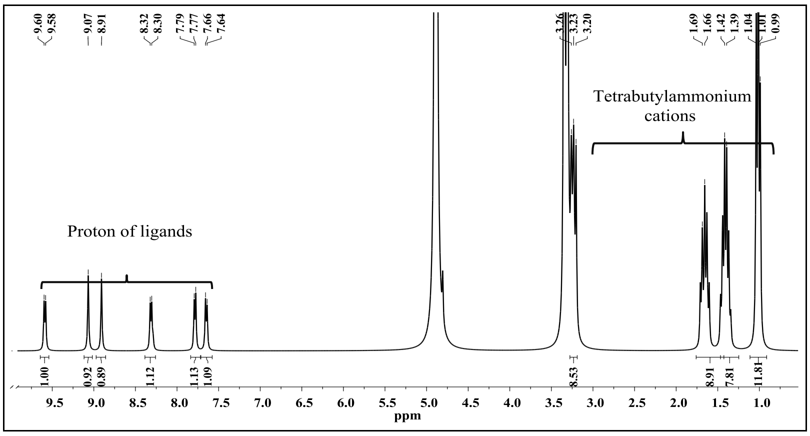

Figure 4.9 The ^{1}H NMR spectrum of N719 in CD_3OD

4.3.3 Cis[bis(thiocyanato)bis(2,2'-biquinoline-4,4'-dicarboxylic acid) (4-carboxy-2,2'-bipyridine-4'-caboxylato)ruthenium(II)] tetrabutylammonium (YN07)

The complexes **YN07** was synthesized from the ligand exchange reaction between **Ru-cymene** and **dcbpy** to give intermediate **1**. Next step, the ligand **dcbiq** was added to obtained intermediate **2**. Then, the Cl^- ligand was exchanged with ^-NCS to afforded the complex **3**. The last step, complex **3** was dissolved in 0.1 M tetrabutylammonium hydroxide in methanol to confer solubility by deprotonation of the carboxylic group [39], [46]. The **YN07** was achieved as dark purple solid, 70% yield. The synthetic of the ligand exchange reaction was explained in the Figure 4.10.

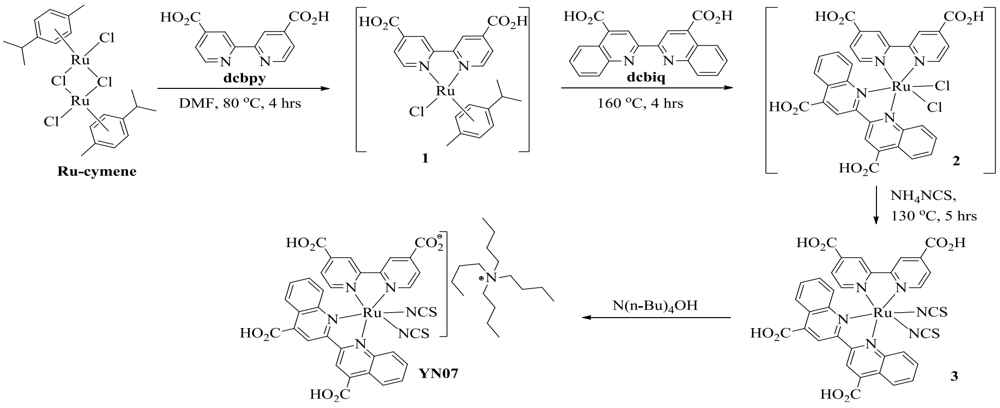

Figure 4.10 The synthetic route of YN07

The molecular structure of **YN07** is an asymmetrical molecule as 52 protons was observed. The ^1H NMR spectra exhibit multiple peaks because of the two different N^N ligands. The proton signals of aromatic rings were located in the downfield from 10.00 - 7.00 ppm. It was that the aromatic signals at chemical shift 9.58 (1H), 9.23 (1H), 9.07 (1H), 9.03 - 8.90 (2H), 8.87 (1H), 8.83 (1H), 8.67 (1H), 8.32 (1H), 8.02 - 7.84 (2H), 7.85 - 7.71 (1H), 7.65 (1H), 7.58 - 7.49 (1H), 7.33 - 7.11 (2H). For the signals of the tetrabutylammonium cation, they were observed in the upfield region at chemical shift 3.27 - 3.16 (8H), 1.71 - 1.56 (8H), 1.47 - 1.32 (8H) and 1.00 (12H). Moreover, it was that the integration ratio of the aromatic proton and the aliphatic proton is 1:8, confirming the present of one ammonium salts in the complex structures shown in Figure 4.11.

The molecular structure of **YN07** was supported with ^{13}C NMR spectra, in Figure A.6 (appendices). Both **YN07** and **P2** give similar ATR-FTIR spectrum. In addition, it was found that the strong peak located around 2103 cm^{-1} assigned to –N=C=S stretching vibration of thiocyanate ligand. The molecular weight of the complex was observed at 828.9761 m/z assigned to M^+-$C_{16}H_{36}N^+$+Na^++H^+ (Figure A.6, appendices).

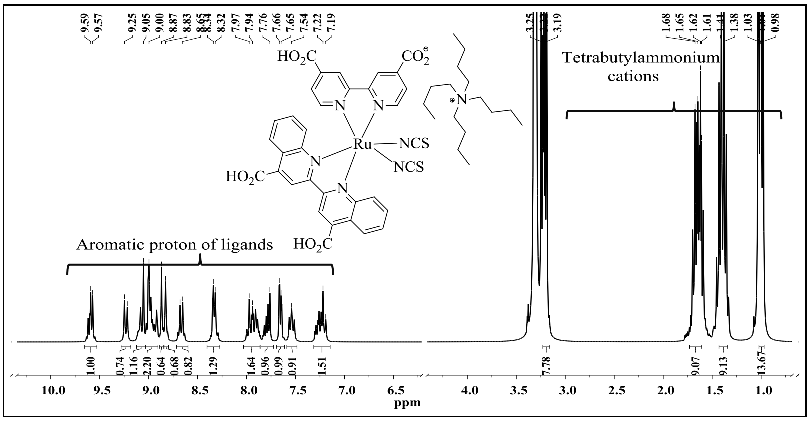

Figure 4.11 The ^{1}H NMR spectrum of YN07 in CD_3OD

4.4 Photophysical properties

UV-Vis absorption spectra of pure and co dyes were measured under the same condition (4×10^{-5} M in ethanol) with 1:1 ratios. The solutions colors of **P2**, **YN07**, **N719**, **P2+N719** and **YN07+N719** are shown in Figure 4.12 (inside).

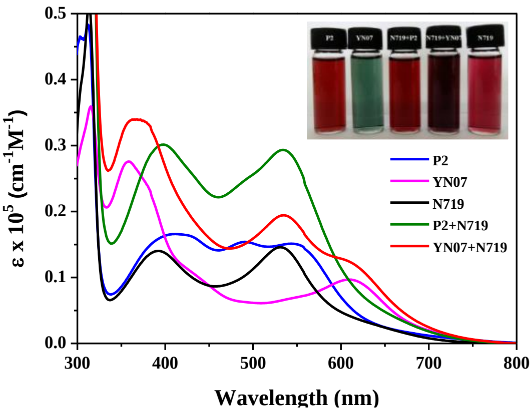

Figure 4.12 UV-Vis absorption spectra and the picture of 4×10^{-5} M (inside) of pure and co-dyes in ethanol

Generally, the absorption spectra of all pure dyes (Figure 4.12) from intense $\pi \rightarrow \pi^*$ of ligand were observed below 390 nm and the absorption band from 400 - 700 nm was assigned as metal to ligand charge transfer (MLCT) from the d-orbital of metal centre to π^* of the N^N ligand [47]. It was found that the **P2** gave a maximum absorption (λ_{max1}) at 411, 490, and 551 nm, **YN07** give λ_{max} at 400 and 612 nm. For **N719** dye, it shows λ_{max} at the 392 and 531 nm, in Table 4.1.

Interestingly, the molar extinction coefficient (**ε**) of **P2+N719** (0.30×10^5 $M^{-1}cm^{-1}$) and **YN07+N719** (0.19×10^5 $M^{-1}cm^{-1}$) was obtained compared with pure a **P2** (0.15×10^5 $M^{-1}cm^{-1}$), **N719** (0.15×10^5 $M^{-1}cm^{-1}$) and **YN07** (0.96×10^5 $M^{-1}cm^{-1}$). In addition, the co-dyes of **YN07+N719** showed a much longer MLCT absorptions range more than that the pure dyes [48], [49].

Table 4.1 Photophysical properties of pure and co-dyes

Dye	λ_{max1}/nm ($\varepsilon_{max}/10^5$ $M^{-1}cm^{-1}$)	λ_{max2}/nm ($\varepsilon_{max}/10^5$ $M^{-1}cm^{-1}$)	λ_{max3}/nm ($\varepsilon_{max}/10^5$ $M^{-1}cm^{-1}$)
P2	411 (0.16)	490 (0.15)	551 (0.15)
YN07	360 (0.27)	612 (0.96)	
N719	392 (0.14)	531 (0.15)	
P2+N719	397 (0.31)	533 (0.30)	
YN07+N719	370 (0.34)	535 (0.19)	610 (0.12)

4.5 Electrochemical properties

Electrochemical measurements were recorded by Autolab Metrohm PG11 with a three-electrode system under argon gas of 0.1 M tetra-n-butylammonium hexafluorophosphate electrolyte. A glassy carbon electrode, a platinum-wire and an Ag/Ag^+ (3 M KCl) electrode were used as the working electrode, counter electrode and reference electrode, respectively. The complexes were prepared at 1×10^{-3} M in a dried DMF solution. The CV curves were recorded compared with the ferrocene/ferrocenium (Fc/Fc^+) redox couple as an external standard which was measured under the same condition [50]. The cyclic voltammograms are shown in Figure 4.13.

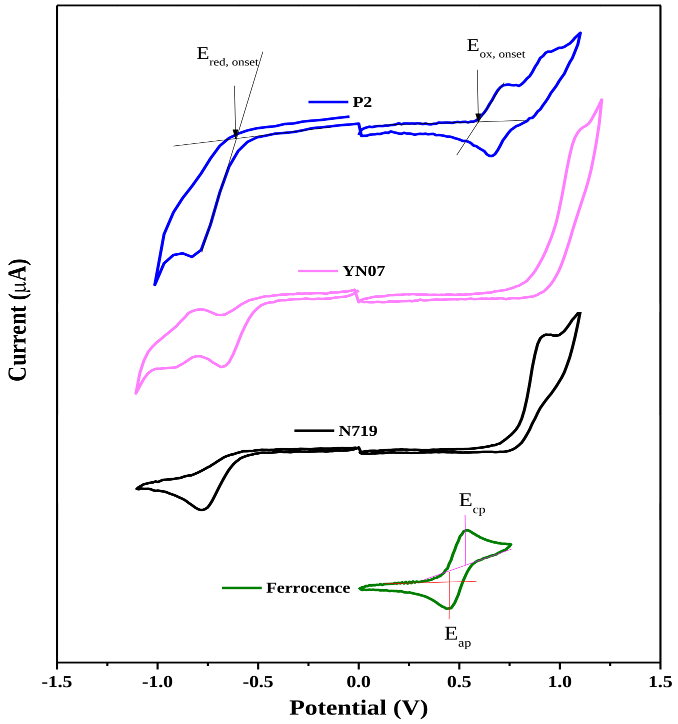

Figure 4.13 The cyclic voltammograms of pure dyes in dry DMF with 100 mV/s scan rate

From the cyclic voltammograms, the complexes show quasi-reversible couples oxidation peak, due to the oxidation of the Ru^{2+}/Ru^{3+} couple at 0.90, 1.02 and 0.85 V for **P2**, **YN07** and **N719**, respectively. The oxidations potentials of the complexes are difference due to the variation of HOMO level form the d-orbitals. The reduction peaks of the complexes are observed at -0.77, -0.60 and -0.72 V for **P2**, **YN07** and **N719**, respectively. Interestingly, **YN07** shows two reductions potentials at -0.60 and -0.85 V due to **dcbpy** and **dcbiq** ligands.

The HOMO and LUMO energy levels of complexes were calculated from equation 8, 9 and 10 [34], [47].

$$E_{HOMO} = -[E_{ox,\ onset} - E_{1/2,\ Fc,Fc^{+}} + 4.8]\ eV \tag{8}$$

$$E_{LUMO} = -[E_{red,\ onset} - E_{1/2,\ Fc,Fc^{+}} + 4.8]\ eV \tag{9}$$

$$E_g = E_{HOMO} - E_{LUMO} \tag{10}$$

The energy level of Fc/Fc$^+$ was used with -4.8 eV vacuum. The half-wave potential of the Fc/Fc$^+$ redox couple ($E_{1/2,\ Fc/Fc^+}$) was estimated from $E_{1/2,\ Fc/Fc^+}$ is $(E_{ap}+E_{cp})/2$, where E_{ap} and E_{cp} are the anodic and cathodic peak potentials, respectively. It was calculated of $E_{1/2,\ Fc/Fc^+}$ = (0.52+0.45)/2 = 0.48 V. The electrochemical properties of the ruthenium complexes are summarized in Table 4.2.

Table 4.2 Electrochemical properties of pure dyes

Dye	**$E_{ox,\ onset}$ (V)**	**$E_{red,\ onset}$ (V)**	**E_{HOMO} (eV)**	**E_{LUMO} (eV)**	**E_g (eV)**
P2	0.60	-0.60	-4.92	-3.72	1.20
YN07	0.90	-0.52	-5.22	-3.80	1.42
N719	0.78	-0.61	-5.10	-3.71	1.39

The LUMO levels of dyes are -3.72, -3.80 and -3.71 eV with respect to the energy level of the conduction band of TiO_2 (-4.40 eV), which is a possible to driving force for charge injection process [8]. The HOMO levels of the sensitizers afforded to -4.92, -5.22 and -5.10 eV, relative to that of the redox couple I^-/I^-_3 (-4.90 eV) can be regenerate form to a ground state. This can successfully provide ample driving force for dye regeneration to complete the circuit and restore the dyes, in Figure 4.14.

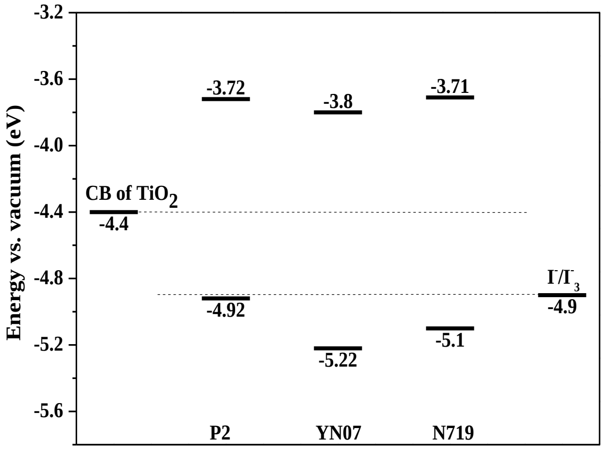

Figure 4.14 Energy level of the pure dyes comparison to the conduction band of TiO_2 and the potential of the iodide/tri-iodide

However, HOMO level of **P2** showed a very close to the potential of the redox couple in the electrolyte that could be affected to recombination process [51]. While **YN07** showed the HOMO level at -5.22 eV which is more than 0.2 eV leading to difficultly dye regeneration process.

4.6 Photovoltaic performance

The incident photon to current conversion efficiency (IPCE) of devices base on **N719**, **P2+N719**, **YN07+N719, P2** and **YN07** are shown in Figure 4.15 (A). All dyes can convert light to photocurrent in the spectral region from 350 to 600 nm. Notably, **N719** show higher IPCE compared to the pure and co-dyes, and reach a maximum at ca 35% at 550 nm [34], [52].

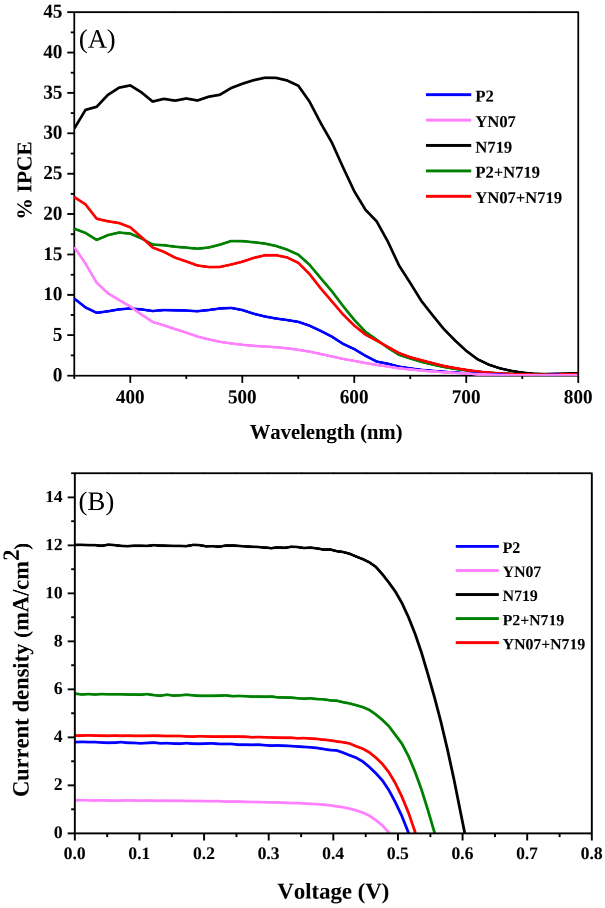

Figure 4.15 Photovoltaic properties: (A) the IPCE spectra and (B) current-voltage characteristics of devices made of pure and co-dyes under AM 1.5

The current-voltage characteristics of photovoltaic of all devices under standard AM 1.5G, the power conversion efficiencies (η) was followed the trend of J_{SC} with the order **N719** (η = 5.17%) > **P2+N719** (η = 2.37%) > **YN07+N719** (η = 1.59%) > **P2** (η = 1.42%) > **YN07** (η = 0.46%), in Figure 4.15 (B). It found that the co-dyes showed a lower performance than pure **N719**. We think that the unsuitable HOMO levels of **P2** and **YN07** affected to dye generation [53], in Figure 4.14. Moreover, **YN07** which is the bulky structure prevent the **N719** absorption on TiO_2 surface [23]. The short-circuit photocurrent density (J_{SC}), open-circuit voltage (V_{OC}), fill factor (FF) and power conversion efficiency (η) are summarized in Table 4.3.

Table 4.3 The photovoltaic parameters of DSSC devices from pure and co-dyes

Dyes	**J_{SC} (mA/cm^2)**	**V_{OC} (mV)**	**FF**	**η (%)**
N719	12.02	600	0.71	5.17
P2	3.82	520	0.72	1.42
YN07	1.41	480	0.68	0.46
P2+N719	5.84	560	0.73	2.37
YN07+N719	4.08	530	0.74	1.59

CHAPTER 5

SYNTHESIS, CHARACTERIZATION, PHOTO PHYSICAL, ELECTROCHEMICAL PROPERTY AND PHOTOVOLTAIC PERFORMANCE OF THIOCYANATE FREE RUTHENIUM COMPLEXES FOR DSSCs

In this chapter, we reported four novel thiocyanate free ruthenium(II) complexes (**PP1**, **PP2**, **PP3** and **PP5**). The new complexes were designed replacing thiocyanate ligand in **N3** by a new C^N ligand The new complexes are named; 2-phenylpyridine-bis(2,2'-bipyridine-4,4'-dicarboxylic acid) ruthenium(II) hexafluorophosphate (**PP1**), 2-phenylpyridine-3-(pyridin-2-yl)benzoate- bis(2,2'-bipyridine-4,4'-dicarboxylic acid) ruthenium(II) hexafluorophosphate (**PP2**), methyl-2-phenylisonicotinate-bis (2,2'-bipyridine-4,4'-dicarboxylic acid) ruthenium(II) hexafluorophosphate (**PP3**) and 2-(3-(methoxycarbonyl)phenyl)isonicotinicacid-bis(2,2'bipyridine-4,4'-dicarboxylic acid) ruthenium(II) hexafluorophosphate (**PP5**) (Figure 5.1).

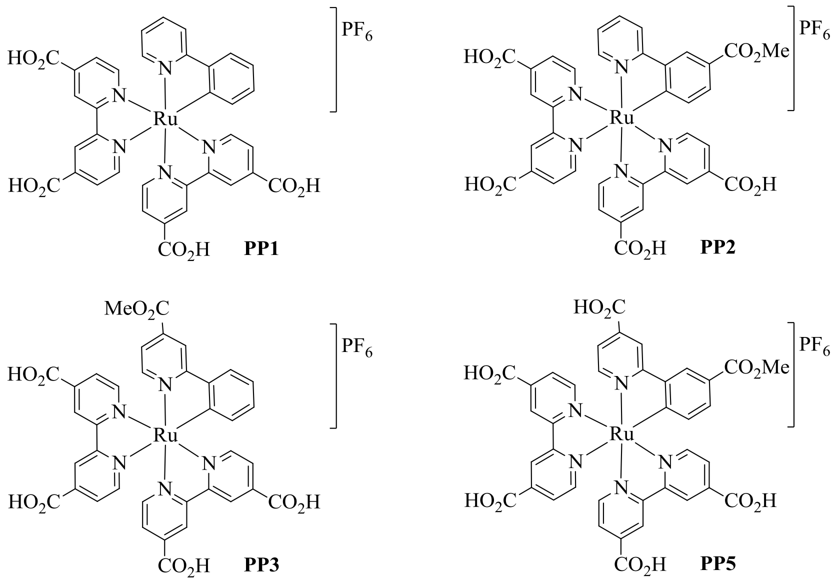

Figure 5.1 Structures of target ruthenium(II) complexes

The new thiocyanate free ruthenium(II) complexes can be synthesized form 2,2'-bipyridine-4,4'-dicarboxylic acid and difference phenyl pyridine (C^N ligand) *via* acetonitrile and *p*-cymene ruthenium(II) intermediate which the C^N ligand can be synthesize from Suzuki coupling reaction and esterification reaction shown in Figure 5.2.

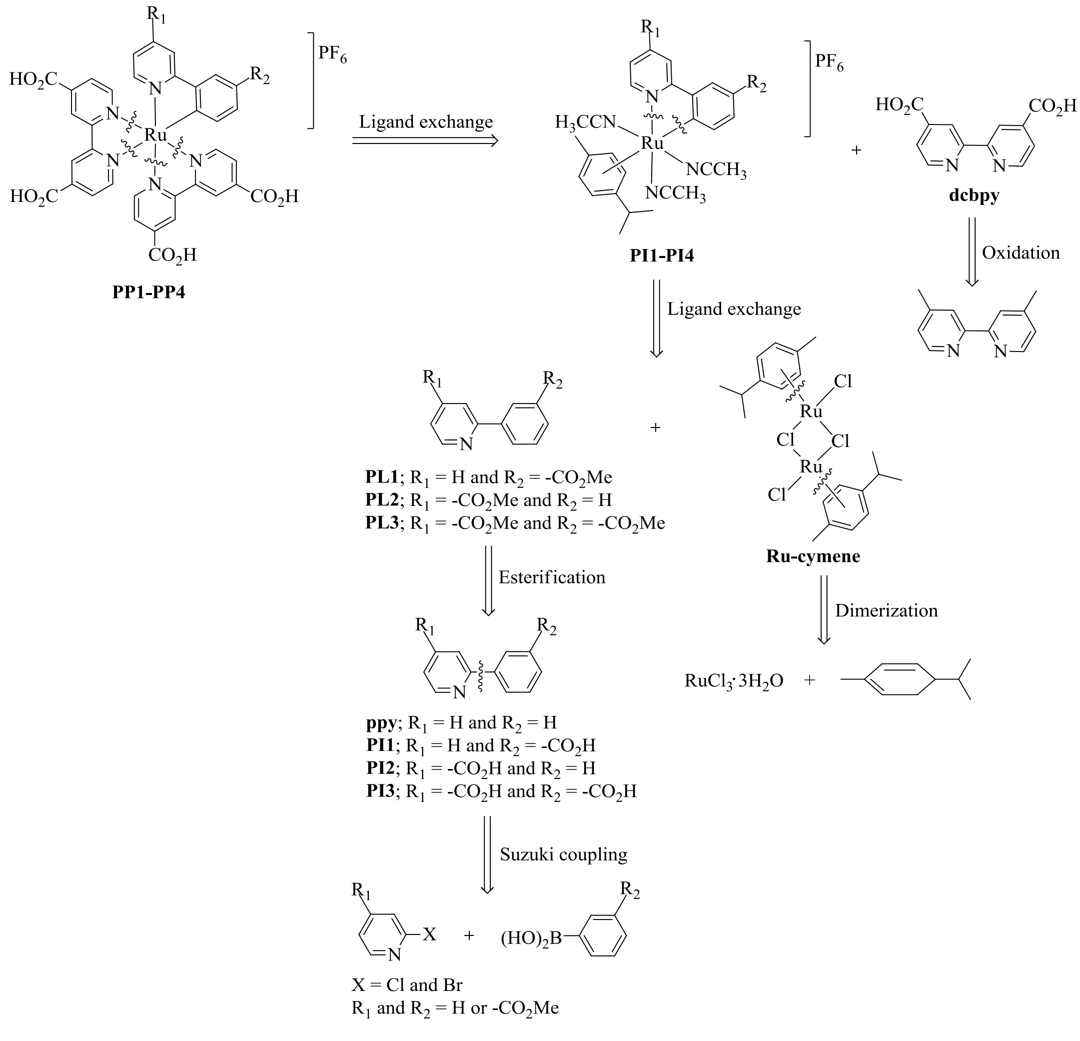

Figure 5.2 The retrosynthetic route of new dyes

5.1 Synthesis and characterization of C^N ligand

5.1.1 Methyl-2-chloroisonicotinate

The methyl-2-chloroisonicotinate was synthesized by esterification reaction from 2-chloroisonicotinic acid and conc. H_2SO_4 in methanol as yellow liquid, 73% yield, shown in Figure 5.3.

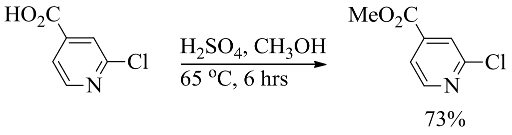

Figure 5.3 The synthesis of methyl-2-chloroisonicotinate

The mechanism of esterification reaction can be explained in Figure 5.4. The 2-chloroisonicotinic acid was protonated with H_2SO_4 to give the carbocation (**1**). Then, it was reacted with methanol nucleophile and loss H_2O to obtain the target product.

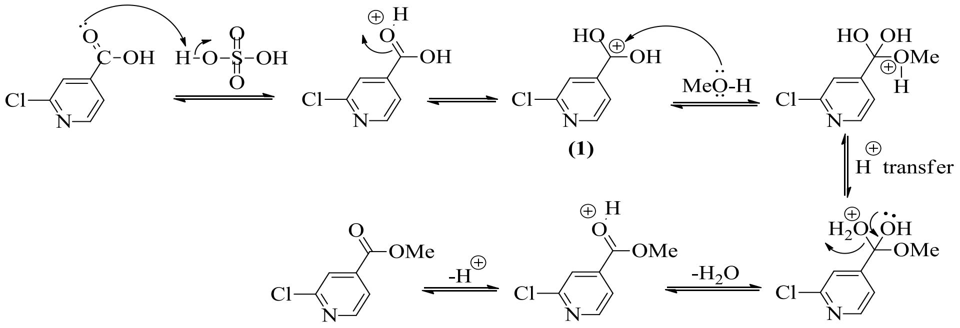

Figure 5.4 The esterification mechanism of methyl-2-chloroisonicotinate

Methyl 2-chloroisonicotinate is an asymmetric molecule as 6 protons of molecule was observed. The ^1H NMR spectrum is show in Figure 5.5. The NMR spectrum shows the signal at chemical shift 8.51 (1H), 7.84 (1H) and 7.74 (1H) ppm assigned as proton of pyridine ring. The result show that the two doublets at 8.51 and 7.84 ppm assigned to H^1 and H^2, respectively. The H^1 show the lower downfield signal because of the nitrogen atom. The singlet signal at chemical shift 7.74 (1H) ppm assigned to H^3. Where the chemical shift at 3.94 (3H) was assigned as the protons of the methyl group. The structure was confirmed by ^{13}C NMR. It was found that the one carbon for carbonyl of ester group appears at 164.2 ppm, and 5 carbon resonances for pyridine ring and one carbon of methyl are reported in Figure A.7, appendices. Moreover, the functional group of methyl 2-chloroisonicotinate was proved by using ATR-FTIR. The IR spectrum of C=O and C–O stretching show at 1732 and 1290 cm^{-1}, respectively (in Figure A.7, appendices).

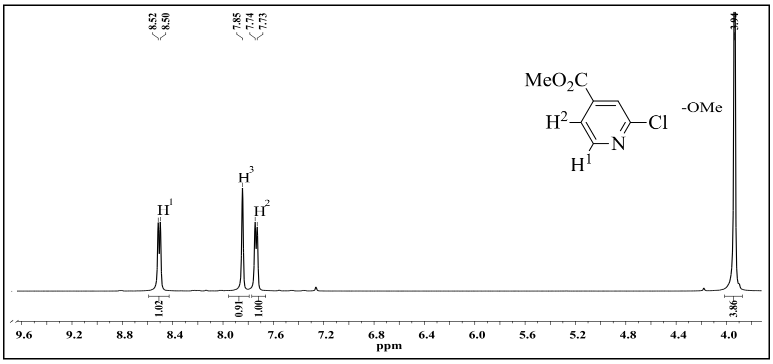

Figure 5.5 The ^{1}H NMR spectrum of methyl-2-chloroisonicotinate in CDCl$_3$

5.1.2 2-Phenylpyridine (ppy)

The 2-phenylpyridine was synthesized by Suzuki coupling reaction between 2-chloropyridine and phenylboronic acid using Pd(0) catalyst to give the product as yellow liquid in 90% yield, shown in Figure 5.6.

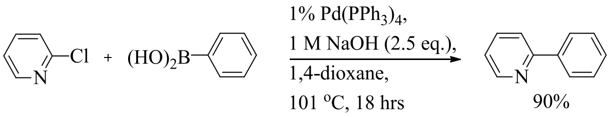

Figure 5.6 The synthesis of 2-phenylpyridine

The Suzuki cross-coupling reaction mechanism was provided in Figure 5.7.

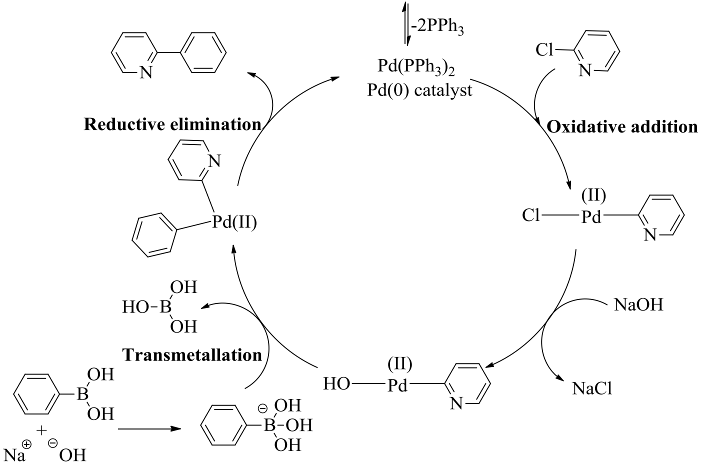

Figure 5.7 The mechanism of Suzuki coupling reaction

The general common steps to cross-coupling reactions, the palladium(0) active catalyst species undergoes oxidative addition with phenylpyridine, followed transmetallation with phenylboronic acid and the last step reductive elimination to form the pyridine and phenyl carbon-carbon bond to give produce [51], [55], [56].

The 2-phenylpyridine is an asymmetric molecule as 9 protons of molecule was observed. The spectrum shows the signal at chemical shift 8.69 (1H), 7.99 (2H) and 7.79 - 7.69 (2H), 7.51 - 7.39 (3H), 7.25 - 7.17 (1H) ppm assigned as proton of aromatic ring, in Figure 5.8. The structure was also confirmed with ^{13}C NMR spectra. The product shows 11 carbon resonances for aromatic carbon. Furthermore, the IR spectrum showing the aromatic C=C and C=N stretching at 1590 and 1400 cm^{-1}, respectively, (in Figure A.8, appendices).

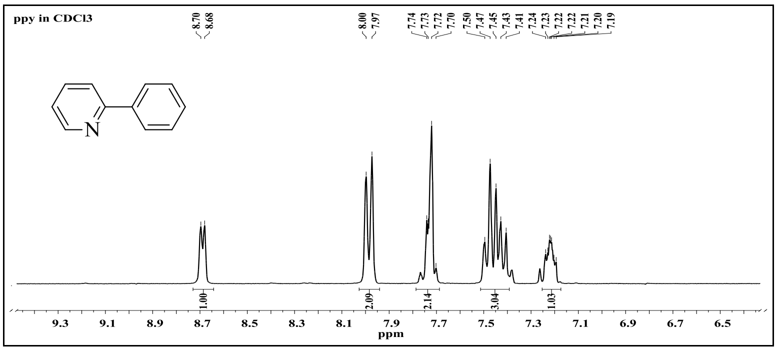

Figure 5.8 The ^{1}H NMR spectrum of 2-phenylpyridine in CDCl$_3$

5.1.3 The target C^N ligand (PL1-Pl3)

PL1-PL3 were successfully formed as outlined, in Figure 5.9. The synthetic procedures for these ligands were obtained from two reaction steps. The first step is the synthesis of **PI1-PI3** by using Suzuki coupling reaction *in situ* hydrolysis. The second step is the synthesis of **PL1-PL3** *via* esterification reaction.

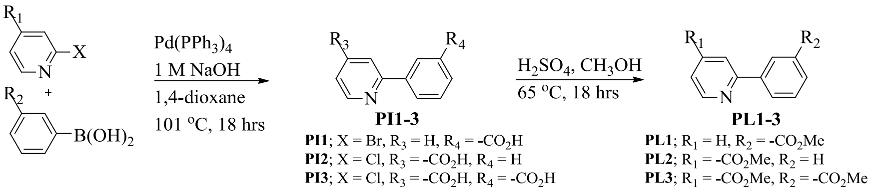

Figure 5.9 The synthetic route of PL1-PL3

5.1.3.1 Synthesis of **PI1-PI3** intermediate

The synthesis of **PI1-PI3** intermediate was completed in high yield from the reaction of aryl halide (1 eq.) and phenylboronic acid (1.1 eq.) using the same methods reported by Thathong [54]. The mechanism of Suzuki cross-coupling reaction can explained similar to 2-phenylpyridine. Interestingly, it found that the final products were obtained as the carboxylic acid instead of the ester group due to the *in situ* hydrolysis under basic condition.

The chemical structure of 3-(pyridin-2-yl)benzoic acid (**PI1**) was confirmed by ^{1}H NMR, in Figure 5.10. The **PI1** is acid molecule, which 7 signals of 8 protons are observed at chemical shift 8.70 (1H), 8.66 (1H) and 8.30 (1H), 8.02 (2H) and 7.90 (1H) and 7.38 (1H) ppm assigned as aromatic position protons. In the DMSO-d_6 solvent, we didn't observe the acid signal proton. Moreover, the ^{13}C NMR spectrum shows one carbon for carbonyl carboxylic acid at 167.6 ppm. The signal of O–H and C=O IR stretching of carboxylic acid were observed at 2500 and 1678 cm^{-1}, respectively. Furthermore, the molecular weight was confirmed by mass spectroscopy. The mass spectra show the peaks at 200.0723 m/z assigned to $M^{+}+H^{+}$ (in Figure A.9, appendices).

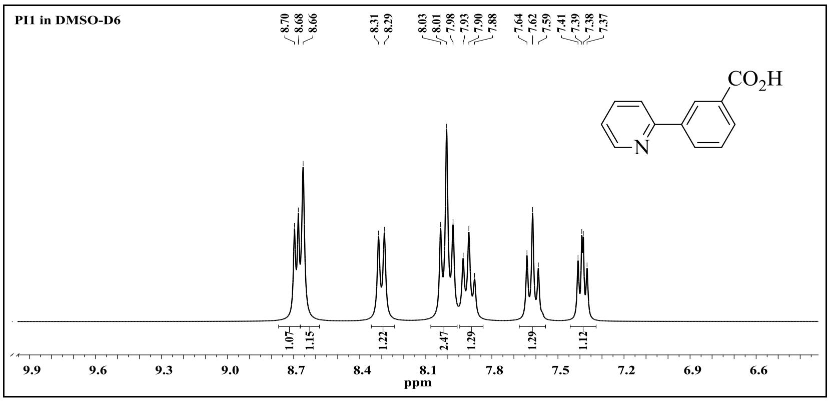

Figure 5.10 The ^{1}H NMR spectrum of 3-(pyridin-2-yl)benzoic acid in DMSO-d_6

The 2-phenyl-isonicotinic acid (**PI2**) and 2-(3-carboxyphenyl) isonicotinic acid (**PI3**) were obtained 70% and 53% yield, respectively, as yellow solid. Their chemical structures were confirmed by ^{1}H NMR, ^{13}C NMR, ATR-FTIR and mass spectrometry (in Figure A.10 - 13, appendices).

5.1.3.2 The synthesis of **PL1-PL3**

2-Phenylpyridine-3-(pyridin-2-yl)benzoate (**PL1)** was synthesized by esterification reaction of **PI1** to give the product as yellow liquid, 73% yield. The **PL1** was characterized by ^{1}H NMR, in Figure 5.11, ^{13}C NMR, ATR-FTIR and mass. The chemical structure of **PL1** is an asymmetric molecule as 11 protons were observed. The ^{1}H NMR spectrum shows the signal at chemical shift 8.72, 8.64, 8.24, 8.09, 7.89, 7.56 and 7.28 ppm. The H^{1} shows singlet signal and one integration number at 8.64 ppm. Correspondingly, the signals patterns of pyridine ring are similar to NMR spectrum of 2-phenylpyridine. Moreover, we observed the chemical shift at 3.95 (3H) ppm assigned as proton of methyl group. The ^{13}C NMR spectra show one carbon at 166.9 for carbonyl, 11 aromatic carbon resonances and one carbon of methyl. The signal of C=O and C–O IR stretching of carboxylic acid were observed at 1710 and 1248 cm^{-1}, respectively. Furthermore, the molecular weight was confirmed by mass spectroscopy. The mass spectra show the peaks at 214.0872 m/z assigned to MW+H^{+}, (in Figure A.14, appendices).

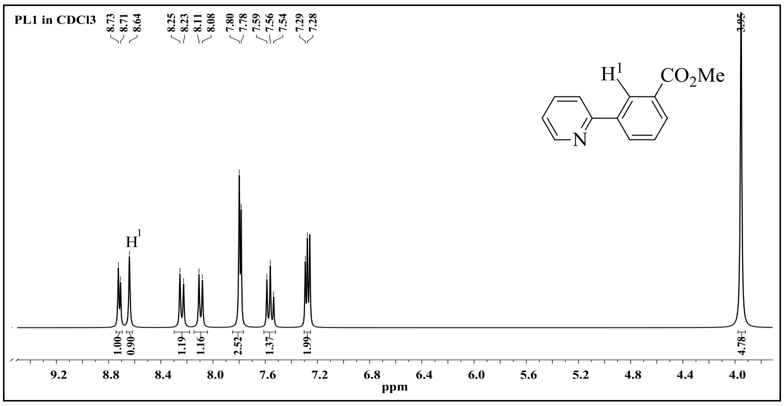

Figure 5.11 The ^{1}H NMR spectrum of PL1 in CDCl$_3$

The synthesis procedure of methyl 2-phenylisonicotinate (**PL2**) is similar to **PL1** ligand. The 61% yellow liquid product was obtained. The **PL2** is an asymmetric molecule as 11 protons. The 3 signals of pyridine ring show doublet, singlet and doublet multiplicity assigned to the H^{1}, H^{2} and H^{3} proton, respectively (Figure 5.12). Furthermore, the correlation of H^{2} and H^{3} were explained based on their coupling constants (about 5 Hz). Furthermore, the ^{13}C NMR spectrum show one carbon at 165.7 ppm for carbonyl, 11 carbon resonances for aromatic ring and one carbon of methyl. The ATR-FTIR give the peak patterns similar **PL1** (in Figure A.15, appendices).

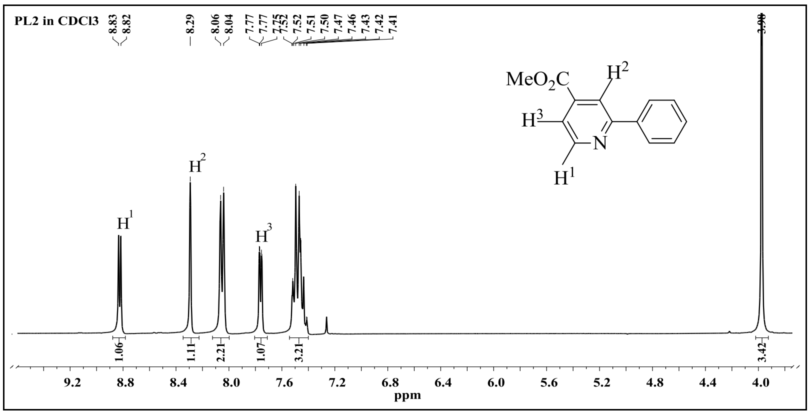

Figure 5.12 The ^{1}H NMR spectrum of PL2 in $CDCl_3$

Methyl-2-(3-(methoxycarbonyl)phenyl)isonicotinate (**PL3**) was synthesized by using the same methods synthesis of **PL1**. We obtained the ligand as white solid in 75% yield and characterized by ^{1}H NMR. The structure of **PL3** is an asymmetric molecule as 13 protons was observed. The signal patterns of pyridine ring are related with pyridine ring of **PL2** ligand (Figure 5.12) and phenyl ring similar to phenyl of **PL1** ligand (Figure 5.11). We found that two singlet signals at chemical shift 8.70 (1H) and 8.36 (1H) referred H^2 and H^3. For the protons of methyl group showing at 4.01 (3H) and 3.97 (3H) ppm were found in Figure 5.13.

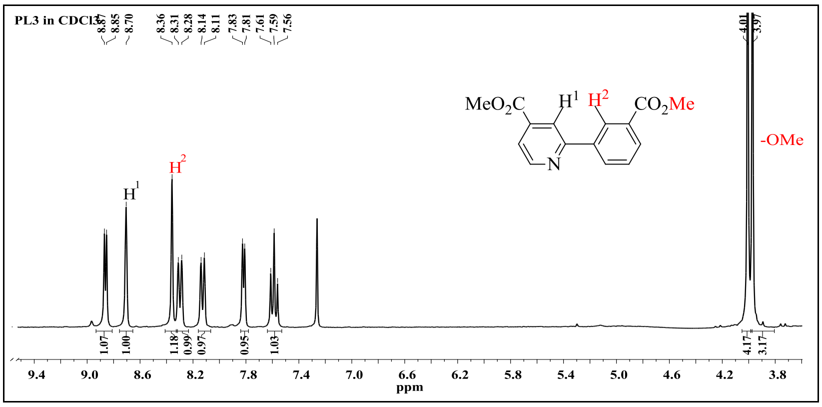

Figure 5.13 The ^{1}H NMR spectrum of PL3 in $CDCl_3$

Furthermore, the ^{13}C NMR spectra of **PL3** show 2 carbons for carbonyl and 2 carbons of methyl. The sharp peak located at 1726 cm^{-1} was assigned to the C=O stretching of carboxylic acid groups. Additionally, the sharp peaks in the region of 1288 cm^{-1} was assigned for the C–O stretching. The molecular weight of the ligand was observed at 272.0924 m/z assigned to $M^{+}+H^{+}$ (in Figure A.16, appendices).

5.2 Synthesis and characterization of thiocyanate free ruthenium complexes

The complexes **PP1-PP4** were synthesized by using the similar procedure to synthesis **P2** (Chapter 4). The **PP1** can be synthesized from the reaction of di-μ-chlorobis[(η^{6}-benzene)dichlororuthenium] (**Ru-cymene**) and 2-phenylpyridine under acetonitrile and potassium hexafluorophosphate at 45 °C for 2 days. The pure intermediate was purified by silica column chromatography using (2:8 v/v) acetonitrile: dichloromethane as eluent. The first green-yellow band was collected to obtain **PI4**. Next step, the 2,2'-bipyridine-4,4'-dicarboxylic acid (**dcbpy**) ligand was added to complete the complex **PI4**. By applying the corresponding **PL1**, **PL2** and **PL3** ligand, the complexes **PP2**, **PP3** and **PP4** were obtained, respectively [25], [37], [53]. The preparation procedures were summarized in Figure 5.14.

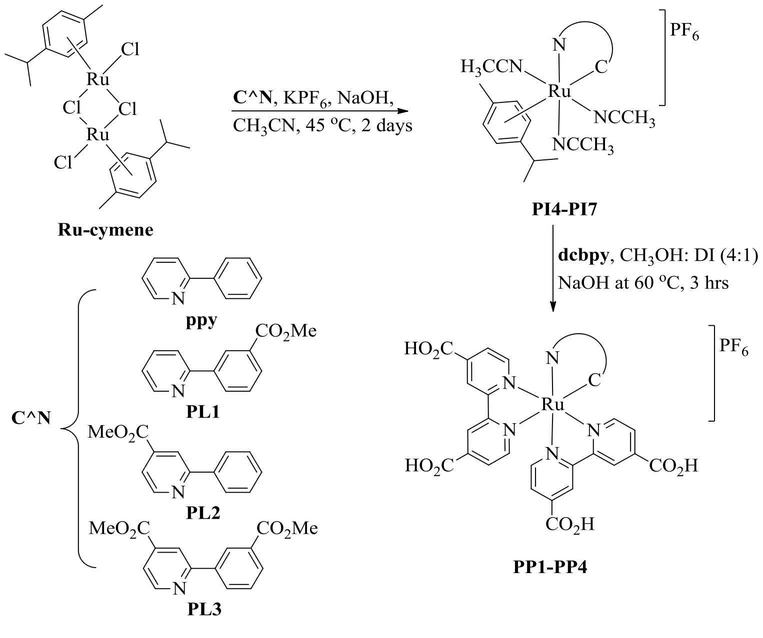

Figure 5.14 The synthesis of PP1-PP4

The intermediate **PI4** was obtained as a green solid, 90% yield. The ^{1}H NMR spectrum of **PI4** is illustrated here as an example in Figure 5.15. The chemical structure was investigated with ^{1}H NMR to confirm the phenyl pyridine, *p*-cymene and acetonitrile ligands were coordinated to the ruthenium. The spectrum obtained in chloroform-d solvent, with a sharp and clearly resolved peak. The result shows that the downfield region about 9.50 - 7.00 ppm assigned to the proton of 2-phenylpyridine ligand and 6.00 - 5.00 ppm represented to proton of *p*-cymene. In aliphatic region, 6 signals of individual chemical shifts for total 19 protons of the methyl, isopropyl and acetonitrile moieties were observed. Furthermore, IR spectrum showed the peaks at 2205 cm^{-1} assigned to -CN stretching of acetonitrile. The structure was confirmed by mass spectroscopy. The mass spectra show the peaks at 390.0742 m/z assigned to M^+-PF^-_6-$3CH_3CN$ (in Figure A.17, appendices).

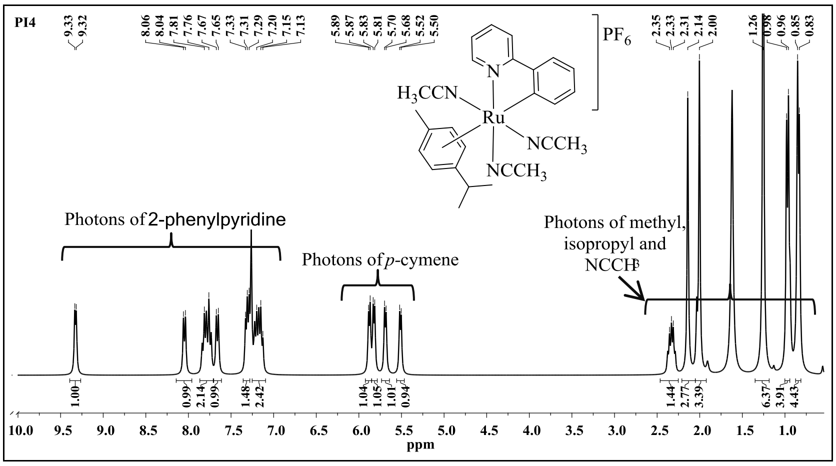

Figure 5.15 The ^{1}H NMR spectrum of PI4 in $CDCl_3$

Analogously, the **PI5**, **PI6** and **PI7** were obtained as a green solid, **PI5** (47%), **PI6** (50%) and **PI7** (65%) by using the similar procedure to synthesis **PI4**. The all complex was confirmed chemical structures by ^{1}H NMR, ATR-FTIR and mass spectrometry (in Figure A.18 - 20, appendices). Particularly, most of the protons in the all intermediates could be precisely assigned with the correlation pattern of the ligand. Target complexes were successfully formed as outlined in Figure 5.14. We obtained the complex as dark purple solid, **PP1** (20%), **PP2** (20%), **PP3** (60%) and **PP5** (35%).

PP1 is an asymmetric molecule as 20 protons were observed from ^1H NMR spectra. The proton signals of aromatic rings were observed in the downfield region at chemical shift 9.05 (1H), 8.97 (1H), 8.91 (2H), 8.19 (1H), 8.08 (1H), 8.00 - 7.82 (4H), 7.76 - 7.58 (4H), 7.58 - 7.39 (1H), 7.20 - 7.01 (1H), 7.02 - 6.88 (1H), 6.90 - 6.68 (2H), 6.39 - 6.28 (1H), in Figure 5.16. Most of the spectra exhibit multiple peaks because of the magnetically non-equivalent two **dcbpy** and **ppy** ligands of all protons. Particularly, the 4 singlet signals from 9.05 - 8.87 were assigned proton of **dcbpy** similar to **P2** (Chapter 4). The NMR spectrum data of compound was also reported in the literature [30], [31].

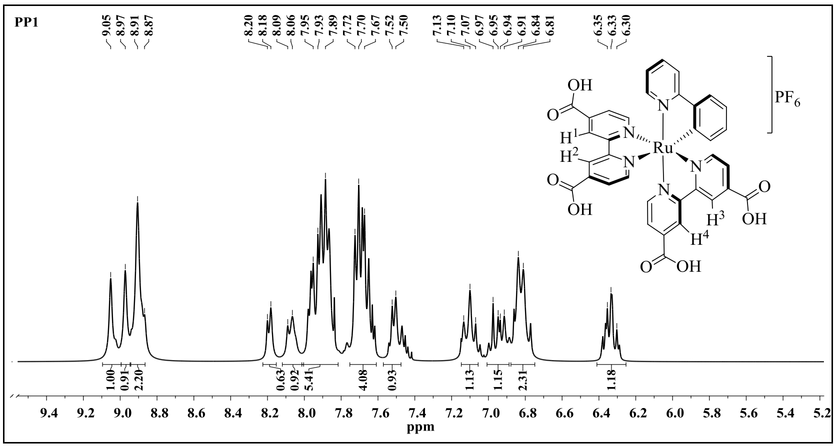

Figure 5.16 The ^1H NMR spectrum of PP1 in CD_3OD

For the reactions to obtain ruthenium(II) sensitizers, the ligands are successively coordinated to the metal center. Therefore, the existence of characteristic peaks for functional groups in the infrared spectra can provide sufficient data for the success of reactions. The ruthenium(II) complex shows the characteristic peaks for each functional group. The broad weak band at 3373 cm^{-1} assigned for the stretching of O–H. The strong peak located at 1596 cm^{-1} and 1366 cm^{-1} are the C=O stretch vibration and C–O stretching of carboxylic acid groups also verifies the existence of the carboxylic acid. The structure was confirmed by mass spectroscopy. The mass spectra show the peaks at 558.3804 m/z assigned to M^+-PF^-_6-$C_{11}H_9N$+$3H^+$ (in Figure A.21, appendices).

PP2 is an asymmetric molecule as 22 protons was observed from 9.50 - 3.00 ppm, see in Figure 5.17. The complex shows 13 signals at chemical shift 9.06 (s, 1H), 8.98 (1H), 8.93 (s, 1H), 8.92 (s, 1H), 8.46 (s, 1H), 8.18 (1H), 8.08 (1H), 8.01 - 7.84 (4H), 7.85 - 7.51 (5H), 7.42 (1H), 7.05 (1H), 6.57 (1H), 3.85 (s, 3H). The signal in aromatic region was assigned to the aromatic proton of **dcbpy** and **PL1** ligands. Interestingly, at 8.46 ppm illustrates the singlet signal and one the integration number of these peaks confirmed to H^1 of phenyl ring in **PL1** ligand. In aliphatic region, the signal at chemical shift 3.85 (3H) was assigned as proton of the methyl group. Additionally, ATR-FTIR spectrum show the sharp peaks at 3383 (broad), 1709 and 1360 cm^{-1} assigned O-H, C=O and C–O stretching, respectively, which illustrates the carboxylic acid. The mass spectra show the peaks at 816.0875 m/z assigned to M^+-PF^-_6+H_2O (in Figure A.22, appendices).

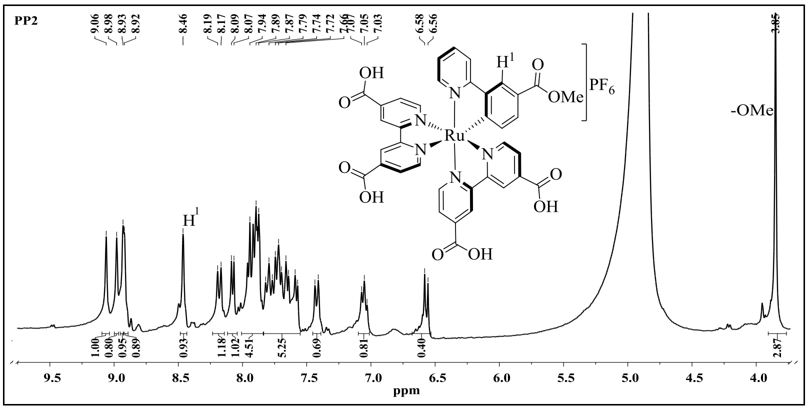

Figure 5.17 The ^1H NMR spectrum of PP2 in CD_3OD

PP3 is an asymmetric molecule as 22 protons was observed from 9.20 - 3.50 ppm. The complex shows 15 signals at chemical shift 9.07 (1H), 8.99 (1H), 8.93 (1H), 8.91 (1H), 8.50 (1H), 8.16 (1H), 8.04 - 7.86 (4H), 7.75 (2H), 7.70 (2H), 7.44 (1H), 7.10 (1H), 6.95 (1H), 6.85 (1H), 6.37 (t, 1H), 3.95 (s, 3H). The signal in aromatic region was assigned to the aromatic proton of **dcbpy** and **PL2** ligands. Interestingly, the singlet signal at 8.50 ppm confirm to H^1 of pyridine ring in **PL2** ligand, in Figure 5.18. The last signal chemical shift at 3.95 (3H) was referred to proton of methyl group. Furthermore, IR spectrum show the peaks at 3383 (broad), 1715 (sharp) and 1228 (sharp) cm^{-1} represented O–H, C=O and C–O stretching, respectively. The mass spectra show the peaks at 802.0744 m/z assigned to M^+-PF^-_6 (in Figure A.23, appendices).

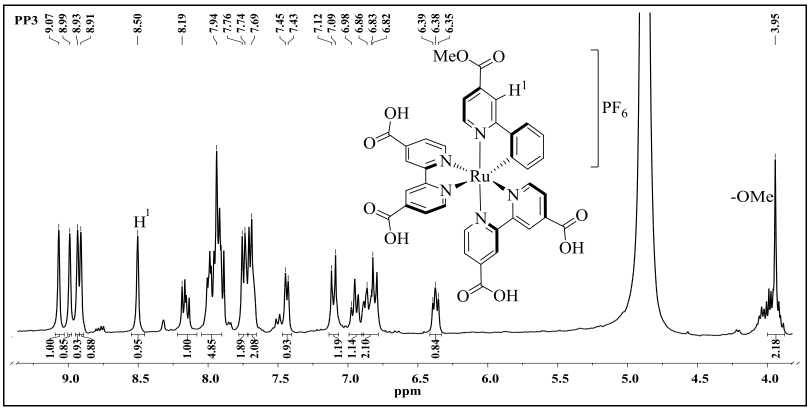

Figure 5.18 The ^{1}H NMR spectrum of PP3 in CD_3OD

The synthesis of complex **PP4** is similar to the **PP1**. The complex structure was characterized by ^{1}H NMR. It was observed 24 protons from 9.20 - 3.50 ppm. The complex shows the 12 signals at chemical shift 9.07 (1H), 8.99 (1H), 8.94 (1H), 8.92 (1H), 8.59 (1H), 8.53 (1H), 8.06 (1H), 7.94 (2H), 7.87 (2H), 7.78 - 7.64 (4H), 7.47 (2H), 6.60 (1H) from aromatic proton. The signal in aromatic region was assigned to the aromatic proton of **dcbpy** and **PL3** ligands. Particularly, the two singlet signals at 8.59 and 8.53 ppm assigned to the H^1 and H^2 of ligand. The H^1 near the nitrogen atom appear at very downfield compare to H^2 (Figure 5.19).

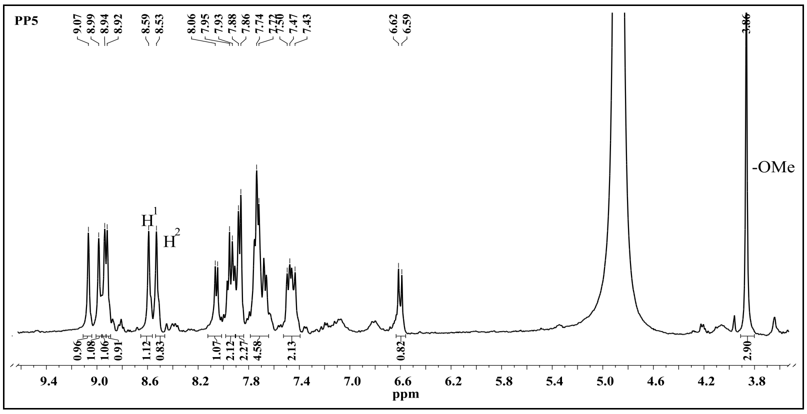

Figure 5.19 The ^{1}H NMR spectrum of PP5 in CD_3OD

Interestingly, we found the methyl ester at 3.86 ppm (3 protons) was observed from methyl ester proton of **PP2** at 3.85 ppm (Figure 5.17). We conclude that the methyl position was assigned in phenyl ring. **PP5** was formed from partial hydrolysis in complexation step. The chemical structure of **PP5** is shown in Figure 5.20.

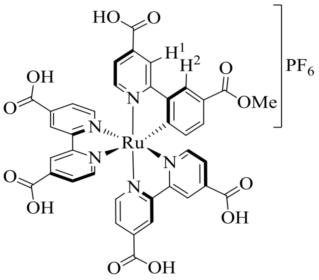

Figure 5.20 The chemical structure of PP5

Furthermore, IR spectrum show the peaks at 3407 cm^{-1} assigned to O-H stretching of carboxylic acid, 1707 and 1229 cm^{-1} assigned to C=O and C-O stretching of carbonyl, respectively. The mass spectra show the peaks at 866.7410 m/z assigned to M$^+$-PF$^-_6$-2H$^+$+Na$^+$ (in Figure A.24, appendices).

From the ^{1}H NMR data, it should note that **PP2**, **PP3** and **PP5** showed the mixtures of unidentified species which can't purify by the recrystallization.

5.3 Photophysical properties

The absorption spectra of these complexes were studied at room temperature (5×10^{-5} M in ethanol) which is displayed in Figure 5.21.

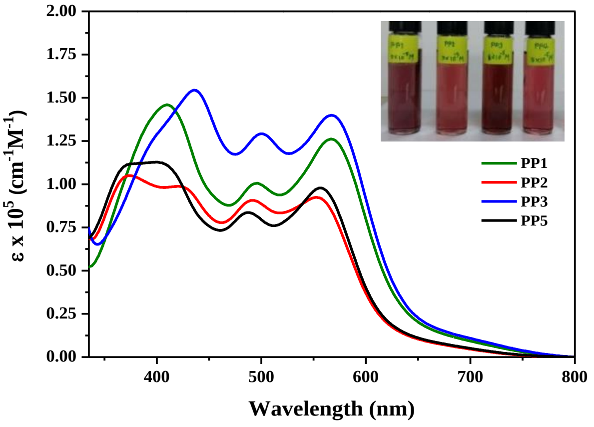

Figure 5.21 UV-Visible absorption spectra and the color solution of PP1, PP2, PP3 and PP5 in ethanol

Generally, all the complexes showed intense $\pi\rightarrow\pi^*$ transitions of the ligands below 390 nm. While the broad absorption coverage originated from metal to ligand charge transfer (MLCT) was detected three main bands at around 560, 490 and 400 nm which are similar to complex **P2** (chapter 4) [30], [57]. The three main absorption spectra were assigned by HOMO+2→LUMO+1, HOMO→LUMO+2 and HOMO-2→LUMO+2, respectively, which are reported in the literature (Figure 5.22) [14].

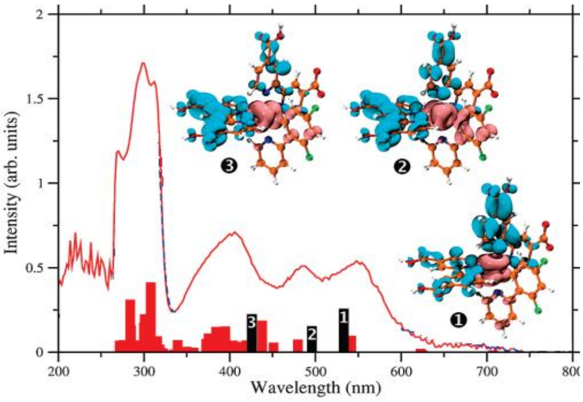

Figure 5.22 UV-visible experimental absorption spectra of complex 1 in DMF solution. Red bars represent the computed vertical electronic excitations intensities (TDDFT) of complex 1. For three selected optically active electronic transitions (black bars with labels 1, 2, and 3 at 533, 496, and 426 nm, respectively)

The maximum absorption (λ_{max}) and molar extinction coefficients (ε_{max}) are summarized in Table 5.1.

Table 5.1 Photophysical properties of PP1, PP2, PP3 and PP5

Dye	**λ_{max1}/nm (ε_{max1}/10^4 $M^{-1}cm^{-1}$)**	**λ_{max2}/nm (ε_{max2}/10^4 $M^{-1}cm^{-1}$)**	**λ_{max3}/nm (ε_{max3}/10^4 $M^{-1}cm^{-1}$)**
PP1	566 (1.23)	495 (1.03)	410 (1.48)
PP2	555 (0.93)	490 (0.91)	424 (0.99)
PP3	567 (1.40)	499 (1.30)	435 (1.56)
PP5	553 (0.98)	487 (0.84)	405 (1.13)

The complexes show the molar extinction coefficients from 0.84 - 1.56×10^4 M^{-1}cm^{-1}. The ε_{max} of **PP3** (1.40×10^4 M^{-1}cm^{-1}) shows the highest intensity others than (**PP1** = 1.23×10^4 M^{-1}cm^{-1}, **PP2** = 0.93×10^4 M^{-1}cm^{-1} and **PP5** = 0.98×10^4 M^{-1}cm^{-1}). It was found that the solutions color of **PP3** shows strong intensity colour more than other dyes, in Figure 5.21 (inside).

5.4 Electrochemical properties

The cyclic voltammograms of the complexes are shown in Figure 5.23.

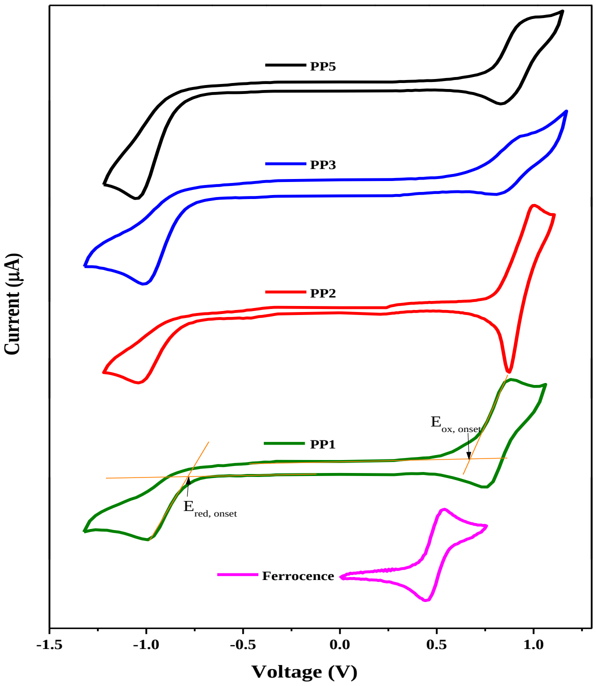

Figure 5.23 The cyclic voltammograms of PP1, PP2, PP3 and PP5 in dry DMF with 100 mV/s scan rate

The complexes **PP1**, **PP2, PP3** and **PP5** show quasi-reversible reaction due to the oxidation of the Ru^{2+}/Ru^{3+} couple at 0.81, 0.93, 0.85 and 0.90 V, respectively. The reduction peaks of the complexes are observed at -0.93 and -0.92, -0.91 and -0.92 V for **PP1**, **PP2**, **PP3** and **PP5**, respectively.

Moreover, the onset oxidation (E$_{ox, onset)}$, onset reduction (E$_{red, onset}$) potentials, HOMO, LUMO and Energy gap can calculate the same way as pure dyes in chapter 4 which are summarized in Table 5.2.

Table 5.2 Electrochemical properties of PP1, PP2, PP3 and PP5

Dye	$E_{ox, onset}$ (V)	$E_{red, onset}$ (V)	E_{HOMO} (eV)	E_{LUMO} (eV)	E_g (eV)
PP1	0.64	-0.78	-4.96	-3.54	1.42
PP2	0.78	-0.81	-5.10	-3.51	1.59
PP3	0.66	-0.79	-4.98	-3.53	1.45
PP5	0.76	-0.82	-5.08	-3.50	1.58

The calculated LUMO levels of dyes are -3.54, -3.51, -3.53 and -3.50 eV which can inject to the conduction band of TiO_2 (-4.40 eV). In contrast, the calculated HOMO levels of all dyes afforded -4.96, -5.10, -4.98 and -5.08 eV, relative to that of the redox couple I^-/I^-_3 (-4.90 eV) which can be regenerate form to a ground state. This can successfully provide ample driving force for dye regeneration to complete the circuit and restore the dyes, in Figure 5.24.

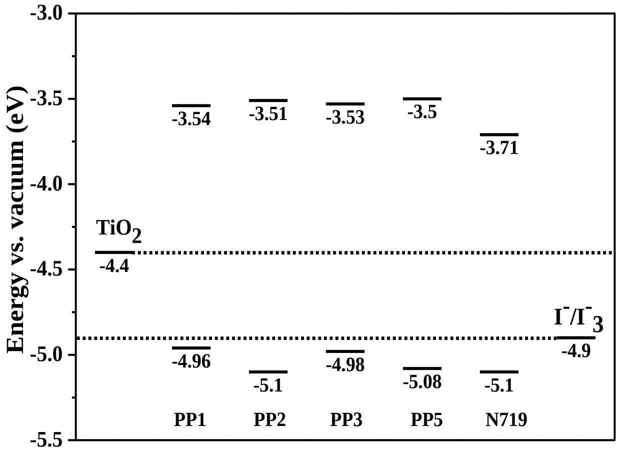

Figure 5.24 Energy level of the ruthenium complexes (PP1-PP5) for comparison with the conduction band of TiO_2 and iodide/tri-iodide couple

The similar LUMO and varied HOMO levels can be explained by density functional theory (DFT), in Figure 2.25 [31]. The fact that the LUMO orbitals are localized on the N^N ligand (2,2'-bipyridine-4,4'-dicarboxylic acid) whereas, the HOMO mainly distributed in ruthenium and C^N ligands. It should note that **PP2** and

PP5 show lower HOMO levels than **PP1** due to the electron withdrawing group in phenyl ring.

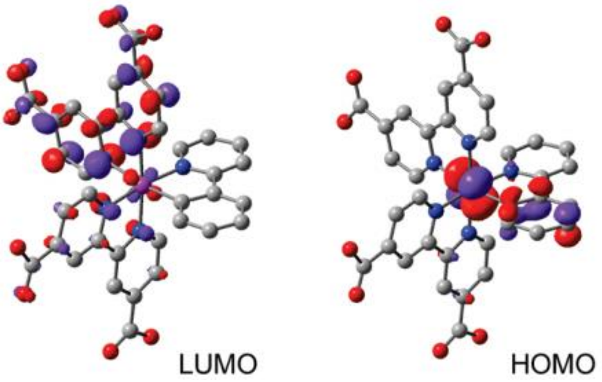

Figure 2.25 Frontier molecular orbitals of 1 illustrating the motivation to install substituents on the phenyl ring of the C∧N ligand to achieve optimal interaction with the HOMO. (Color scheme: Ru = purple; N = blue; O = red; C = gray; H atoms not shown) [31]

5.5 Photovoltaic performance

The I-V characteristic of the DSSCs based on **PP1**, **PP2, PP3**, **PP5** and **N719** is shown in Figure 5.26.

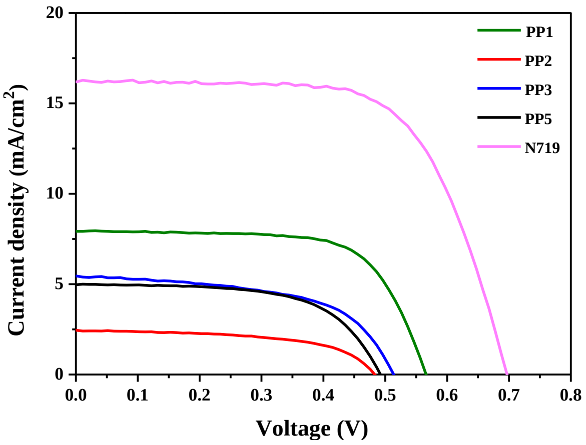

Figure 5.26 The I-V curve of DSSCs based on PP1, PP2, PP3, PP5 and N719

Overall performance including J_{SC}, V_{OC}, FF and η are summarized in Table 4.5. It was found that, **PP1**, **PP2**, **PP3** and **PP5** show efficiency of 3.10%, 0.69%, 1.54% and 1.53% respectively, compared with **N719** of 7.44%.

The I-V characteristics of photovoltaic of all devices under standard AM 1.5 was found that the thiocyanate free ruthenium complexes showed a lower performance than **N719**. We think that the LUMO and condition of TiO_2 show the big different more than 0.2 eV affected to difficultly the electron injection, in Figure 5.24 [53]. The DSSC results showed that **PP1** gave high efficiencies at 3.10% compared with other synthetic complexes because of high the J_{SC}, V_{OC} and FF. The purity of complex could be a responsible.

Table 5.3 The photovoltaic parameters of DSSC devices from PP1-PP5

Dyes	J_{SC} (mA/cm^2)	V_{OC} (mV)	FF	η (%)
PP1	7.99	563	0.69	3.10
PP2	2.47	484	0.58	0.69
PP3	5.03	492	0.62	1.54
PP5	5.24	511	0.57	1.53
N719	16.19	697	0.65	7.44

CHAPTER 6

CONCLUSIONS

The ruthenium complexes for DSSCs were successfully synthesized by ligand substitution reaction. The molecular structural of ruthenium complexes were characterized by NMR, FTIR and Mass technique. The FTIR spectrum show the broad peaks of O-H stretching of carboxylic acid, C=O and C-O stretching of carbonyl and C=C of aromatic. These results confirm the carboxylic acid and ester functional group. The photophysical was studied by UV-Visible absorption. The results show that the high extinction coefficient. Furthermore, the electrochemical was studied by cyclicvoltammetry (CV) method. It was found the LUMO level of dye shows higher than that of the conduction band of the TiO_2 and the HOMO of dye shows more negative than the iodide/tri-iodide.

In the first part, the DSSCs performances of co-sensitizers (**P2+N719** and **YN07+N719**) were studied compared with the **N719** dye under AM 1.5 irradiation. It was found that, the power efficiencies of **P2+N719** and **YN07+N719** show efficiency of 2.37% and 1.59%, respectively, compared with standard **N719** (5.14%). However, the molecular size and unsuitable HOMO can be a responsible to low power efficiencies.

In the second part, four novel thiocyanate free ruthenium(II) complexes based on differance C^N ligand were successfully synthesized and characterized. It was found that, the **PP1**, **PP2**, **PP3** and **PP5** show efficiency of 3.10%, 0.69%, 1.54% and 1.53%, respectively compared with standard **N719** (7.44%). The low performance can be explained by the unsuitable LUMO and purity of the synthetic complexes.

The photovoltaic parameters of co-sensitization (Part 1) and thiocyanate free ruthenium(II) complexes (Part 2) are summarized in Table 6.1.

Table 6.1 The photovoltaic parameters of DSSC devices

Part 1: co-sensitization from ruthenium(II) complexes				
Dye	**J_{SC} (mA/cm^2)**	**V_{OC} (mV)**	**FF**	**η (%)**
N719	12.02	600	0.71	5.17
P2	3.82	520	0.72	1.42
YN07	1.41	480	0.68	0.46
P2+N719	5.84	560	0.73	2.37
YN07+N719	4.08	530	0.74	1.59
Part 2: thiocyanate free ruthenium(II) complexes				
Dye	**J_{SC} (mA/cm^2)**	**V_{OC} (mV)**	**FF**	**η (%)**
PP1	7.99	563	0.69	3.10
PP2	2.47	484	0.58	0.69
PP3	5.03	492	0.62	1.54
PP5	5.24	511	0.57	1.53
N719	16.19	697	0.65	7.44

REFERRENCES

REFERRENCES

[1] Green, M. A., "The path to 25% silicon solar cell efficiency: History of silicon cell evolution", **Progress in Photovoltaics: Research and Applications**. 17: 183-189; April, 2009.

[2] Dimroth, F. and et al. "Wafer bonded four-junction GaInP/GaAs//GaInAsP/ GaInAs concentrator solar cells with 44.7% efficiency", **Progress in Photovoltaics: Research and Applications**. 22(3): 277-282; March, 2014.

[3] O'regan, B., and Grätze, M. "A low-cost, high-efficiency solar cell based on dye-sensitized colloidal TiO_2 films", **Nature**. 353(6346): 737-740; October, 1991.

[4] Qin, Y., and Peng, Q. "Ruthenium sensitizers and their applications in dye-sensitized solar cells", **International Journal of Photoenergy**. 2012: 6346-9385; February, 2012.

[5] Basheer, B. and et al. "An overview on the spectrum of sensitizers: the heart of dye sensitized solar cells", **Solar Energy**. 108: 479-507; October , 2014.

[6] Nazeeruddin, M. K. and et al. "Dye-sensitized solar cells: A brief overview", **Solar Energy**. 85(6): 1172-1178; June, 2011.

[7] Yali Sun. **The development of novel ru(II) polypyridyl complexes for application in dye sensitized solar cells**. Doctor's Thesis: Bowling Green State University, 2009.

[8] Huang. W. K. and et al. "Design and characterization of heteroleptic ruthenium complexes containing benzimidazole ligands for dye-sensitized solar cells: the effect of fluorine substituents on photovoltaic performance", **Journal of Physical Chemistry Letters**. 3(13): 1830-1835; June, 2012.

[9] Han, L. and et al. "High-efficiency dye-sensitized solar cell with a novel co-adsorbent", **Energy & Environmental Science**. 5: 6057-6060; January, 2012.

[10] Nazeeruddin, M. K. and et al. "Combined experimental and DFT-TDDFT computational study of photoelectrochemical cell ruthenium sensitizers", **Journal of the American Chemical Society**. 127(48): 16835-47; November, 2005.

REFERRENCES (CONTINUED)

[11] Kim, J. J. and et al. “New efficient ruthenium sensitizers with unsymmetrical indeno[1,2-b]thiophene or a fused dithiophene ligand for dye-sensitized solar cells”, **Inorganic Chemistry**. 49(18): 8351-8357; September, 2010.

[12] Kalyanasundaram, K. and Grätze, M. “Efficient dye-sensitized solar cells for direct conversion of sunlight to electricity”, **Material Matters**. 4(4): 88-94; January, 2009.

[13] Liu, K.Y. and et al. “Photovoltaic properties of dye-sensitized solar cells associated with amphiphilic structure of ruthenium complex dyes”, **Journal of Colloid and Interface Science**. 372(1): 73-79; April, 2012.

[14] Bessho, T. and et al. “New Paradigm in Molecular Engineering of Sensitizers for Solar Cell Applications”, **Journal of the American Chemical Society**. 131(16): 5930-5934; March, 2009.

[15] Hagfeldt, A., and Grätze, M. “Light-induced redox reactions in nanocrystalline systems”, **Chemical Reviews**. 95(1): 49-68; January, 1995.

[16] Nazeeruddin, M. K. and et al. “Conversion of light to electricity by cis X_2bis(2,2'-bipyridyl-4,4'-dicarboxylate)ruthenium(II) charge-transfer sensitizers ($X = Cl^-$, Br^-, I^-, CN^-, and SCN^-) on nanocrystalline titanium dioxide electrodes”, **Journal of the American Chemical Society**. 115(14): 6382-6390; July, 1993.

[17] Hara, K., and Arakawa, H. “Dye-sensitized solar cells”, **National Institute of Advanced Industrial Science and Technology (AIST)**. https://www.researchgate.net/publication/228038382_Dye-Sensitized_Solar_Cells. 18 May 2016.

[18] Kuang, D. and et al. “Co-sensitization of organic dyes for efficient ionic liquid electrolyte based dye-sensitized solar cells”, **Langmuir**. 23(22): 10906-10909; September, 2007.

[19] Lin, L. Y. and et al. “Insights into the co-sensitizer adsorption kinetics for complementary organic dye-sensitized solar cells”, **Journal of Power Sources**. 247: 906-914; February, 2014.

REFERRENCES (CONTINUED)

[20] Yu, L. and et al. “Efficient panchromatic light harvesting with co-sensitization of zinc phthalocyanine and bithiophene-based organic dye for dye-sensitized solar cells”, **American Chemical Society sustainable chem engineering**. 2(4): 718-725; January, 2014.

[21] Singh, S. P. and et al. “Co-sensitization of amphiphilic ruthenium (II) sensitizer with a metal free organic dye: Improved photovoltaic performance of dye sensitized solar cells”, **Organic Electronics**. 14(5): 1237-1241; May, 2013.

[22] Ogura, R. Y. and et al. “High-performance dye-sensitized solar cell with a multiple dye system”, **Applied Physics Letters**. 94: 073308-073308-3; February, 2009.

[23] Shi, Y. and et al. “New ruthenium sensitizers featuring bulky ancillary ligands combined with a dual functioned coadsorbent for high efficiency dye-sensitized solar cells”, **ACS Applied Materials & Interfaces**. 5(1): 144-153; December, 2013.

[24] Ranasinghe, C. S. K. and et al. “An enhancement of efficiency of a solid-state dye-sensitized solar cell due to cocktail effect of N719 and black dye”, **Optik**. 125(2): 813-815; January, 2014.

[25] Siu, S. H. and et al. “Thiocyanate-free ruthenium(II) cyclometalated complexes containing uncommon thiazole and benzothiazole chromophores for dye-sensitized solar cells”, **Journal of Organometallic Chemistry**. 748: 75-83; December, 2013.

[26] Dragonetti, C. and et al. “Thiocyanate-free ruthenium(ii) sensitizer with a pyrid-2-yltetrazolate ligand for dye-sensitized solar cells”, **Inorganic Chemistry**. 52(19): 10723-10725; September, 2013.

[27] Singh, S. P. and et al. “Development of a new class of thiocyanate-free cyclometalated ruthenium(ii) complex for sensitizing nanocrystalline TiO_2 solar cells”, **International Journal of Photoenergy**. 2011: 520848-520853; January, 2011.

REFERRENCES (CONTINUED)

[28] Funaki, T. and et al. “New class of thiocyanate-free cyclometalated ruthenium(II) complexes having a pyridylquinoline derivative for near-infrared sensitization of dye-sensitized solar cells”, **Inorganic Chemistry Communications**. 35: 281-283; September, 2013.

[29] Claudia, D. and et al. “A new thiocyanate-free cyclometallated ruthenium complex for dye-sensitized solar cells: Beneficial effects of substitution on the cyclometallated ligand”, **Journal of Organometallic Chemistry**, 714(2012): 88-93; March, 2012.

[30] Schott, E., Zarate, X., and Perez, R. A. “Substituents effects on two related families of dyes for dye sensitized solar cells: $[Ru(4,4'\text{-}R,R\text{-}2,2'\text{-}bpy)_3]^{2+}$and $[Ru(4,4'\text{-}COOH\text{-}2,2'\text{-}bpy)(4,4'\text{-}R,R\text{-}2,2'\text{-}bpy)_2]^{2+}$”, **The Journal of Physical Chemistry A**. 116(27): 7436-7442; June, 2012.

[31] Paolo G, B. and et al. “On the viability of cyclometalated Ru(II) complexes for light-harvesting applications”, **Inorganic Chemistry**. 48(20): 9631-9643; September, 2009.

[32] Paolo G, B. and et al. “Cyclometalated Ru complexes of type $[RuII(N\^{}N)_2(C\^{}N)]^z$: physicochemical response to substituents installed on the anionic ligand”, **Inorganic Chemistry**. 49: 4960-4971; May, 2010.

[33] Ocakoglu, K. and et al. “Design and synthesis of heteroleptic ruthenium (II) complexes and their applications in nanocrystalline TiO_2 solar cells”, **Inorganic Chemistry Communications**. 24: 118-124; October, 2012.

[34] Huang, J. F. and et al. “Highly efficient and stable cyclometalated ruthenium(II) complexes as sensitizers for dye-sensitized solar cells”, **Electrochimica Acta**. 174: 494-501; August, 2015.

[35] Liu, K. Y. and et al. “Synthesis and characterization of cross-linkable ruthenium complex dye and its application on dye-sensitized solar cells”, **Journal of Polymer Science**. 48(2): 366-372; December, 2010.

[36] Bennett, M. A. and Smith, A.K. “Arene ruthenium(II) complexes formed by dehydrogenation of cyclohexadienes with ruthenium(III) trichloride”, **Journal of the Chemical Society, Dalton Transactions**. 3(2): 233-241; March, 1974.

REFERRENCES (CONTINUED)

[37] Prompan, P. and et al. “Design and synthesis of ruthenium (II) complexes and their applications in dye sensitized solar cells (DSSCs)”, **Advanced Materials Research**. 770: 92-95; September, 2013.

[38] Nazeeruddin, M. K. and et al. “Acid-base equilibria of (2,2'-bipyridyl-4,4'-dicarboxylic acid) ruthenium(II) complexes and the effect of protonation on charge-transfer sensitization of nanocrystalline titania”, **Inorganic Chemistry**. 38(26): 6298-6305; December, 1999.

[39] Yuranan Thathong. **The synthesis and characterization of ruthenium complexes for dye sensitized solar cells application**. Master’s Thesis: Ubon Ratchathani University, 2013.

[40] Mothajit, K. and et al. “A Novel charged iridium(III) complex for amine sensor application”, **Advanced Materials Research**. 893: 91-94; February, 2014.

[41] Khammultri, N. and et al. “Suzuki-Miyaura reaction; novel synthesis of C-N and N-N Ligands for organic light-emitting eevices”, **Advanced Materials Research**. 622-623: 236-240; December, 2013.

[42] Alessandro, A. and et al. “Thiocyanate-free cyclometalated ruthenium sensitizers for solar cell on heteroaromatic-substituted 2-arylpyridines”, **Dalton Transactions**. 41(38): 11731-11738; August, 2012.

[43] Erten-Ela, S., and Ocakoglub, O. “Fabrication of thin film nanocrystalline TiO_2 solar cells using ruthenium complexes with carboxyl and sulfonyl groups”, **Journal of Industrial and Engineering Chemistry**. 20(2): 474-479; March, 2014.

[44] Chonchanok Talodthaisong. **Novel ruthenium complexes for dye sensitized solar cell**. Master’s Thesis: Ubon Ratchathani University, 2015.

[45] Nazeeruddin, M. K. and et al. “Combined Experimental and DFT-TDDFT computational study of photoelectrochemical cell ruthenium sensitizers”, **Journal of the American Chemical Society**. 127(48): 16835-16847; November, 2005.

REFERRENCES (CONTINUED)

[46] Fan, S.H. and et al. “A triphenylamine-grafted imidazo[4,5-f][1,10] phenanthroline ruthenium(II) complex: acid-base and photo electric properties”, **Inorganic Chemistry**. 49(8): 3752-3763; March, 2010.

[47] Chen, C. T. and et al. “A ruthenium complex with superhigh light-harvesting capacity for dye-sensitized solar cells”, **Angewandte Chemie International Edition**. 45(35): 5822-5825; September, 2006.

[48] Chang, J. and et al. “Co-sens itization promoted light harvesting for organic dye-sensitized solar cells using unsymmetrical squaraine dye and novel pyrenoimidazole-based dye”, **Journal of Power Sources**. 240: 779-785; October, 2013.

[49] Bayliss, S. L. and et al. “Predicting solar-cell dyes for cosensitization”, **The Journal of Physical Chemistry C**. 118(26): 14082-14090; June, 2014.

[50] Huang, W. K. and et al. “Design and characterization of heteroleptic ruthenium complexes containing benzimidazole ligands for dye-sensitized solar cells: the effect of fluorine substituents on photovoltaic performance”, **The Journal of Physical Chemistry Letters**. 3(13): 1830-1835; June, 2012.

[51] Lennox, A. J. J. and Lloyd-Jones, G. C. “Selection of boron reagents for Suzuki-Miyaura coupling”, **Chemical Society Reviews**. 43: 412-443; October, 2013.

[52] Hua, Y. and et al. “Significant improvement of dye-sensitized solar cell performance using simple phenothiazine-based dyes”, **Chemistry of Materials**. 25(10): 2146-2153; April, 2013.

[53] Siu, C. H. and et al. “Optimizing the photovoltaic performance of thiocyanate-free ruthenium photosensitizers by structural modification of C^N cyclometalating ligand in dye-sensitized solar cells”, **Polyhedron**. 82: 71-79; October, 2014.

[54] Thathong, T. and et al. “Air-stable anthracene-phosphine oxide adduct ligand in Pd catalysed Suzuki-Miyaura reactions”, **APCBEE Procedia**. 3: 154-160; December, 2012.

REFERRENCES (CONTINUED)

[55] Hamilton, A. E. and et al. “An operationally simple aqueous Suzuki-Miyaura cross-coupling reaction for an undergraduate organic chemistry laboratory”, **Journal of Chemical Education**. 90(11): 1509-1513; October, 2013.

[56] Martin, R., and Buchwald, S. L. “Palladium-catalyzed Suzuki-Miyaura cross-coupling reactions employing dialkylbiaryl phosphine ligands”, **Accounts of Chemical Research**. 41(11): 1461-1473; July, 2008.

[57] Wadman, S. H. and et al. “Consequences of N,C,N′- and C,N,N′ coordination modes on electronic and photophysical properties of cyclometalated aryl ruthenium(II) complexes”, **Inorganic Chemistry**. 48(5): 1887-1990; January, 2009.

APPENDICES

APPENDICES A

Characterization data

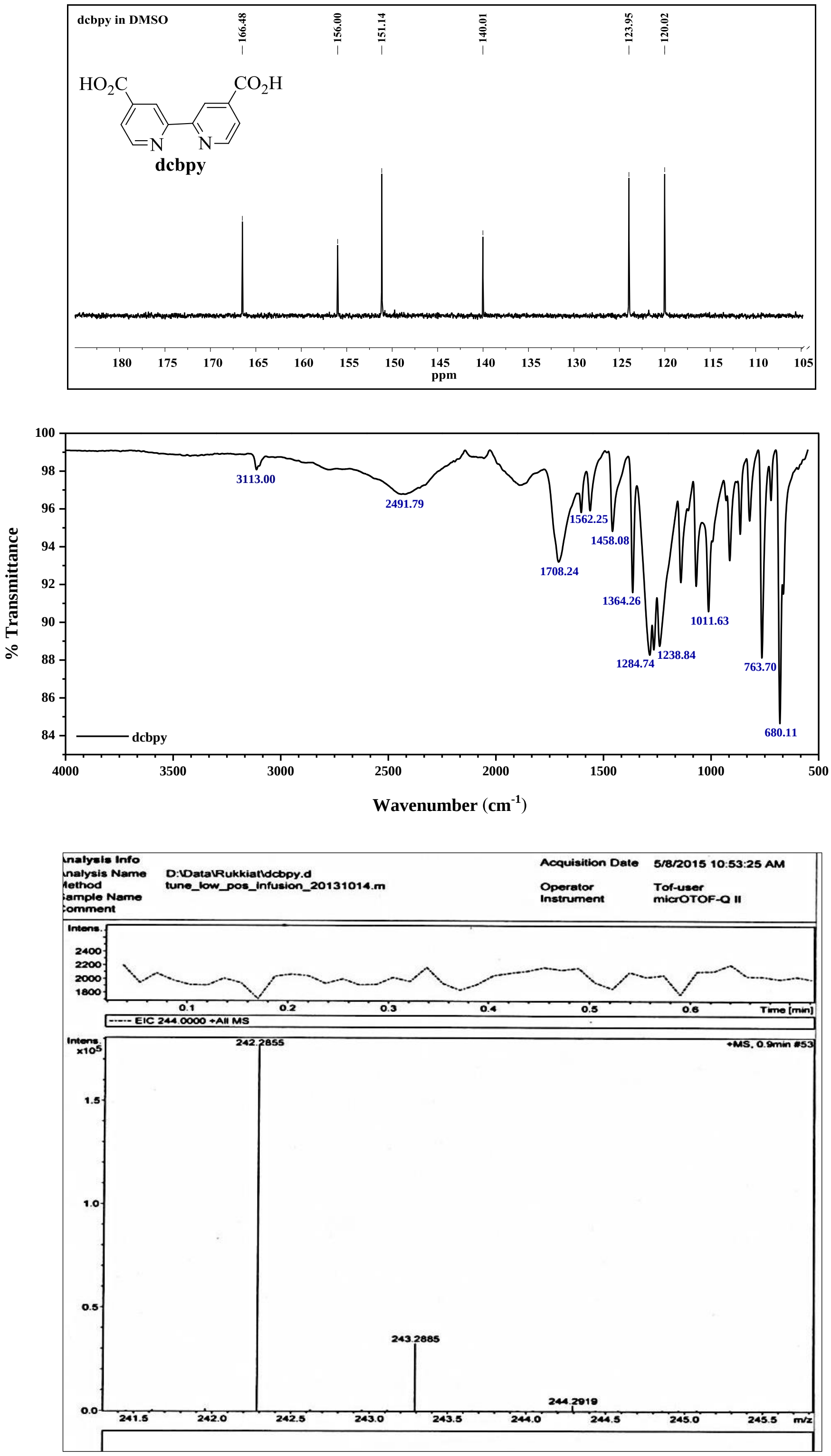

nalysis Info
nalysis Name D:\Data\Rukkiat\dcbpy.d
lethod tune_low_pos_infusion_20131014.m
ample Name
omment
Acquisition Date 5/8/2015 10:53:25 AM
Operator Tof-user
Instrument micrOTOF-Q II

Figure A.1 ^{13}C NMR in DMSO-d$_6$, ATR-FTIR (neat) and mass spectra of dcbpy

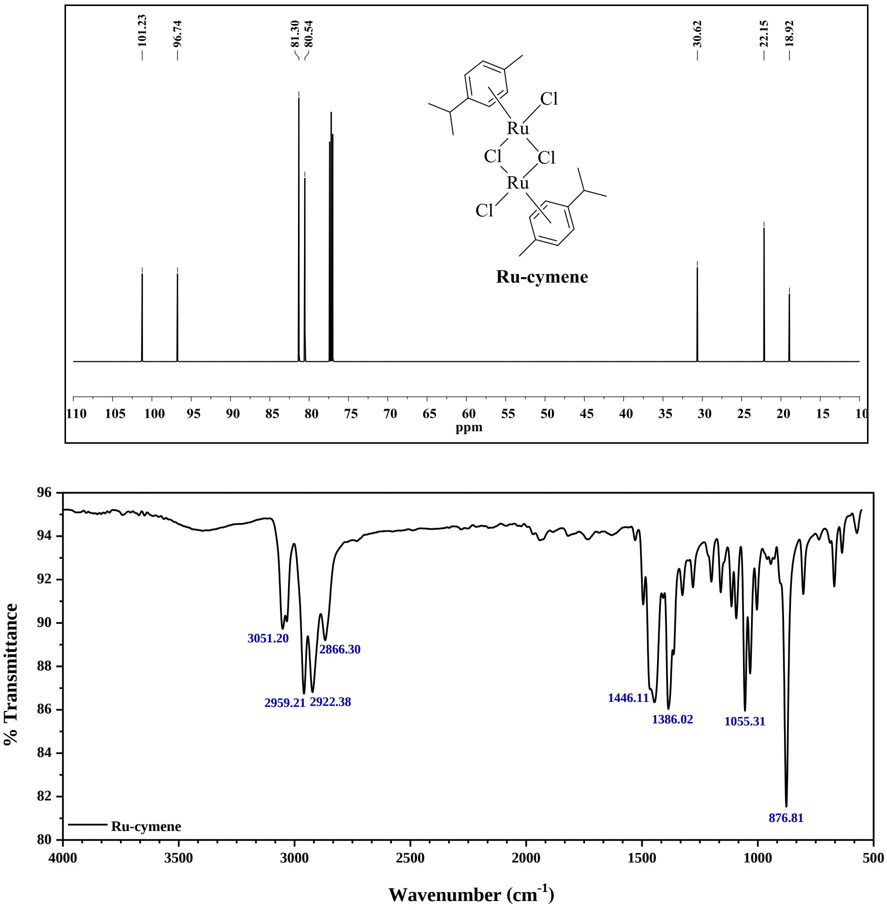

Figure A.2 ^{13}C NMR in $CDCl_3$ and ATR-FTIR (neat) Ru-cymene

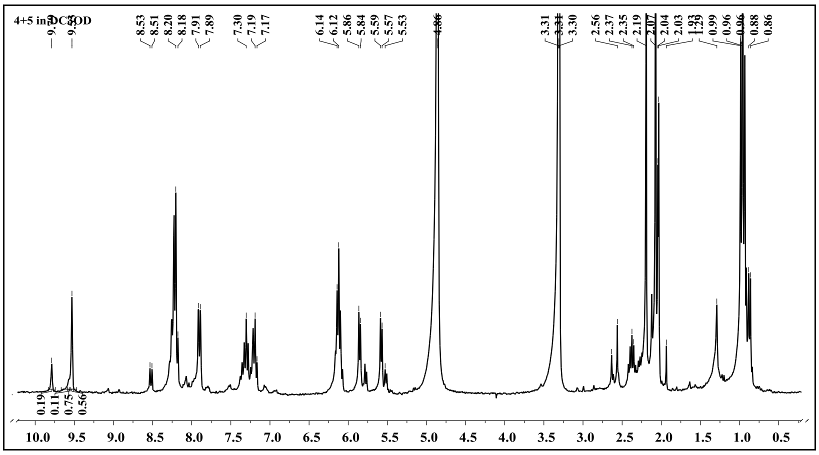

Figure A.3 ^{1}H NMR in CD_3OD of mixing 4 and 5

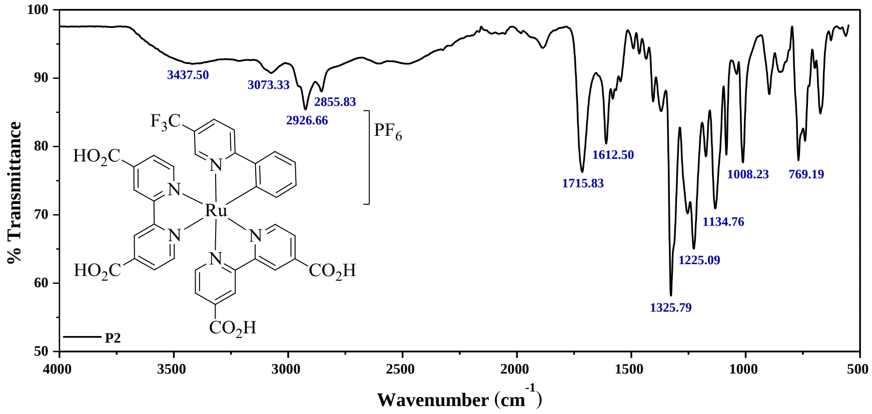

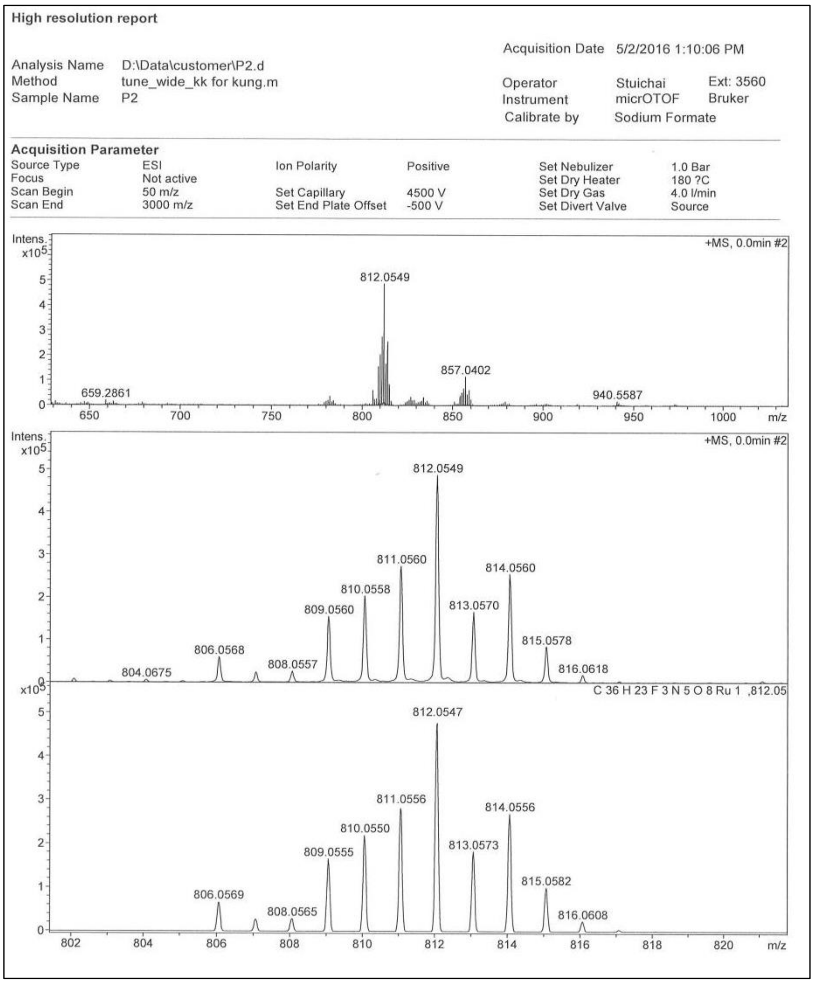

High resolution report

Acquisition Date 5/2/2016 1:10:06 PM

Analysis Name D:\Data\customer\P2.d
Method tune_wide_kk for kung.m
Sample Name P2

Operator Stuichai Ext: 3560
Instrument micrOTOF Bruker
Calibrate by Sodium Formate

Acquisition Parameter

Source Type ESI
Focus Not active
Scan Begin 50 m/z
Scan End 3000 m/z
Ion Polarity Positive
Set Capillary 4500 V
Set End Plate Offset -500 V
Set Nebulizer 1.0 Bar
Set Dry Heater 180 ?C
Set Dry Gas 4.0 l/min
Set Divert Valve Source

Figure A.4 ATR-FTIR (neat) and mass spectrum of P2

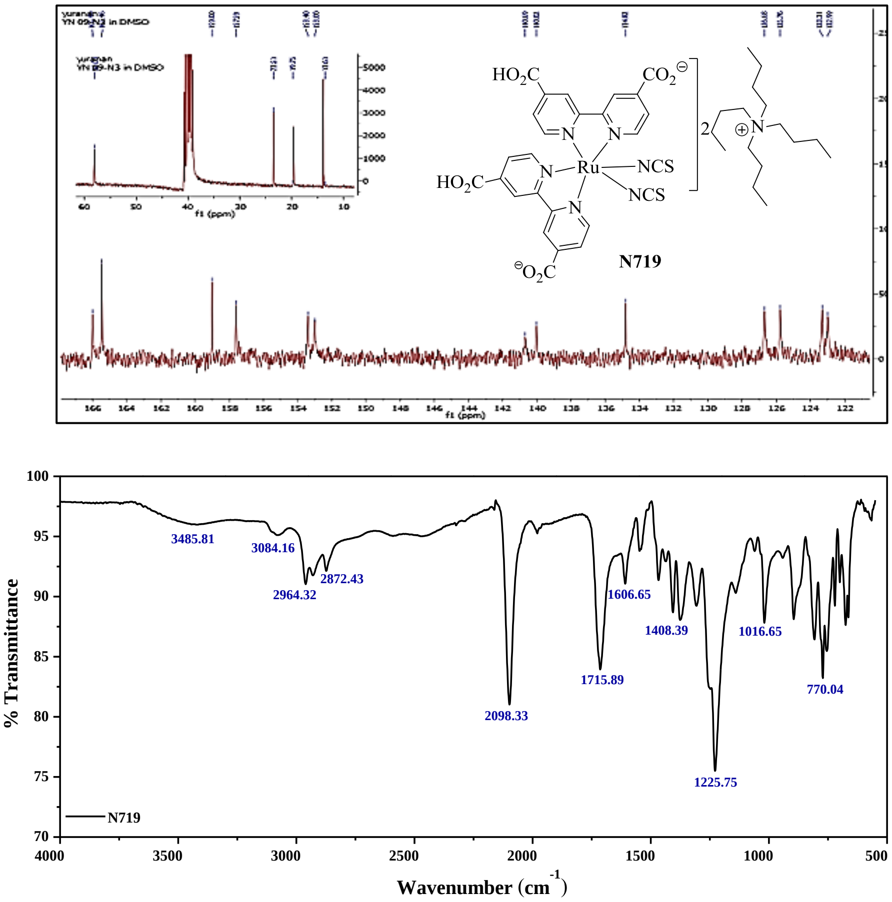

Figure A.5 ^{13}C NMR in CD_3OD [36] and ATR-FTIR (neat) of N719

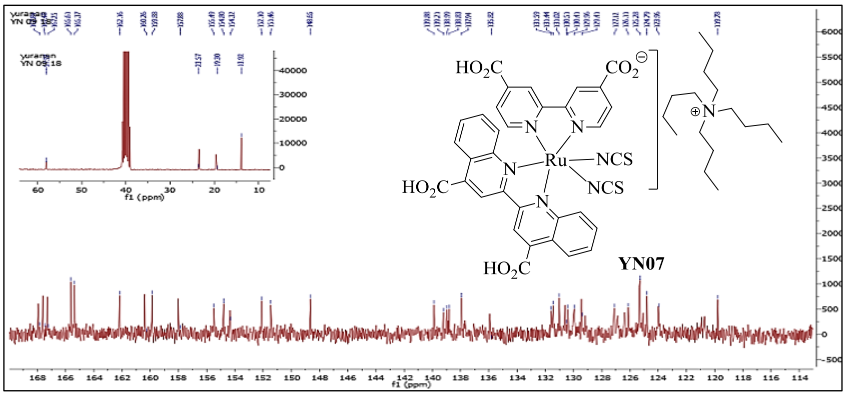

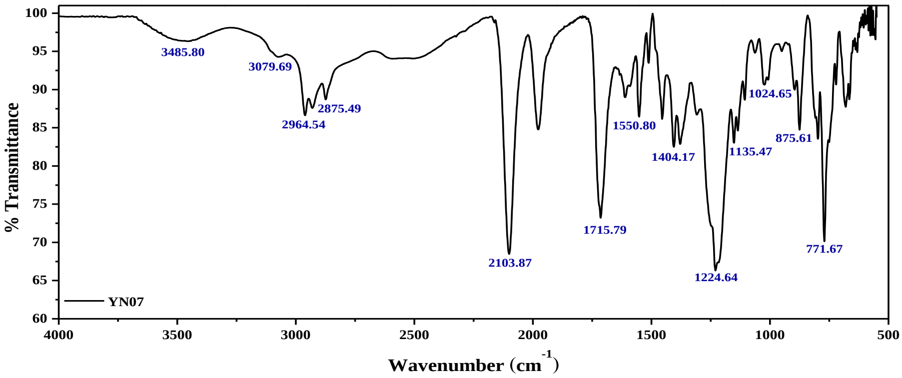

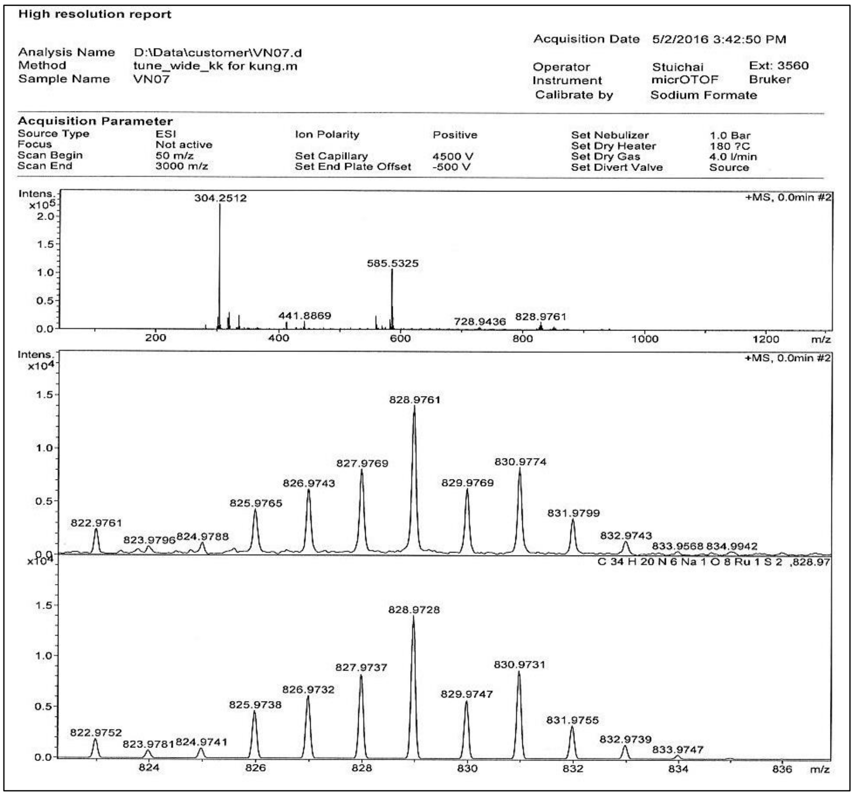
High resolution report

Analysis Name D:\Data\customer\VN07.d
Method tune_wide_kk for kung.m
Sample Name VN07

Acquisition Date 5/2/2016 3:42:50 PM

Operator Stuichai Ext: 3560
Instrument micrOTOF Bruker
Calibrate by Sodium Formate

Acquisition Parameter

Source Type	ESI	Ion Polarity	Positive	Set Nebulizer	1.0 Bar
Focus	Not active			Set Dry Heater	180 ?C
Scan Begin	50 m/z	Set Capillary	4500 V	Set Dry Gas	4.0 l/min
Scan End	3000 m/z	Set End Plate Offset	-500 V	Set Divert Valve	Source

Figure A.6 ^{13}C NMR in DMSO-d$_6$ [37], ATR-FTIR (neat) and mass spectrum of YN07

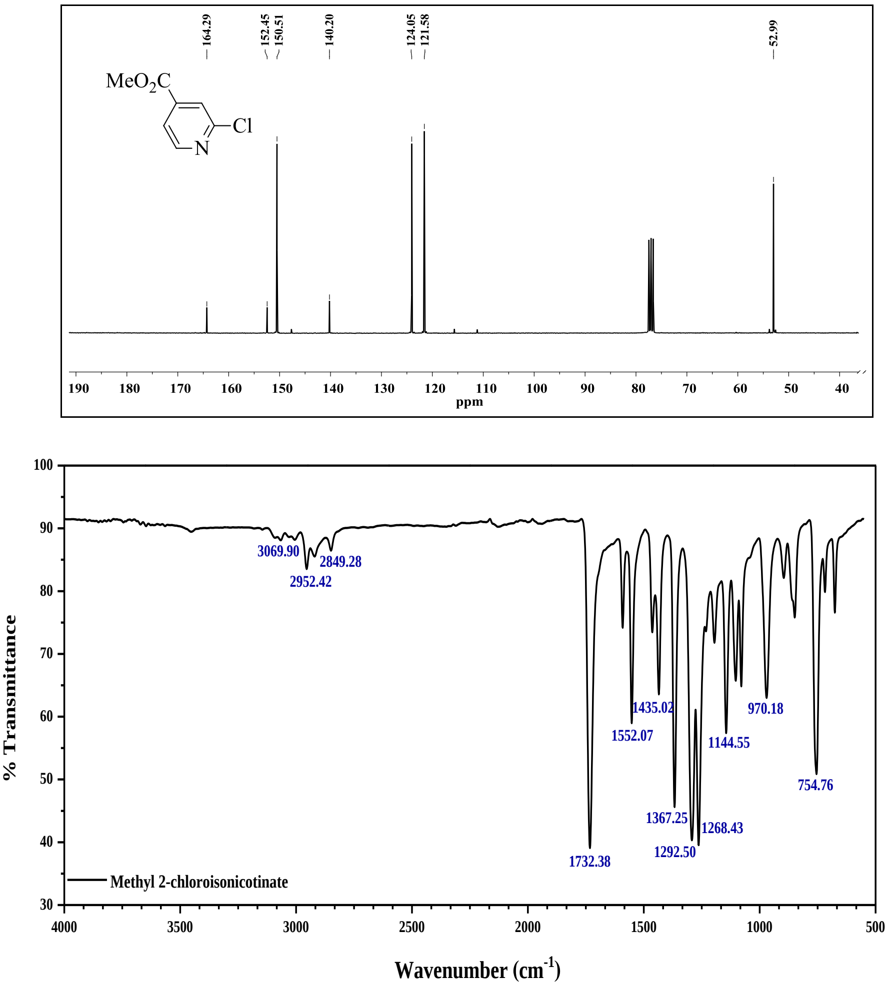

Figure A.7 ^{13}C NMR in $CDCl_3$ and ATR-FTIR (neat) of methyl-2-chloroisonicotinate

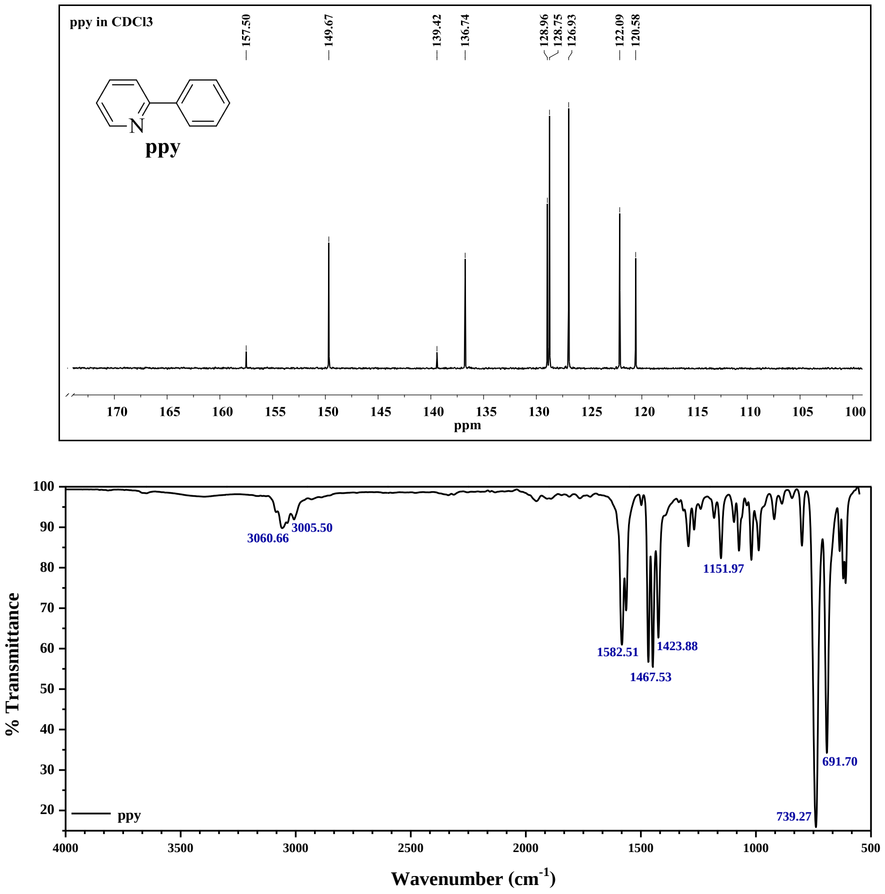

Figure A.8 ^{13}C NMR in $CDCl_3$, ATR-FTIR (neat) and mass spectrum of 2-phenylpyridine

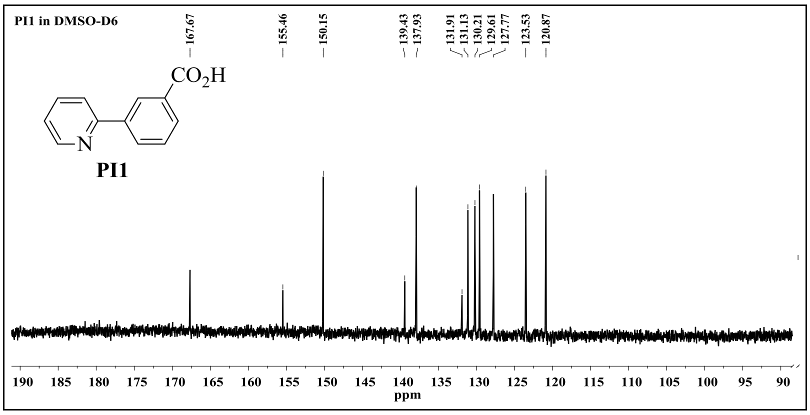

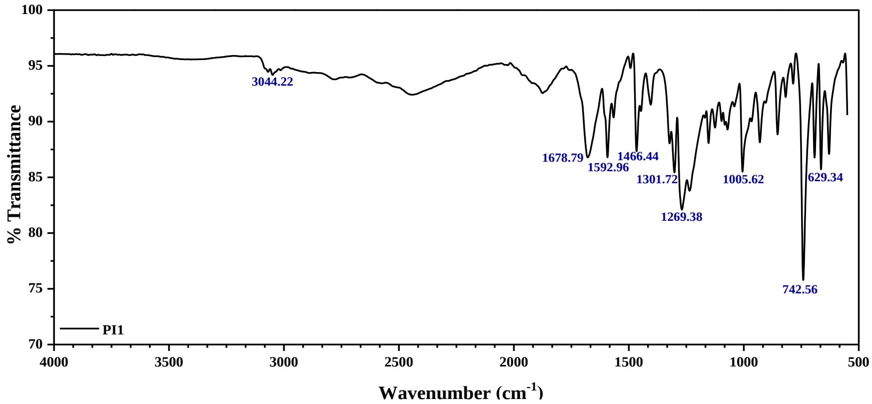

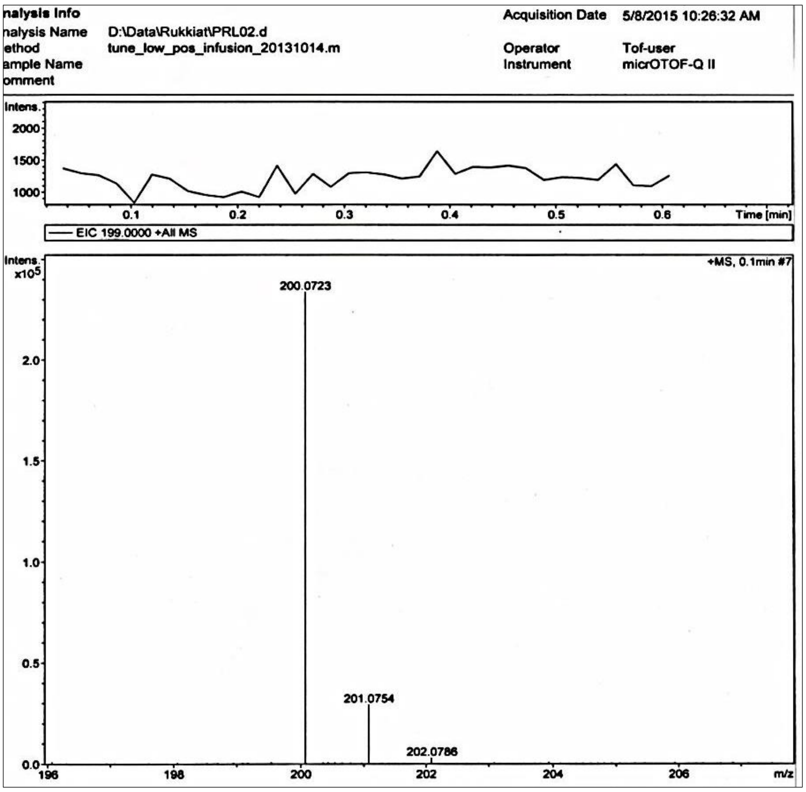

nalysis Info
nalysis Name D:\Data\Rukkiat\PRL02.d
ethod tune_low_pos_infusion_20131014.m
ample Name
omment

Acquisition Date 5/8/2015 10:26:32 AM
Operator Tof-user
Instrument micrOTOF-Q II

Figure A.9 ^{13}C NMR in DMSO-d_6, ATR-FTIR (neat) and mass spectrum of PI1

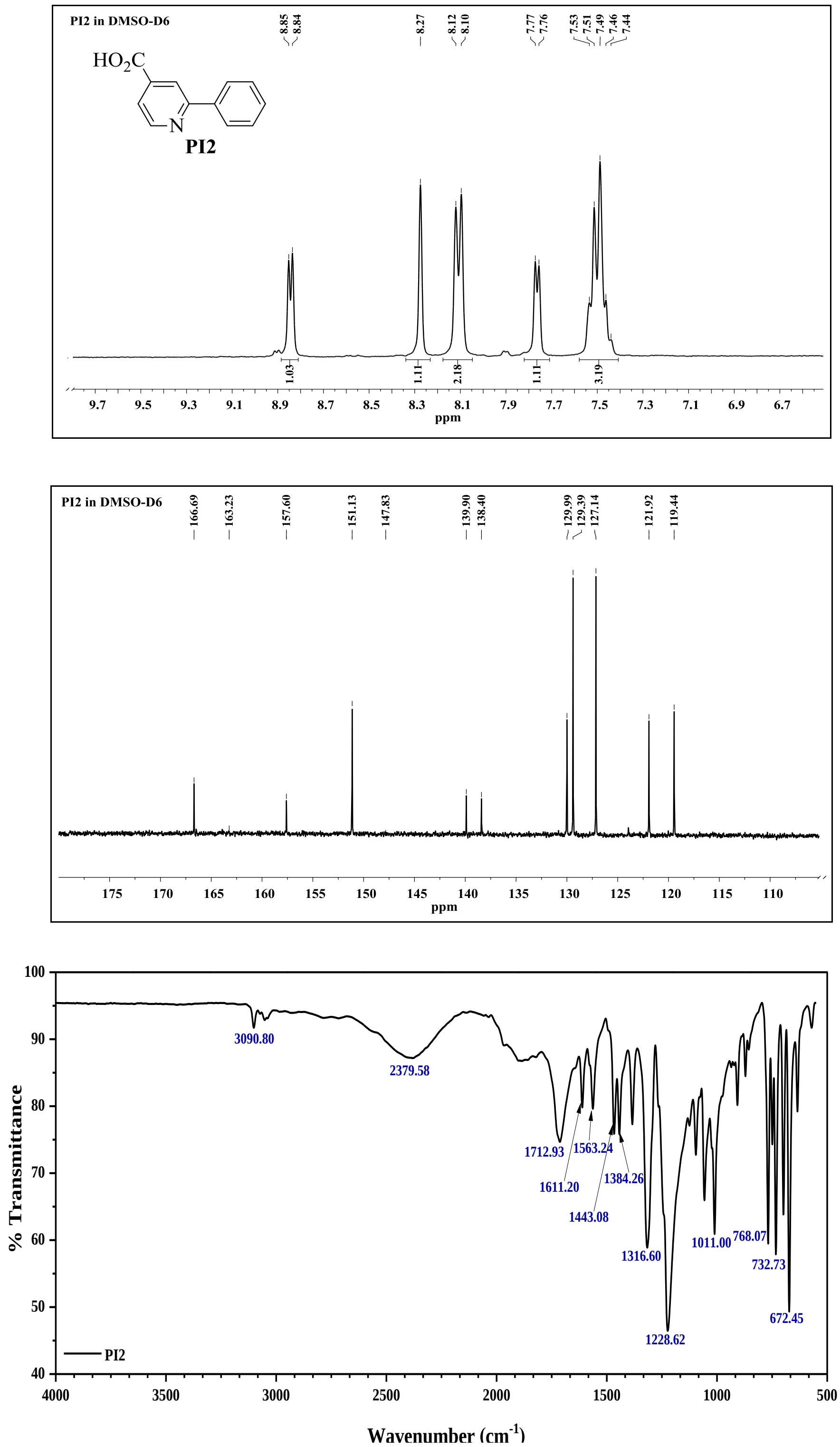

Figure A.10 ^{1}H, ^{13}C NMR in DMSO-d$_6$ and ATR-FTIR (neat) of PI2

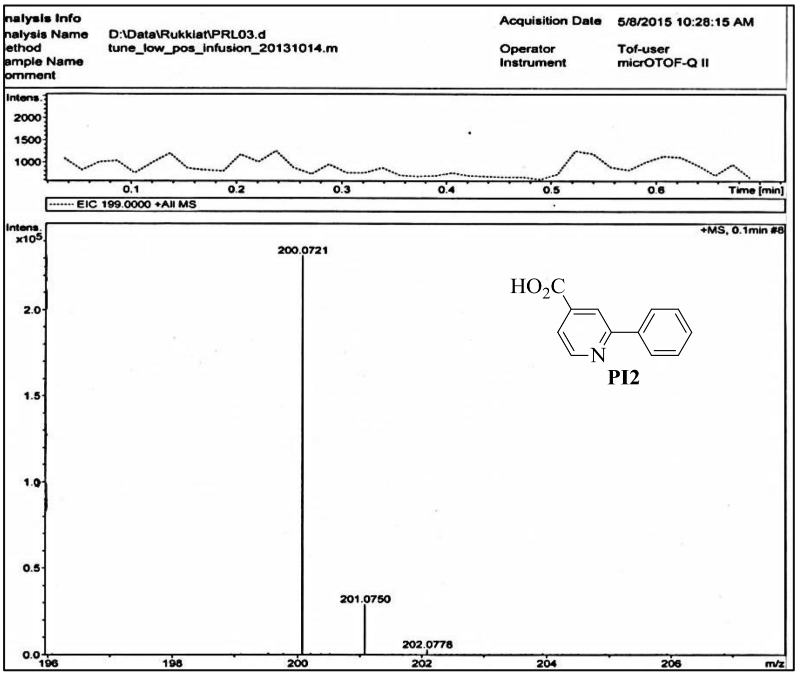

nalysis Info
nalysis Name D:\Data\Rukkiat\PRL03.d
ethod tune_low_pos_infusion_20131014.m
ample Name
omment
Acquisition Date 5/8/2015 10:28:15 AM
Operator Tof-user
Instrument micrOTOF-Q II

Figure A.11 Mass spectrum of PI2

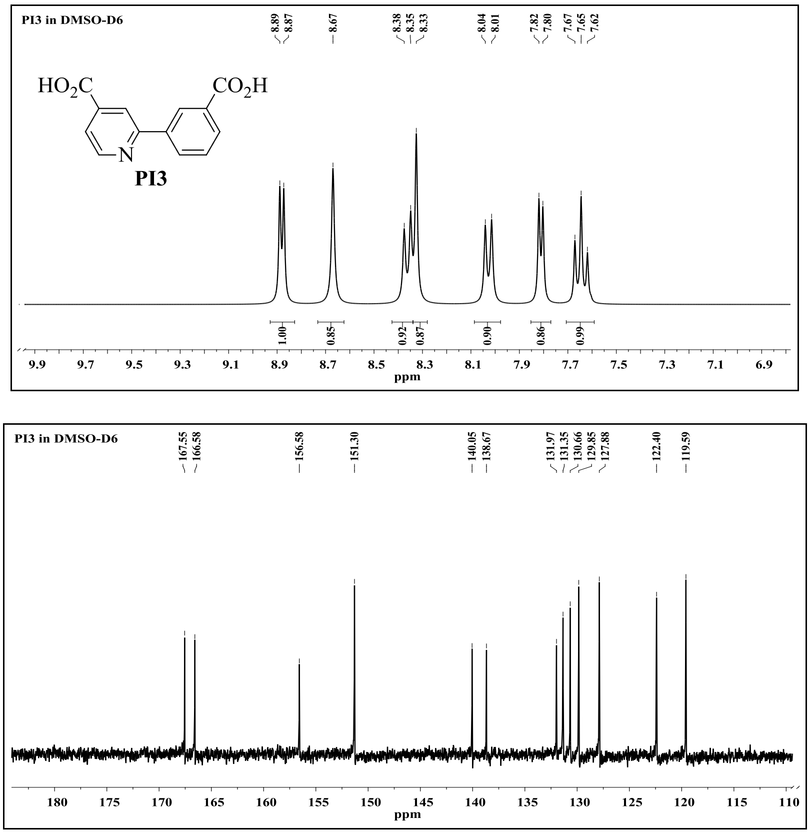

Figure A.12 ^1H and ^{13}C NMR in DMSO-d_6 of PI3

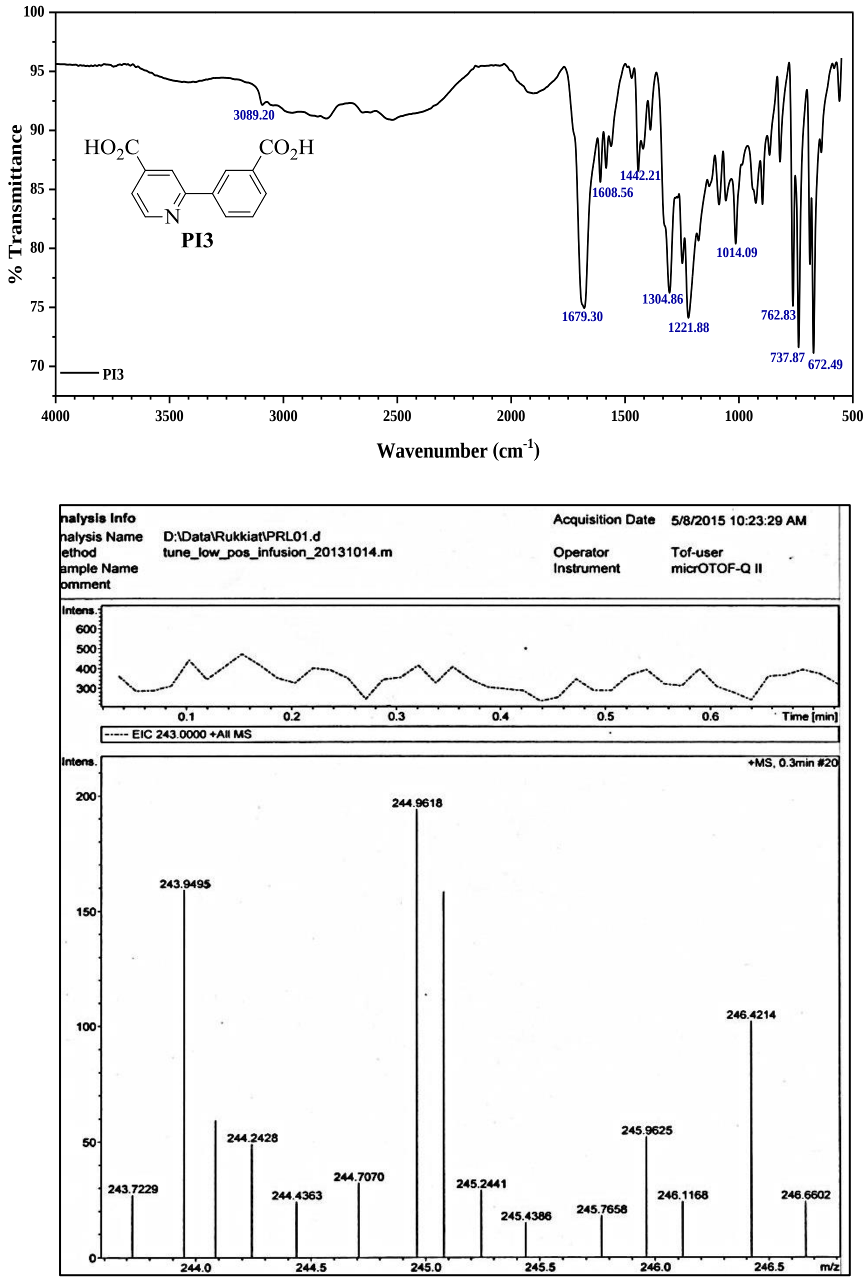

nalysis Info
nalysis Name D:\Data\Rukkiat\PRL01.d
ethod tune_low_pos_infusion_20131014.m
ample Name
omment

Acquisition Date 5/8/2015 10:23:29 AM
Operator Tof-user
Instrument micrOTOF-Q II

Figure A.13 ATR-FTIR (neat) and mass spectrum of PI3

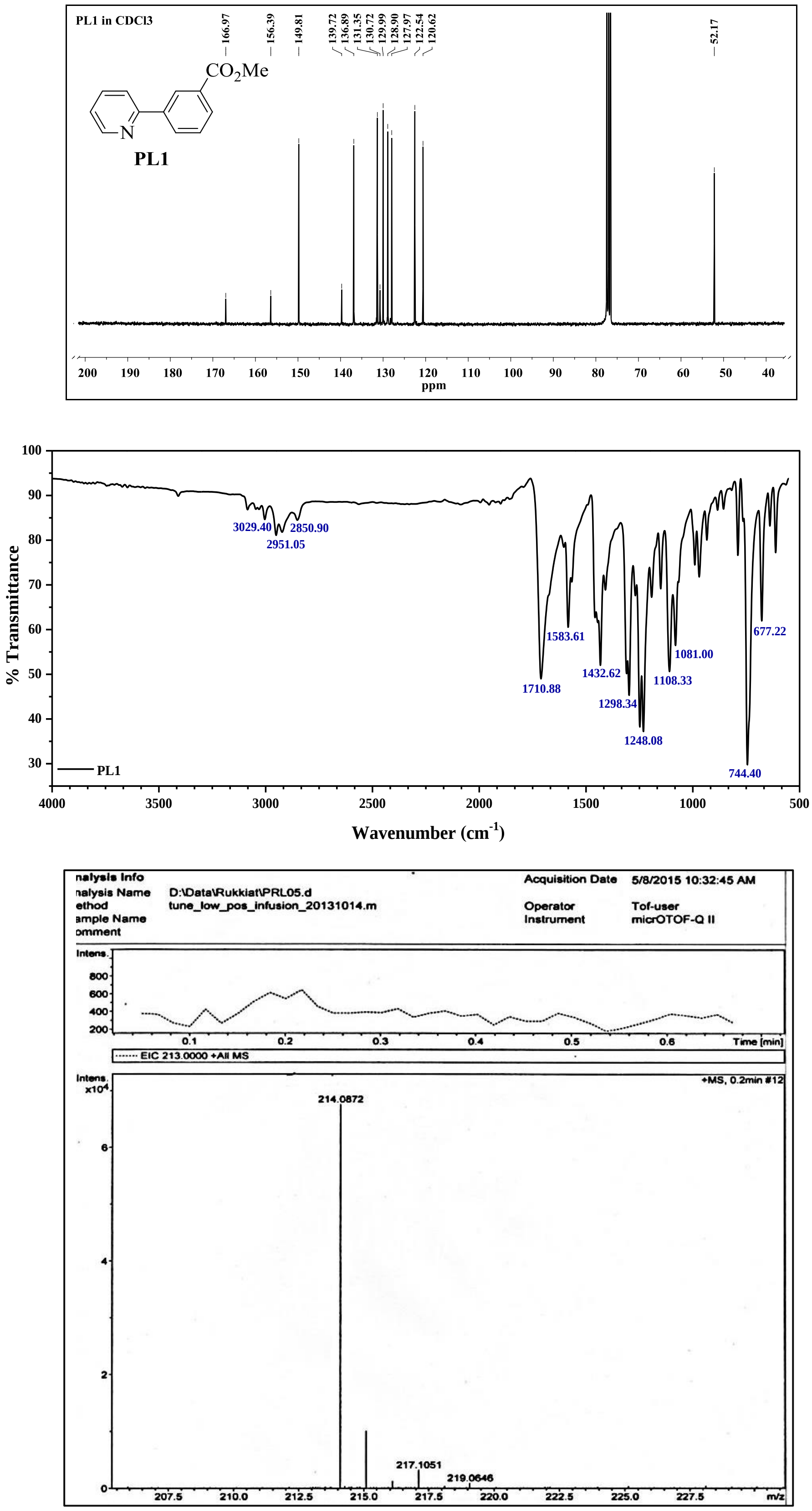

nalysis Info
nalysis Name D:\Data\Rukkiat\PRL05.d
ethod tune_low_pos_infusion_20131014.m
ample Name
omment
Acquisition Date 5/8/2015 10:32:45 AM
Operator Tof-user
Instrument micrOTOF-Q II

Figure A.14 ^{13}C NMR in $CDCl_3$, ATR-FTIR (neat) and mass spectrum of PL1

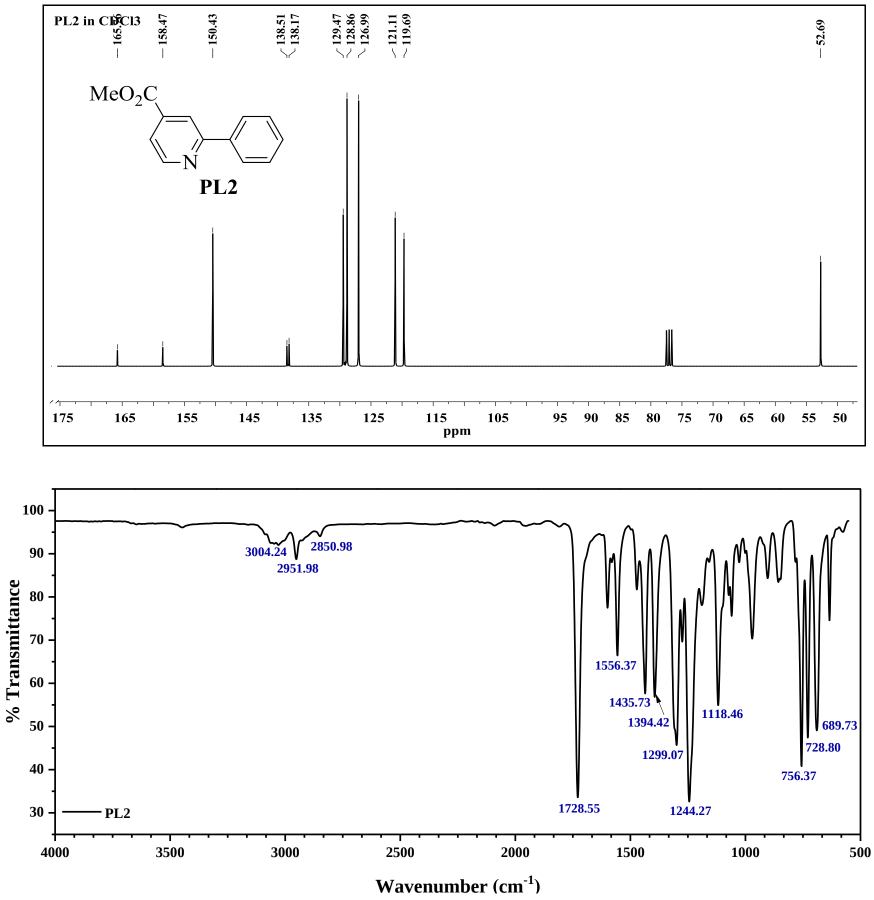

Figure A.15 ^{13}C NMR in CDCl$_3$, ATR-FTIR (neat) and mass spectrum of PL2

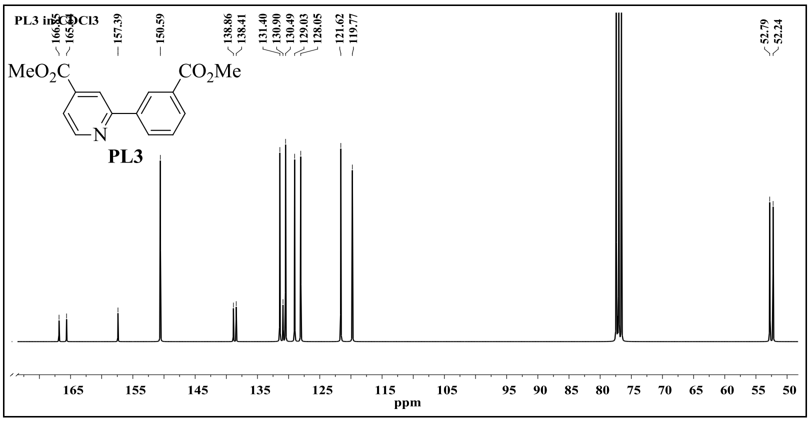

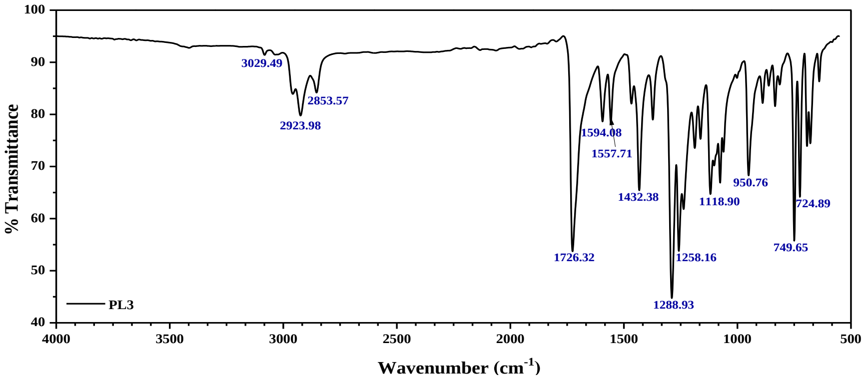

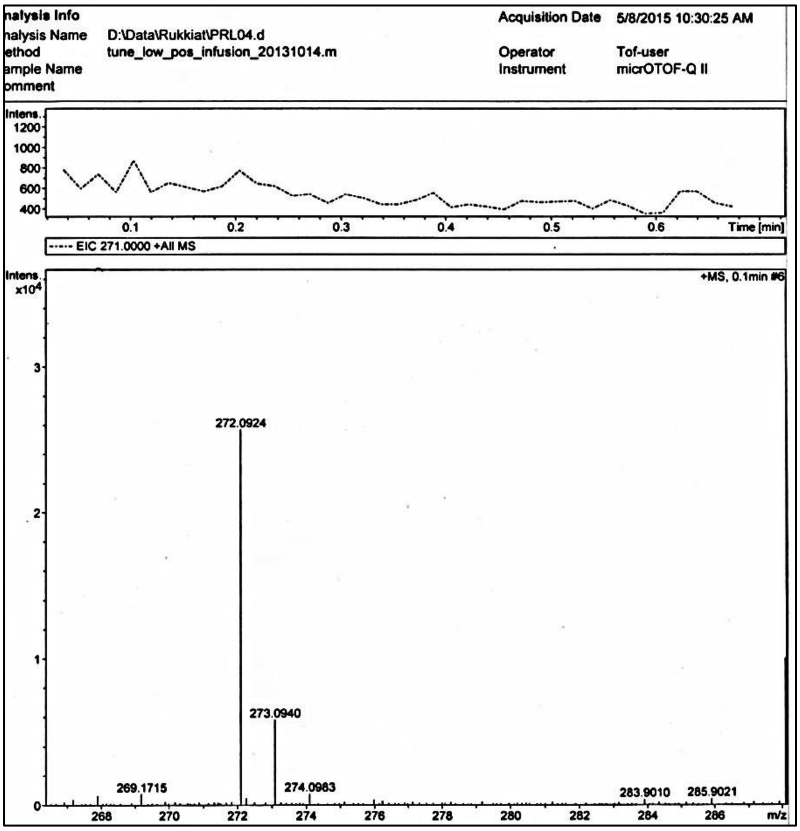
nalysis Info
nalysis Name D:\Data\Rukkiat\PRL04.d
ethod tune_low_pos_infusion_20131014.m
ample Name
omment

Acquisition Date 5/8/2015 10:30:25 AM
Operator Tof-user
Instrument micrOTOF-Q II

Figure A.16 ^{13}C NMR in CDCl$_3$, ATR-FTIR (neat) and mass spectrum of PL3

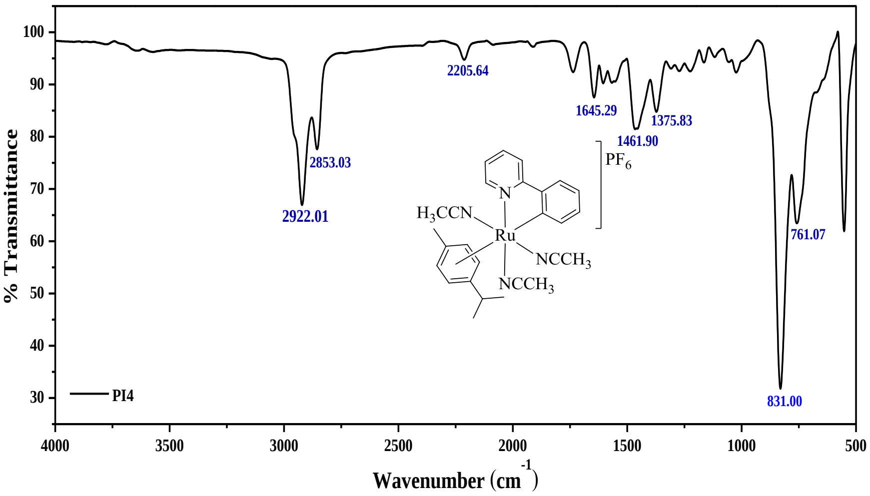

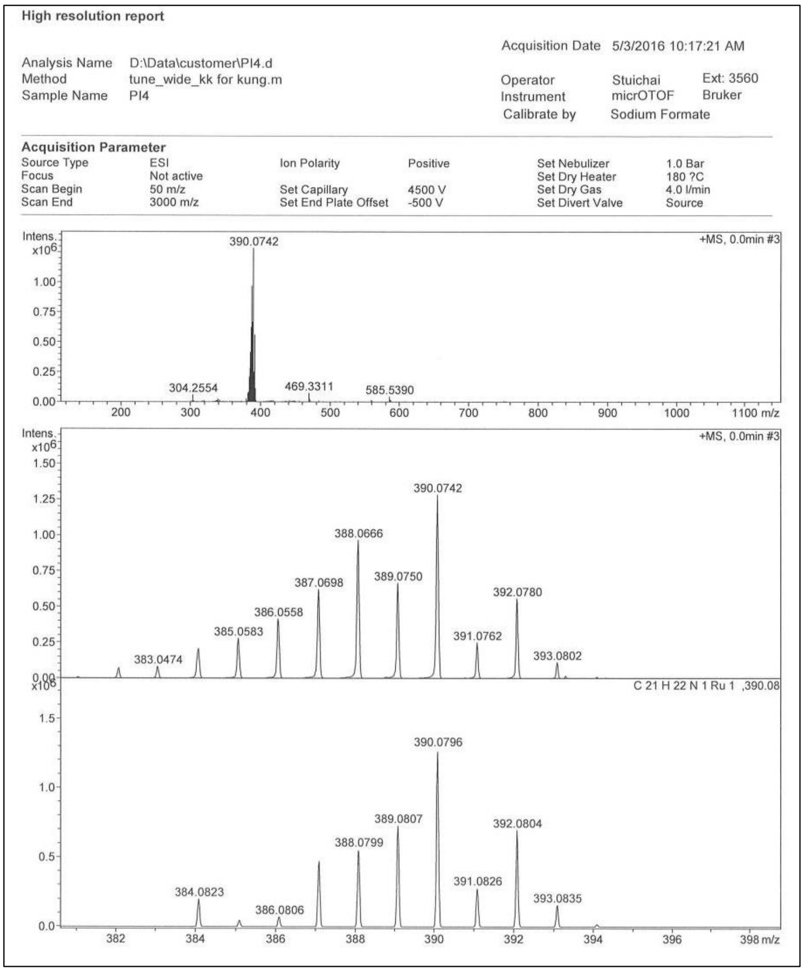

High resolution report

Analysis Name	D:\Data\customer\PI4.d	Acquisition Date	5/3/2016 10:17:21 AM
Method	tune_wide_kk for kung.m	Operator	Stuichai Ext: 3560
Sample Name	PI4	Instrument	micrOTOF Bruker
		Calibrate by	Sodium Formate

Acquisition Parameter

Source Type	ESI	Ion Polarity	Positive	Set Nebulizer	1.0 Bar
Focus	Not active			Set Dry Heater	180 ?C
Scan Begin	50 m/z	Set Capillary	4500 V	Set Dry Gas	4.0 l/min
Scan End	3000 m/z	Set End Plate Offset	-500 V	Set Divert Valve	Source

Figure A.17 ATR-FTIR (neat) and mass spectrum of PI4

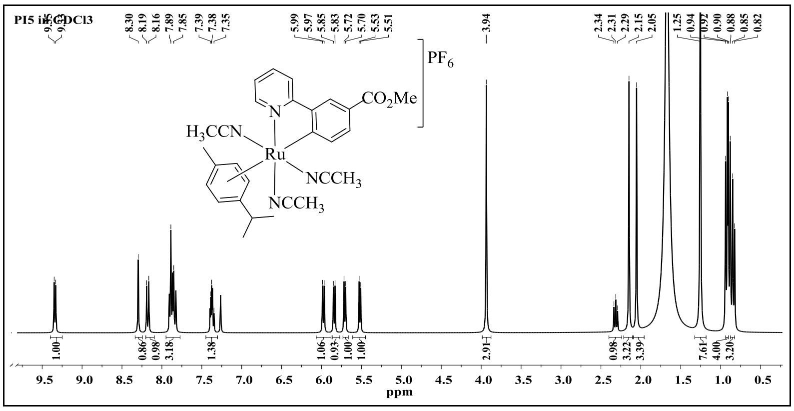

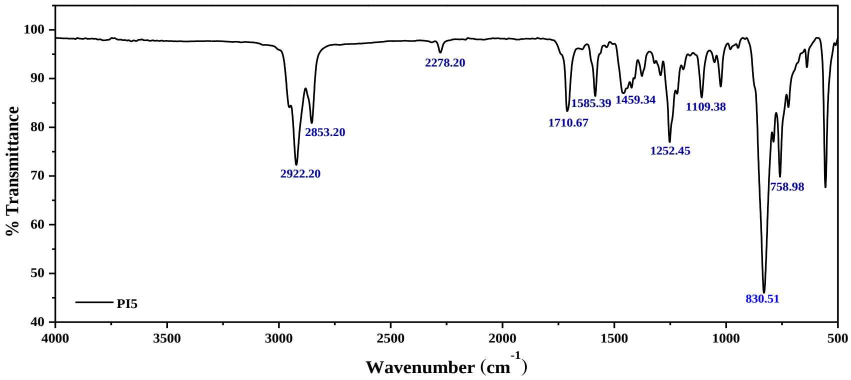

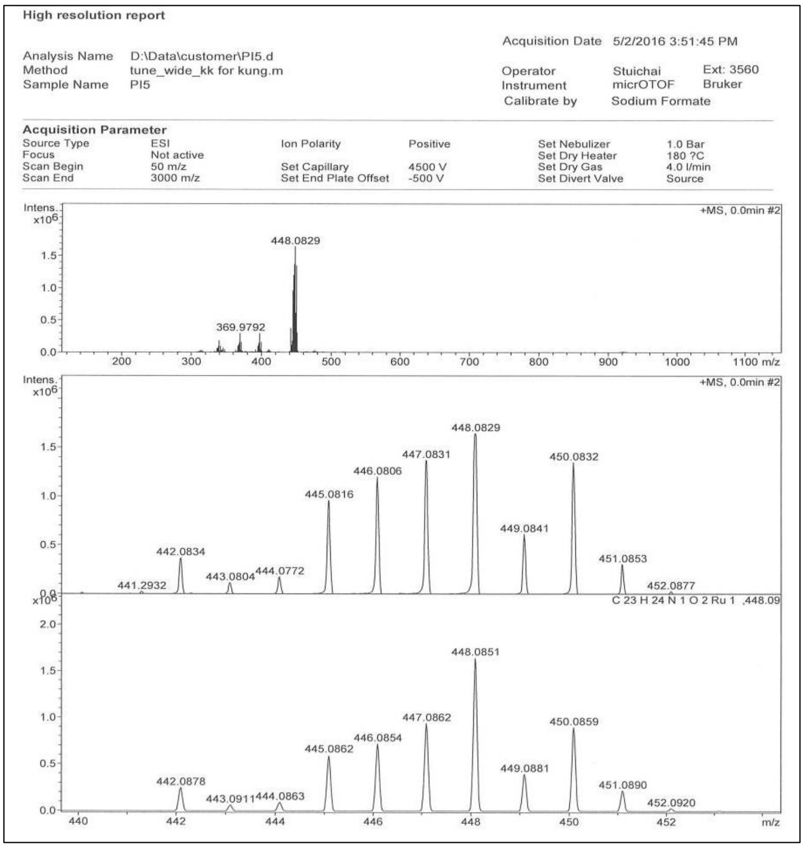

High resolution report

Acquisition Date 5/2/2016 3:51:45 PM

Analysis Name D:\Data\customer\PI5.d
Method tune_wide_kk for kung.m
Sample Name PI5

Operator Stuichai Ext: 3560
Instrument micrOTOF Bruker
Calibrate by Sodium Formate

Acquisition Parameter

Source Type ESI
Focus Not active
Scan Begin 50 m/z
Scan End 3000 m/z
Ion Polarity Positive
Set Capillary 4500 V
Set End Plate Offset -500 V
Set Nebulizer 1.0 Bar
Set Dry Heater 180 ?C
Set Dry Gas 4.0 l/min
Set Divert Valve Source

Figure A.18 ^{1}H NMR in $CDCl_3$, ATR-FTIR (neat) and mass spectrum of PI5

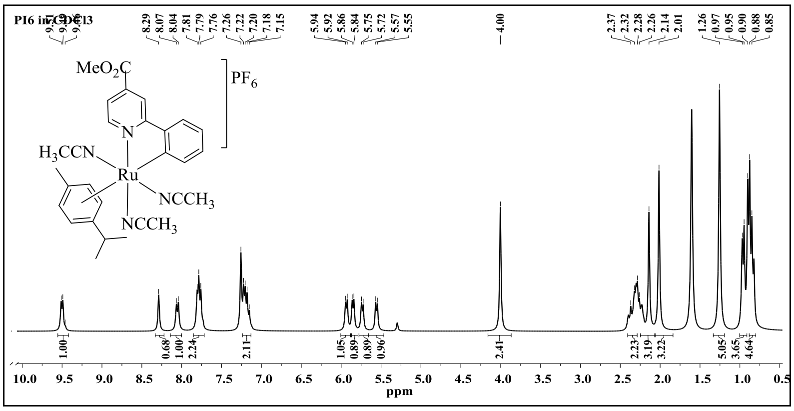

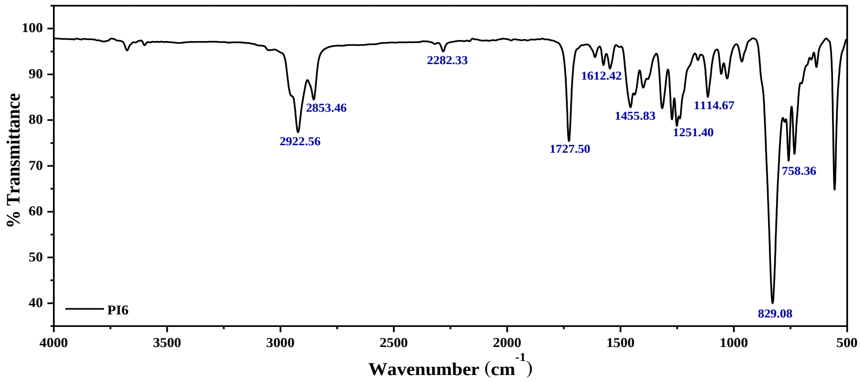

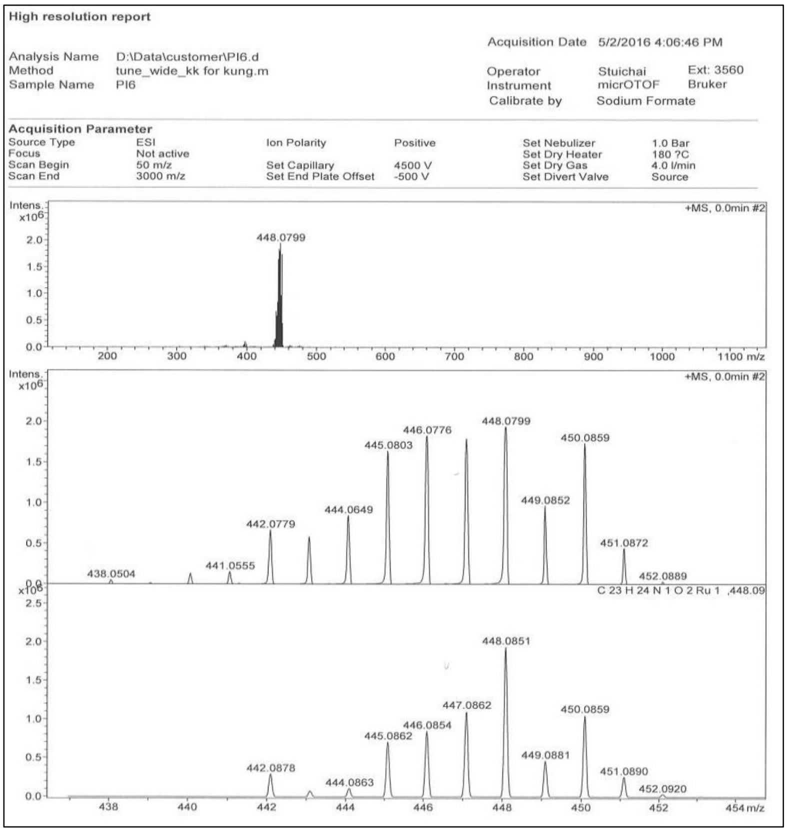

High resolution report

		Acquisition Date	5/2/2016 4:06:46 PM	
Analysis Name	D:\Data\customer\PI6.d			
Method	tune_wide_kk for kung.m	Operator	Stuichai	Ext: 3560
Sample Name	PI6	Instrument	micrOTOF	Bruker
		Calibrate by	Sodium Formate	

Acquisition Parameter

Source Type	ESI	Ion Polarity	Positive	Set Nebulizer	1.0 Bar
Focus	Not active			Set Dry Heater	180 ?C
Scan Begin	50 m/z	Set Capillary	4500 V	Set Dry Gas	4.0 l/min
Scan End	3000 m/z	Set End Plate Offset	-500 V	Set Divert Valve	Source

Figure A.19 ^{1}H NMR in $CDCl_3$, ATR-FTIR (neat) and mass spectrum of PI6

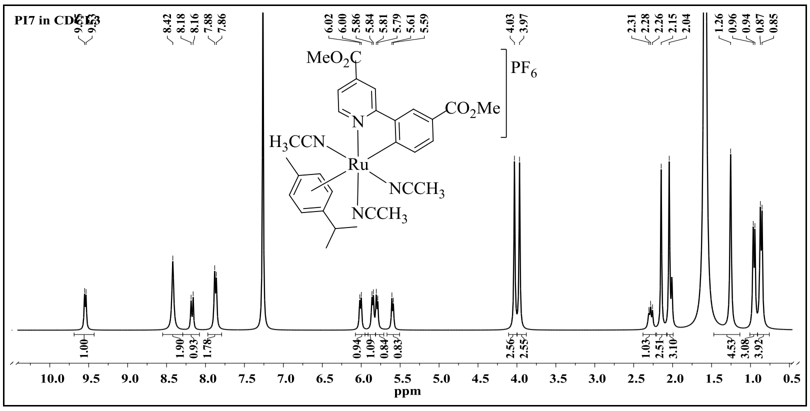

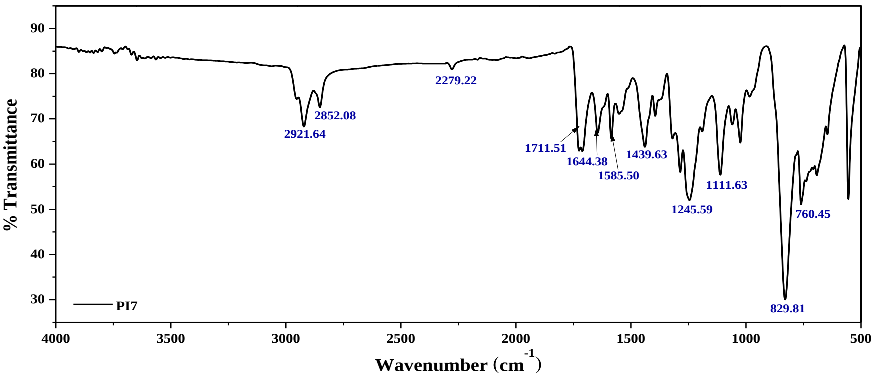

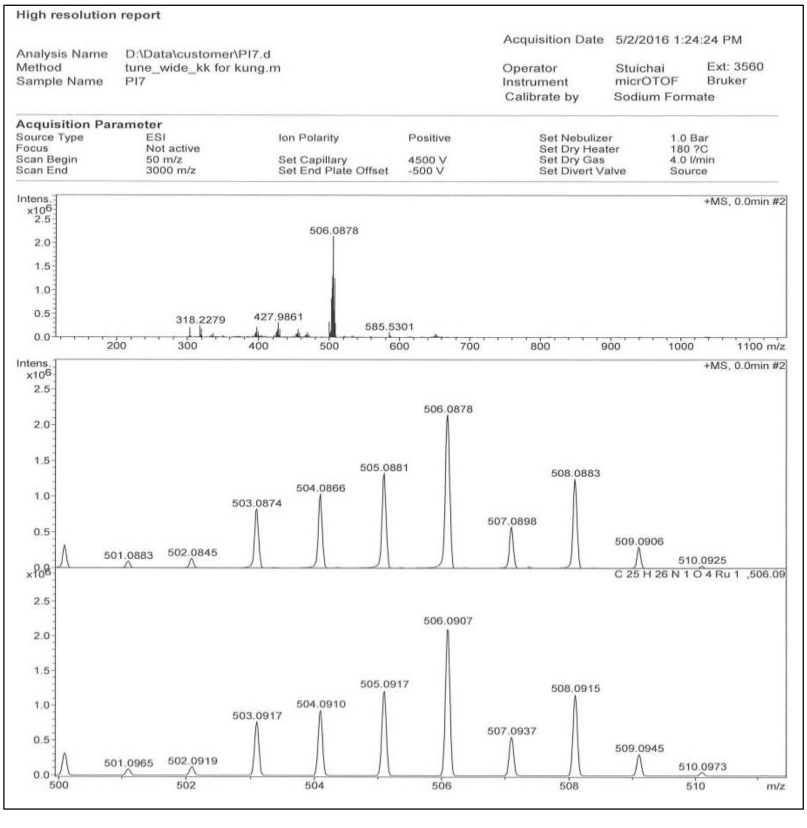
High resolution report

Acquisition Date 5/2/2016 1:24:24 PM

Analysis Name D:\Data\customer\PI7.d
Method tune_wide_kk for kung.m
Sample Name PI7

Operator Stuichai Ext: 3560
Instrument micrOTOF Bruker
Calibrate by Sodium Formate

Acquisition Parameter

Source Type	ESI	Ion Polarity	Positive	Set Nebulizer	1.0 Bar
Focus	Not active			Set Dry Heater	180 ?C
Scan Begin	50 m/z	Set Capillary	4500 V	Set Dry Gas	4.0 l/min
Scan End	3000 m/z	Set End Plate Offset	-500 V	Set Divert Valve	Source

Figure A.20 ^{1}H NMR in $CDCl_3$, ATR-FTIR (neat) and mass spectrum of PI7

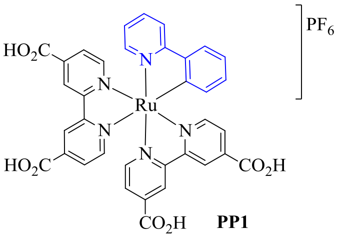

PP1

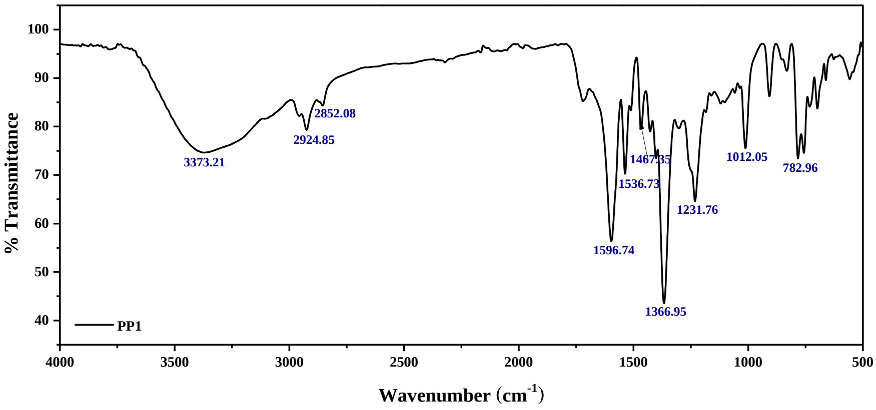

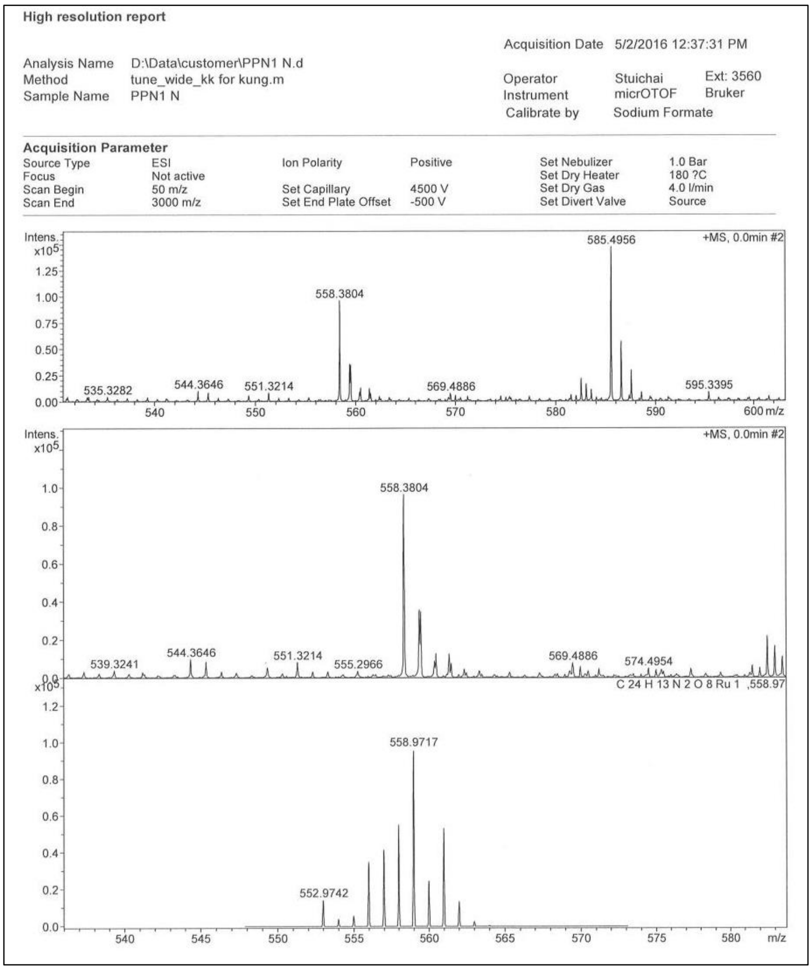

High resolution report

Acquisition Date 5/2/2016 12:37:31 PM

Analysis Name D:\Data\customer\PPN1 N.d
Method tune_wide_kk for kung.m
Sample Name PPN1 N

Operator Stuichai Ext: 3560
Instrument micrOTOF Bruker
Calibrate by Sodium Formate

Acquisition Parameter

Source Type ESI
Focus Not active
Scan Begin 50 m/z
Scan End 3000 m/z
Ion Polarity Positive
Set Capillary 4500 V
Set End Plate Offset -500 V
Set Nebulizer 1.0 Bar
Set Dry Heater 180 ?C
Set Dry Gas 4.0 l/min
Set Divert Valve Source

Figure A.21 ATR-FTIR (neat) and mass spectrum of PP1

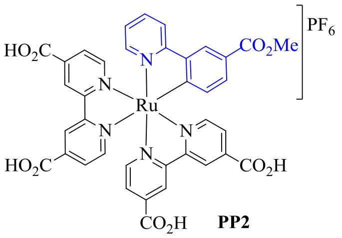

PP2

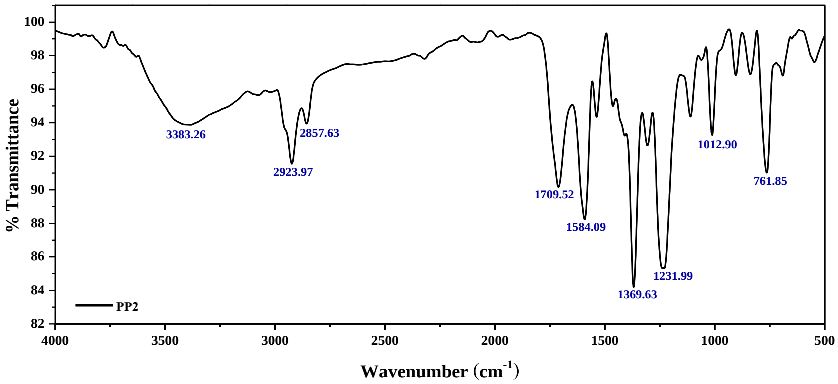

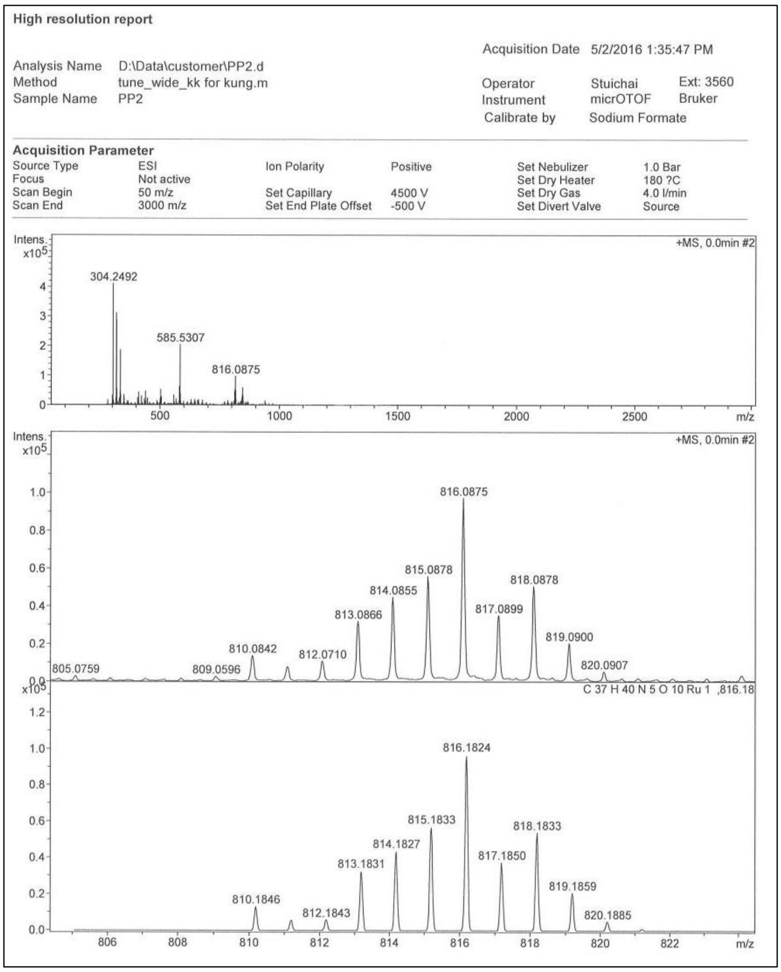

High resolution report

Analysis Name	D:\Data\customer\PP2.d	Acquisition Date	5/2/2016 1:35:47 PM
Method	tune_wide_kk for kung.m	Operator	Stuichai Ext: 3560
Sample Name	PP2	Instrument	micrOTOF Bruker
		Calibrate by	Sodium Formate

Acquisition Parameter

Source Type	ESI	Ion Polarity	Positive	Set Nebulizer	1.0 Bar
Focus	Not active			Set Dry Heater	180 ?C
Scan Begin	50 m/z	Set Capillary	4500 V	Set Dry Gas	4.0 l/min
Scan End	3000 m/z	Set End Plate Offset	-500 V	Set Divert Valve	Source

Figure A.22 ATR-FTIR (neat) and mass spectrum of PP2

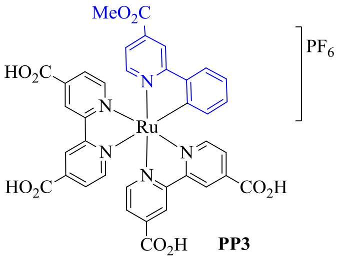

PP3

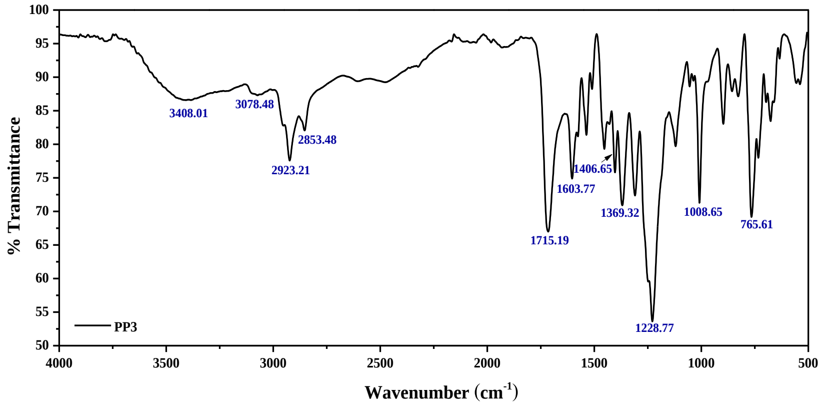

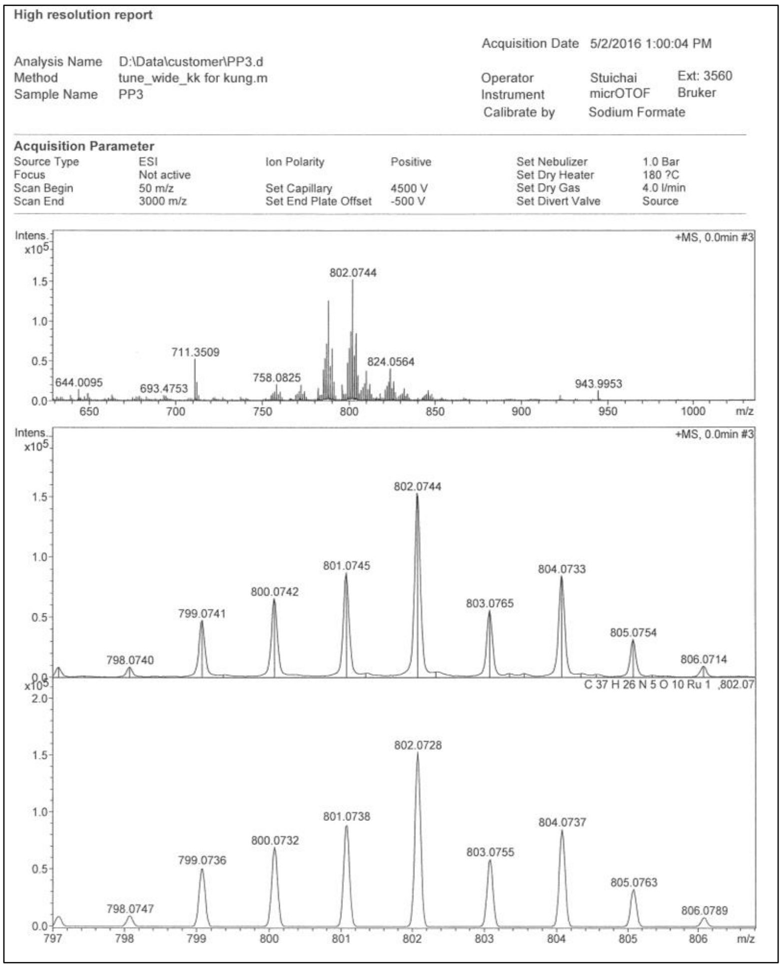

High resolution report

Acquisition Date 5/2/2016 1:00:04 PM

Analysis Name D:\Data\customer\PP3.d
Method tune_wide_kk for kung.m
Sample Name PP3

Operator Stuichai Ext: 3560
Instrument micrOTOF Bruker
Calibrate by Sodium Formate

Acquisition Parameter

Source Type ESI
Focus Not active
Scan Begin 50 m/z
Scan End 3000 m/z
Ion Polarity Positive
Set Capillary 4500 V
Set End Plate Offset -500 V
Set Nebulizer 1.0 Bar
Set Dry Heater 180 ?C
Set Dry Gas 4.0 l/min
Set Divert Valve Source

Figure A.23 ATR-FTIR (neat) and mass spectrum of PP3

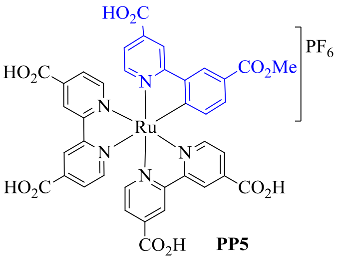

PP5

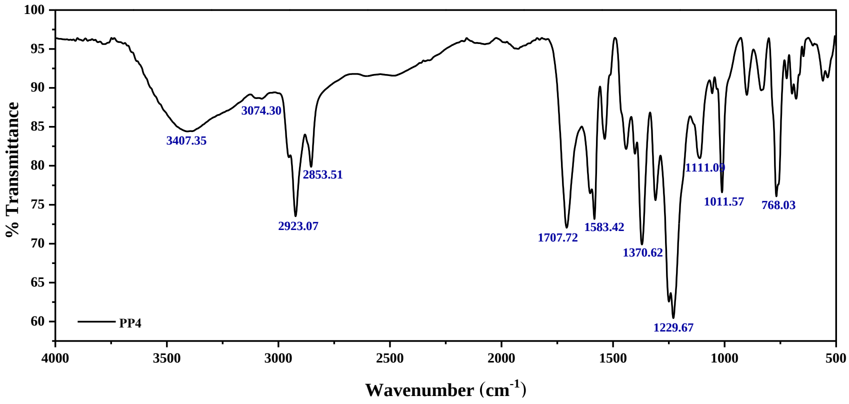

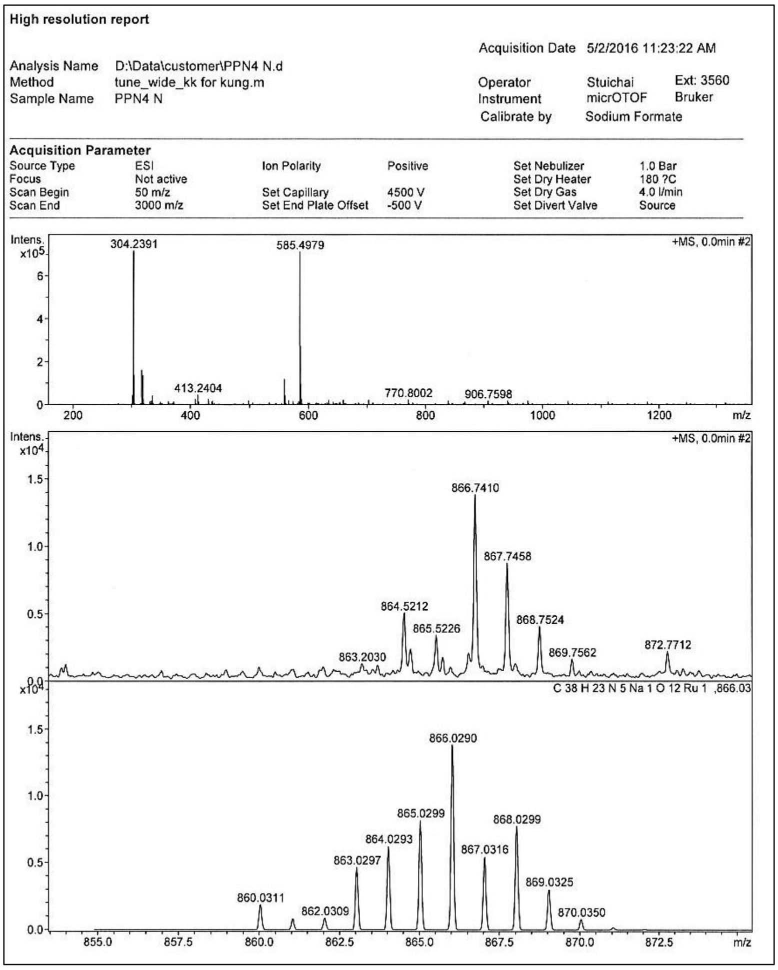

High resolution report

		Acquisition Date	5/2/2016 11:23:22 AM	
Analysis Name	D:\Data\customer\PPN4 N.d			
Method	tune_wide_kk for kung.m	Operator	Stuichai	Ext: 3560
Sample Name	PPN4 N	Instrument	micrOTOF	Bruker
		Calibrate by	Sodium Formate	

Acquisition Parameter

Source Type	ESI	Ion Polarity	Positive	Set Nebulizer	1.0 Bar
Focus	Not active			Set Dry Heater	180 ?C
Scan Begin	50 m/z	Set Capillary	4500 V	Set Dry Gas	4.0 l/min
Scan End	3000 m/z	Set End Plate Offset	-500 V	Set Divert Valve	Source

Figure A.24 ATR-FTIR (neat) and mass spectrum of PP5

APPENDIX B

Publication

Advanced Materials Research Vol. 770 (2013) pp 92-95
© (2013) Trans Tech Publications, Switzerland
doi:10.4028/www.scientific.net/AMR.770.92

Design and synthesis of ruthenium (II) complexes and their applications in dye sensitized solar cells (DSSCs)

Preeyapat Prompan, Kittiya Wongkhan[a] and Rukkiat Jitchati[b*]

Center for Organic Electronic and Alternative Energy (COEA), Department of Chemistry, Faculty of Science, UbonRatchathani University, Warinchumrap,Ubon Ratchathani Province, 34190, Thailand

kitt_w_2000@yahoo.ie,[a] rukkiat_j@hotmail.com[b]

Keywords: Dye-syntizingsolar cell (DSSCs); ruthenium complex; bipyridine

Abstract. Three thiocyanate-free ruthenium(II) sensitizers, [Ru^{II}(**dcppy**)(**L1-L3**)](PF$_6$)] where dcppy = 4, 4'-dicarboxylic acid-2, 2'-bipyridine, **L1** = 2-(2,4-difluorophenyl)-5-(trifluoromethyl) pyridine, **L2** = 2-(2,4-difluorophenyl) pyridine and **L3** = 2-phenyl-5-(trifluoromethyl)pyridine were synthesized and applied for dye-sensitized solar cells (DSSCs). The structures of ruthenium complexes were characterized by ^{1}H, ^{13}C NMR and IR spectra. The absorption was studied by UV-Vis spectroscopy and the electrochemical property was determined by cyclic voltammetry. The surface morphology of ruthenium complexes on mica was examined by atomic force microscopy. The performance of this complexes as photosensitizer in TiO$_2$ based dye sensitized solar cells is studied under standard AM 1.5 sunlight and by using an electrolyte.

Introduction

The dye-sensitised solar cell (DSSC) has been proposed as a low-cost and high-efficiency alternative to conventional photovoltaic cells in 1991 [1]. At present, efficiencies of more than 10% can be obtained for DSSCs using electrolytes based on volatile organic solvents [2]. One of the most important components of DSSC is the photosensitizer that is the dye which absorbs light from the sun and transfers an electron from its excited state to the conduction band of TiO$_2$. The most common sensitizers are Ru(II) complexes based on 2,2'-bipyridine (bpy) ligands, such as cis-di(thiocyanato)bis(bpy-4,4'-dicarboxylate)ruthenium(II) (**N3**) [3] . However, a limitation of these types of materials is a presence of thiocyanate (-NCS) ligand, which can easily be replaced by other competing ligands yielding less efficient species [4,5].

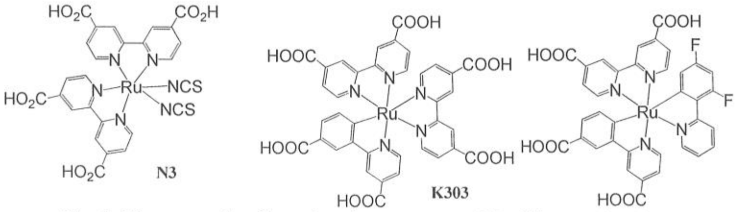

Fig. 1. The example of a molecular structure of Ru(II) complex dyes

Herein, we report the synthesis and characterization of a new thiocyanate-free cyclometallated 2-phenylpyridine Ru(II) complexes which were used as a materials in DSSCs application.

Materials and methods

Ligands (**L1-L3** and **dcbpy**) and ruthenium cymene complex (**1**) were synthesized in our laboratory as reported elsewhere [6-8]. Anhydrous dimethyl formamide (DMF) was distilled using calcium hydride before used. ^{1}H and ^{13}C NMR spectra were recorded on a Bruker Avance 300 spectrometer. Chemical shifts are quoted downfield from internal standard TMS. IR spectra were measured on a Perkin–Elmer FT-IR spectroscopy spectrum RXI spectrometer as KBr or NaCl disc. Melting points were measured in open-end capillaries using a Bűchi 530 melting point apparatus. The temperatures at the melting points were ramped at 2.5 °C/min and were uncorrected.

[Ru(dcbpy)$_2$ (L1)]PF$_6$ (2): ligand **L1** (0.17 g, 0.66 mmol), ruthenium cymene **1** (0.21 g, 0.34 mmol), NaOH (0.03 g, 0.75 mmol) and KPF$_6$ (0.24 g, 1.30 mmol) were added to the 50 ml a two necked round bottom flask under nitrogen balloon atmosphere. Acetonitrile (5 ml) was added to dissolve the content and then heated to reflux at 45°C for 24 hours. The complete reaction mixture was cooled to room temperature before removed the solvent. The crude solid was filtered using DCM:CH_3CN (9:1) solvent through the celite pad to obtain the yellow-brown solid mixture intermediate products which were used in the step without further purification.

Next step, compound **dcbpy** (0.05 g, 0.20 mmol), NaOH (0.02 g, 0.40 mmol) were placed in a 50 ml two necked round bottom flask in 5 ml of H_2O/MeOH (1:4 v/v) under N_2 balloon. The reaction was heated to 60 °C for 40 minute, the intermediate mixture complexes (0.07 g, 0.09 mmol) were added and continued reflux for 3 hours. After the reaction completed, the solvent was removed by rotary evaporator and adjusted to pH = 1.8 by 0.02 M HNO_3 to afford a purple-red solid. The solid was washed with water and diethyl ether to a target complex (**1**) (0.02 g, 26%); ^{1}H NMR (300 MHz, CD_3OD) δ 9.12 (s, 1H), 9.05 (s, 1H), 8.99 (s, 2H), 8.49 (d, J = 8.0 Hz, 1H), 8.16 (d, J = 5.7 Hz, 1H), 8.12 – 7.90 (m, 4H), 7.91 – 7.68 (m, 5H), 6.55 – 6.44 (m, 1H), 5.94 (d, J = 6.0 Hz, 1H); IR (NaCl) 3447, 2363, 1718, 1603, 1366, 1329, 1268, 1141, 1071, 1013, 766 and 682 cm^{-1}.

[Ru(dcbpy)$_2$(L2]PF$_6$ (3); The synthesis method was done as the synthesis of complex **2**. Compound **1** (0.20 g, 0.33 mmol), ligand **L2** (0.14 g, 0.63 mmol), NaOH (0.03 g, 0.75 mmol) and KPF$_6$ (0.24 g, 1.30 mmol) were used to give a mixture intermediate. Then, **dcbpy** (0.05 g, 0.20 mmol), NaOH (0.02 g, 0.40 mmol) and the intermediet mixtures (0.07 g, 0.10 mmol) gave a purple-red solid (**3**) (0.04 g, 40%); ^{1}H NMR (300 MHz, CD_3OD) δ 9.12 (s, 1H), 9.03 (s, 1H), 8.95 (d, J = 4.4 Hz, 2H), 8.28 (d, J = 8.6 Hz, 1H), 8.19 (d, J = 5.8 Hz, 1H), 8.08 (d, J = 5.4 Hz, 1H), 8.00 (d, J = 5.5 Hz, 4H), 7.90 (d, J = 5.9 Hz, 1H), 7.84 – 7.65 (m, 4H), 6.95 (dt, J = 20.3, 6.8 Hz, 2H), 6.41 (d, J = 7.1 Hz, 1H); ^{13}C NMR (75 MHz, CD_3OD) δ 192.0, 170.8, 166.0, 157.9, 157.1, 156.7, 155.5, 154.5, 150.7, 150.4, 149.6, 146.0, 143.5, 134.7, 133.0, 130.0, 126.8, 125.9, 125.6, 125.5, 125.3, 122.3, 121.8, 119.0, 48.4, 48.2, 47.9, 47.6, 47.3, 47.0, 46.7; IR (NaCl) 3422, 2345, 1718, 1610, 1367, 1330, 1311, 1230, 1136, 1085, 1012, 768 and 681 cm^{-1}.

[Ru(dcbpy)$_2$(L3)]PF$_6$ (4); The synthesis method was done as the synthesis of complex **2**. Compound **1** (0.20 g, 0.33 mmol), ligand **L3** (0.13 g, 0.68 mmol), NaOH (0.03 g, 0.66 mmol) and KPF$_6$ (0.25 g, 1.35 mmol) were used to give a mixture intermediate. Then, **dcbpy** (0.05 g, 0.20 mmol), NaOH (0.02 g, 0.40 mmol) and intermediet mixtures (0.07 g, 0.10 mmol) gave a purple-red solid (**4**) (0.05 g, 56%); ^{1}H NMR (300 MHz, CD_3OD) δ 9.08 (s, 1H), 9.02 (s, 1H), 8.97 (s, 2H), 8.33 (d, J = 8.8 Hz, 1H), 8.20 (d, J = 5.8 Hz, 1H), 8.01 – 7.86 (m, 4H), 7.78 (s, 4H), 7.60 (d, J = 5.3 Hz, 1H), 7.04 (dd, J = 13.8, 7.4 Hz, 2H), 6.49 – 6.38 (m, 1H), 5.86 (d, J = 7.7 Hz, 1H); IR (NaCl) 3409, 2924, 1718, 1595, 1366, 1234, 1013, 983, 767 and 682 cm^{-1}

Fabrication of DSSC: The transparent (Ti-Nanoxide 20T/SP, Solaronix) and a scattering (Ti-Nanoxide R/SP, Solaronix) TiO_2 layer were prepared by a screen-printing method on a transparent FTO glass (8 Ω/sq, Solaronix) and then sintered at 450 °C for 30 minute and cooled to 80 °C. Nanocrystalline TiO_2 films were coated with dyes by dipping the film in 3×10^{-4} M dye solutions in ethanol overnight. The dye-coated TiO_2 electrode was incorporated into a thin-layer sandwich-type cell with a Pt-coated FTO as counter electrode, a spacer film, and an organic electrolyte solution to measure the solar cell performance. The Pt counter electrode was prepared by spin-coating a 7 mM H_2PtCl_6 in 3-methoxyethanolsolution on FTO glass followed by sintering at 385 °C for 30 minute. The electrolyte contained 0.05M I_2, 0.1M LiI, 0.4 M *t*-butylpyridine (tBPy), and 0.6 M tetrapropy ammonium iodide (TPAI) in 85:15v/v acetonitrile/valeronitrile solvent was used. Light-to-electricity conversion efficiency values were measured using Newport sun simulator 96000 equipped with an AM 1.5 G filter. The current density-voltage of DSSCs was measured by Keithley 2400 source meter unit in a terminal sense configuration.

Results and discussions

The new thiocyanate-free cyclometallated 2-phenylpyridine Ru(II) complexes were synthesized from dimer $[(\eta^6\text{-}p\text{-cymene})RuCl_2]_2$ (**1**) and ligand (**L1-L3**) to give intermediate mixtures of ruthenium acetonitrile complexes which the ratio of the intermediate mixtures can be identified by ^{1}H

NMR. Then, the intermediate mixtures were reacted with 2 equivalents of bipyridine carboxylic acid (**dcbpy**) without purification to afford 26%, 40% and 56% for complex **2**, **3** and **4**, respectively. The molecular structures of ruthenium complex were characterized and identified by ^{1}H, ^{13}C NMR and IR spectra. The IR spectra clearly show a vibration of O-H, C=O and C-F bond at 3300, 1730 cm^{-1} and 1010 cm^{-1}, respectively.

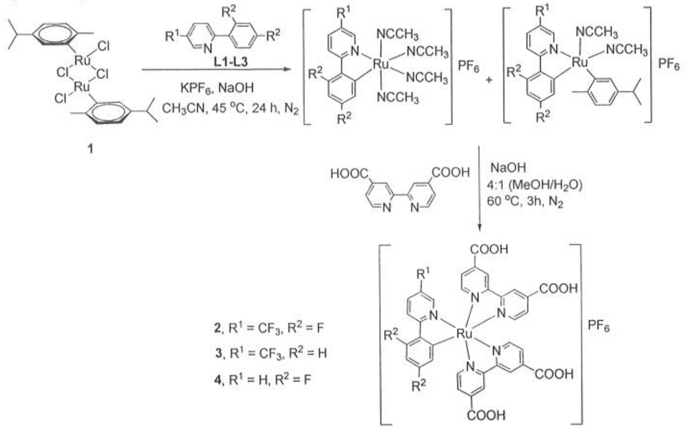

Fig. 2. The synthetic route of cyclometallated Ru(II) **2**, **3** and **4** complexes

The absorption spectra of the dyes in DMF solution show three absorption bands which are observed in the 300–800 nm region; the first band below 350 nm is attributed to the intraligand π–π* transition of **dcbpy** ligand. The second band appeared from 360–410 nm is attributed to the π–π* transition of the cyclometallated 2-phenylpyridine ligand (**L1-L3**). The final band around 500-600 nm shows a lower-energy MLCT band, that is, the ruthenium *d* orbital to π* orbital. The λ_{max} values of the complexes show in Table 1 whereas the molar absorption coefficients (ε) give about 1 x 10^4 M^{-1}cm^{-1} for **2**, **3** and **4** complexes.

Table 1. The characterized data and photovoltaic parameters of devices from complex **2**, **3** and **4**

complex	λ_{max} ^{a} (nm)	$\varepsilon \times 10^4$ ^{a} (M^{-1}cm^{-1})	$E_{1/2}$ ^{b} (V)		R_a ^{c} (nm)	DSSCs performance parameters ^{d}			
			E_{ox}	E_{red}		J_{sc} (mA cm^{-2})	V_{oc} (mV)	FF	η (%)
2	403 481 542	0.83 0.72 0.76	0.62	-0.71	15.689	7.02	521	72.1	2.64
3	422 294 563	1.55 1.26 1.14	0.41	-0.75	15.640	4.74	492	70.5	1.65
4	403 486 556	0.92 0.65 0.87	0.54	-0.76	15.419	4.09	493	70.1	1.42

a) λ_{max} and ε were determined by 2.5 x 10^{-5} M in ethanol.

b) $E_{1/2}$ was measured by 1 x 10^{-4} in DMF, 0.1 M TBAPF$_6$ and a scan rate of 100 mV s^{-1}.

c) The average roughness (R_a) was examined with AFM with non contracted mode.

d) DSSCs devices were determined by using **2**, **3** and **4** dyes with composed of 0.25 cm^2 dye-adsorbed TiO$_2$ film, 0.05 M I$_2$, 0.1 M LiI, 0.4 M tBPy, and 0.6 M TPAI as the electrolyte under AM 1.5 G illumination (100 mWcm^{-2}).

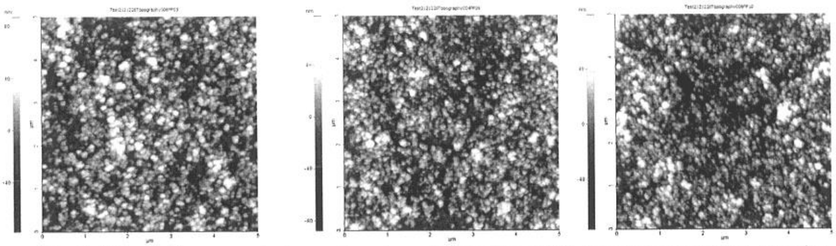

Fig. 3. The surface morphology of cyclometallated Ru(II) **2**, **3** and **4** complexes on mica

The average roughness (R_a) of coated **2**, **3** and **4** dyes on TiO_2 surface was checked by AFM image which is a similar value about 15 nm which can be explained by the same molecular length for all three complexes. The DSSCs performance of these 3 complexes as photosensitizer in TiO_2 based dye sensitized solar cells studied under standard AM 1.5 sunlight and by using I_2/I_3^- as an electrolyte show the conversion efficiency about 2% (Table 1).

Conclusion

In conclusion, we have successfully synthesized and characterized the new family of cyclometallated Ru(II) **2**, **3** and **4** complexes. The conversion efficiency of **2**, **3** and **4** complexes are 2.64%, 1.65 and 1.42%, respectively. We believe that this work will contribute to the development of new family of cyclometallated Ru(II) for enhancing the DSSCs performance in the future.

Acknowledgment

The authors would like to thank Ubon Ratchathani University for the financial support.

References

[1] B. O'Regan, M. Grätzel, A low-cost, high-efficiency solar cell based on dye-sensitized colloidal TiO_2 films, Nature 353 (1991) 737-740.

[2] Y. Luo, D. Li, Q. Meng, Towards optimization of materials for dye-sensitized solar cells, Adv. Mater. 21 (2009) 4647-4651.

[3] M. K. Nazeeruddin, A. Kay, I. Rodicio, R. Humphry-Baker, E. Mueller, P. Liska, N. Vlachopoulos, M. Grätzel, Conversion of light to electricity by cis-X_2bis (2,2'-bipyridyl-4,4'-dicarboxylate)ruthenium(II) charge-transfer sensitizers (X = Cl-, Br-, I-, CN-, and SCN-) on nanocrystalline titanium dioxide electrodes, J. Am. Chem. Soc. 115 (1993) 6382-6390.

[4] K. Ocakoglu, E. Harputlu, P. Guloglu, S. Erten-Ela, Design and synthesis of heteroleptic ruthenium (II) complexes and their applications in nanocrystalline TiO2 solar cells, Inorg. Chem. Commun. 24 (2012) 118-124.

[5] T. Bessho, E. Yoneda, J.-H. Yum, M. Guglielmi, I. Tavernelli, H. Imai, U. Rothlisberger, M. K. Nazeeruddin, M. Grätzel, New Paradigm in Molecular Engineering of Sensitizers for Solar Cell Applications, J. Am. Chem. Soc. 131 (2009) 5930–5934.

[6] R. Jitchati, Y. Thathong, K. Wongkhan, A cheap synthetic route to commercial ruthenium N3 dye for sensitizing solar cell applications, Adv. Mat. Res. 488-489 (2012) 1049-1054.

[7] R. Jitchati, Y. Thathong, K. Wongkhan, Three synthetic routes to a commercial N3 dye, Int. J. App. Phy Mat. 2 (2012) 107-110.

[8] N. Khammultri, N. Senamart, N. Deepuppha, K. Wongkhan, R. Jitchati, Suzuki-Miyaura Reaction; Novel Synthesis of C-N and N-N Ligands for Organic Light-Emitting Devices, Adv. Mat. Res. 622-623 (2013) 236-240.

FREE THIOCYANATE RUTHENIUM COMPLEX FOR DYE-SENSITIZED SOLAR CELL

Preeyapat Prompan [1], Kittiya Wongkhan [1] and Rukkiat Jitchati [*1]

[1]Center for Organic Electronic and Alternative Energy (COEA), Department of Chemistry, Faculty of Science, Ubon Ratchathani University, Warinchumrap, Ubon Ratchathani Province, 34190, Thailand
*Corresponding author: rukkiat_j@hotmail.com

Introduction

The dye-sensitised solar cell (DSSC) has been proposed as a low-cost and high-efficiency alternative to conventional photovoltaic cells in 1991 [1]. At present, efficiencies of more than 10% can be obtained for DSSCs using electrolytes based on volatile organic solvents [2]. One of the most important components of DSSC is the photosensitizer, that is the dye which absorbs light from Sun and transfers an electron from its excited state to the conduction band of TiO_2. The most common sensitizers are Ru(II) complexes based on 2,2'-bipyridine (bpy) ligands, such as cis-di(thiocyanato)bis(bpy-4,4'-dicarboxylate)ruthenium(II) (**N3**) [3]. However, a limitation of these types of materials is a presence of thiocyanate (-NCS) ligand, which can easily replaced by other competing ligands yielding less efficient species [4]. Herein, we report the synthesis and charactrization of a new thiocyanate-free cyclometallated 2-phenylpyridine Ru(II) complex which the material will be used in DSSC application.

Synthetic Methodology

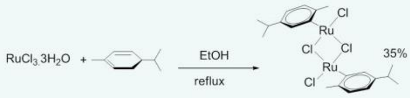

The ruthenium dimer $[(\eta^6\text{-}p\text{-cymene})RuCl_2]_2$ was synthesized by ruthenium chloride trihydrate and α-phellandrene in ethanol for 4 hours.

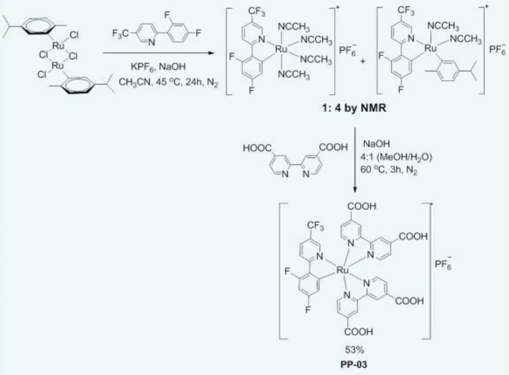

The new free thiocyanate ruthenium complex was synthesized from dimer $[(\eta^6\text{-}p\text{-cymene})RuCl_2]_2$ and 2-(2,4-difluorophenyl)-5-trifluoromethyilpyridineto give a mixture of ruthenium acetonitrile complexes which can indentify in the ratio of 1: 4 by ^1H NMR. Then, the intermediate mixtures were reacted with 2 equivalents of bipyridine carboxylic acid without purification to afford 53% yield **PP-03**. The molecular structure of ruthenium complex was characterized and identified by ^1H and ^{13}C NMR spectra.

Results and Discussion

^1H NMR of **PP-03** in CD_3OD

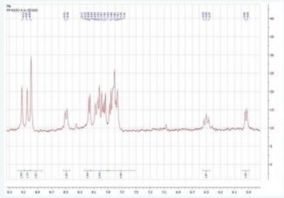

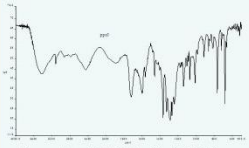

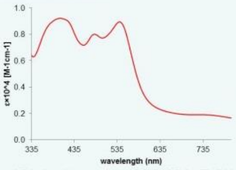

IR spectra of **PP-03** with NaCl disc

UV-vis absorption of **PP-03** in EtOH

AFM surface of **PP-03** with noncontract mode

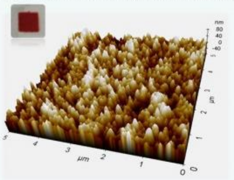

The IR spectra clearly show a vibration of O-H, C=O and C-F bond at 3300, 1730 cm^{-1} and 1010 wave number, respectively. The UV-Vis absorption spectra of the ruthenium sensitizer in ethanol solution show in the visible region due to metal-to-ligand (MLCT) charge transfer transitions, thus allowing a broad harvesting of the solar radiation. The λ_{max} values of the complex show around 400, 450 and 550 whereas the molar absorption coefficient (ε) give nearly $1 \times 10^{-4}\ M^{-1}cm^{-1}$.
The average roughness (Ra) of coated dye on TiO_2 surface was checked by AFM image which is about 15.64 nm. The preliminary performance of this complex as photosensitizer in TiO_2 based dye sensitized solar cells studied under standard AM 1.5 sunlight and by using I2/II3- as an electrolyte show the conversion efficiency about 2% (compared with N3 about 3%)

Conclusions and Acknowledgements

We report the synthesis and characterization of free thiocyanate ruthenium complex for using as sensitizer dye in DSSCs.

The authors would like to acknowledge the financial support from the Research, Development and Engineering (RD&E) Fund through National Nanotechnology Center (NANOTEC) (P-10-11346) and Energy Policy and Planning Office (EPPO) (P 07-01-53-027).

References

[1] O'Regan, B.; Grätzel, M. *Nature* **1991**, *353*, 737. [2] a) Hagfeldt, A.; Grätzel, M. *Acc. Chem. Res.* **2000,** *33, 269.* b) Hagfeldt, A.; Boschloo, G.; Sun, L.; Kloo, L.; Pettersson, H. *Chem. Rev.* **2010**, *110*, 6595. [3] Nazeeruddin, M. K.; Kay, A.; Rodicio, I.; Humphry-Baker, R.; Mueller, E.; Liska, P.; Vlachopoulos, N.; Grätzel, M. *J. Am. Chem. Soc.* **1993**, *115*, 6382. [4] Bessho, T.; Yoneda, E.; Yum, J.-H.; Guglielmi, M.; Tavernelli, I.; Imai, H.; Rothlisberger, U.; Nazeeruddin, M. K.; Grätzel, M. *J. Am. Chem. Soc.* **2009**, *131*, 5930.

Energy Policy and Planning Office
MINISTRY OF ENERGY

Co-sensitizers for Dye-Sensitized Solar Cell (DSSC)

Preeyapat Prompan, Taweesak Sudyoadsuk,
Kittiya Wongkhan and Rukkiat Jitchati*

Organometallic and Catalytic Center (OCC), Department of Chemistry, Faculty of Science,
Ubon Ratchathani University, Warinchamrap, Ubon Ratchathani Province, 34190, Thailand

*E-mail: rukkiat_j@hotmail.com

Himpunan Optika Indonesia (HOI)
Indonesian Optical Society (InOS)

10th ISMOA 2015

INTRODUCTION

The dye-sensitized solar cell (DSSC) has been proposed as a low-cost and high-efficiency alternative to conventional solar cells in 1991 [1]. At present, the efficiency more than 11% can be obtained for DSSC using the volatile organic solvents [2]. One of the most important components of DSSC is the photosensitizer which absorbs sun light and transfers an electron from its excited state to the TiO_2 conduction band. A limitation of these materials are a weak absorption in the red and IR regions. However, co-sensitizer with a dye combination of two or more can solve this problem [3]. Herein, we report the study of pure and co-sensitizer which are **P2, YN07** and **N719** in DSSCs in Fig 1.

MATERIALS AND METHODS

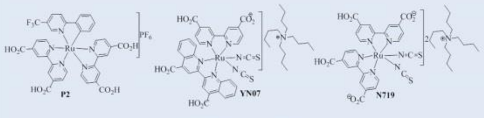

Fig 1. Structures of sensitizers.

(2-Phenyl-5-(trifluoromethyl)pyrido)-bis(4,4'-dicarboxy-2,2'-bipyridine)ruthenium(II) hexafluorophosphate (**P2**) and cis-bis(thiocyanato)bis(4,4'-dicarboxy-2,2'-bipyridine)ruthenium(II) bis(tetrabutyl-ammonium) (**N719**) were synthesized in our laboratory as reported elsewhere [4-5]. Both molecular structures were characterized and identified by ^1H, ^{13}C NMR and FTIR techniques.

Cis-bis(thiocyanato)bis(4,4'-dicarboxy-2,2'-biquinoline)(4-carboxy-2,2'-bipyridine-4'-caboxylate)ruthenium(II) tetrabutylammonium) (**YN07**) was synthesized from the reaction of di-μ-chloro-bis[(η^6-benzene) chlororuthenium(II)] (**Ru-cymene**) and 4,4'-dicarboxy-2,2'-bipyridine (**dcbpy**). Then, 2,2'-biquinoline 4,4'-dicarboxylic acid (**dcbiq**) was added to the reaction mixtures. In the work up step, the basic MeOH solution $N(nBu)_4OH$ was used before separated by sephadex LH-20 column. The **YN07** complex was achieved as a dark purple solid (90%) and characterized by ^1H NMR, see Fig 2.

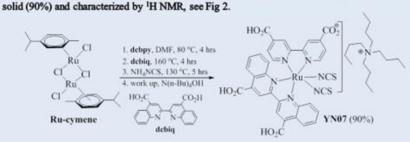

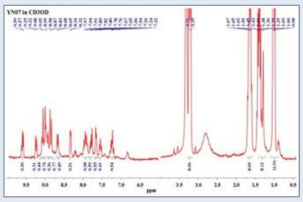

Fig 2. ^1H NMR spectrum of **YN07** in CD_3OD.

The co-sensitization

The preparation of 3×10^{-4} M co-dye using two sensitizers for complementary absorption are shown in Fig. 3 to achieve DSSC panchromatic light harvesting dyes.

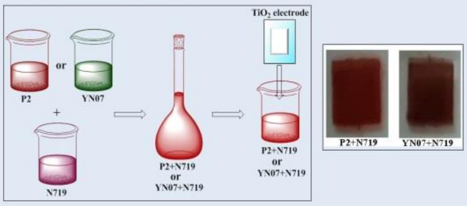

Fig 3. The co-sensitization mixing steps (left) and the f co-dye on TiO_2 film (right).

RESULTS AND DISCUSSION

UV-Vis absorption

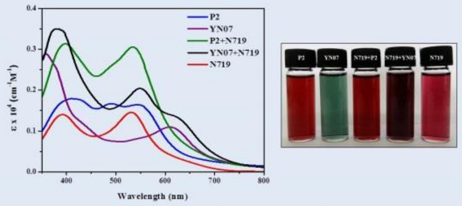

Fig 4. Absorption spectra (left) and the color of 4 x 10^{-4} M ethanolic dye solution (right).

The solution absorption spectra are shown in Fig. 4. We found that the main absorption peaks are π-π* transition (below 400 nm) and MLCT transitions (400-700 nm). Interestingly, the co-dyes show a much higher extinction coefficient and also give longer MLCT absorptions range than those pure **P2, YN07** and **N719**.

DSSC photovoltaic performance

Fabrication of DSSC: the transparent (Ti-Nanoxide 20T/SP, Solaronix) and a scattering (Ti-Nanoxide R/SP, Solaronix) TiO_2 layers were prepared by a screen-printing method on a transparent FTO glass (8 Ω/sq, Solaronix) and then sintered at 450 °C for 30 minute and cooled to 80 °C. Nanocrystalline TiO_2 films were overnight coated with pure dye and co-dyes by dipping in ethanolic. The coated TiO_2 electrode was incorporated to sandwich-type cell with a Pt-coated FTO by using a spacer film. Then, a liquid electrolyte was injected to complete DSSC shown in Fig. 5 (right).

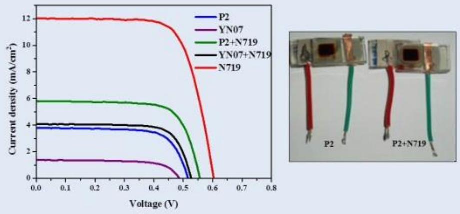

Fig 5. Current–voltage characteristics of pure and co-dyes under standard AM 1.5 (left) and DSSC device (right).

The photovoltaic parameters of DSSC were investigated with pure and co-dyes under standard AM 1.5 sun light. The result from I-V curve (Fig. 5) was summarized in Table 1. The results show that the power conversion efficiency of **P2+N719** and **YN07+N719** were found at 2.37% and 1.59%, respectively (compared with pure **P2** (1.42%) and pure **YN07** (0.46%) which can be explained by the high J_{SC} values at 5.84 and 4.08 mA/cm^2.

Table 1. The photovoltaic parameters of DSSC devices from pure and co-dye.

Complexes	J_{SC} (mA/cm^2)	V_{OC} (mV)	FF	η (%)
P2	3.82	0.52	0.72	1.42
YN07	1.41	0.48	0.68	0.46
P2+N719	5.84	0.56	0.73	2.37
YN07+N719	4.08	0.53	0.74	1.59
N719	12.02	0.60	0.71	5.17

CONCLUSIONS

We report the synthesis and characterization of ruthenium complex for using as sensitizers in DSSCs. The co-sensitized device (**P2+N719** and **YN07+N719**) show significantly enhancing the J_{SC} (5.84 and 4.08 mA/cm^2, respectively). As a result, both co-sensitization show higher power efficiencies (2.37% and 1.59%, respectively) than the sensitizer alone.

ACKNOWLEDGEMENTS

The financial supported by the Energy Policy and Planning Office, Ministry of Energy, Thailand.
The authors would like to thank Ubon Ratchathani University and Center for Organic Electronic and Alternative Energy (COEA).

REFERENCES

[1] O'Regan, B. and Grätzel, M. *Nature*. **13**, 353 – 737, 1991. [2] a) O'Regan, B. and Grätzel, M. *Acc. Chem. Res.* **33**, 269, 2000. b) Chiba, Y. et al. *J. Appl. Phys.* **45**, L638-L640, 2006. c) Gao, F. et al. *J. Am. Chem. Soc.* **130**, 10720-10728, 2008. [3] Singh, S. P. et al. *Org. Electron.* **14**, 1237 (2013). [4] Prompan, P. et al. *Adv. Mater. Res.* **770**, 92-95, 2013. [5] Luo, Y. et al. *Adv. Mater.* **21** (45), 4647-4651, 2009.

FACULTY OF SCIENCE
UBON RATCHATHANI UNIVERSITY

VITAE

NAME	Miss. Preeyapat Prompan
BORN	18 August 1990, Nakhonphanom, Thailand
EDUCATION	2009-2012, Ubon Ratchathani University, Bachelor’s Degree of Science, Chemistry
RESEARCH GROUP	Organometallic and Catalytic Center (OCC)
PUBLICATIONS	Preeyapat Prompan, Kittiya Wongkhan and Rukkiat Jitchati “Design and synthesis of ruthenium (II) complexes and their applications in dye sensitized solar cells (DSSCs)”, **Advanced Materials Research**. 770: 92-95; September, 2013
PRESENTATIONS	1) 2013 International Conference on Applied Physics and Material Applications (ICAPMA 2013), Oral presentation in the topic of “Design and Synthesis of Ruthenium (II) Complexes and Their Applications in Dye Sensitized Solar Cells (DSSCs)” at Phetchaburi, Thailand, 2013 2) Pure and Applied Chemistry International Conference 2013 (PACCON 2013), Poster Presentation in the topic of “Thiocyanate free ruthenium complex for dye sensitized solar cell” at Chonbury, Thailand, 2013 3) 10th International Symposium on Modern Optics and Its Applications 2015, Poster Presentation in the topic of “Co-sensitizers for Dye-Sensitized Solar Cells (DSSCs)” at Bandung, Indonesia, 2015